공학박사 학위논문

Problem Identification and Performance Enhancement of Video Multicast over WLAN

무선랜 비디오 멀티캐스트의 문제 발견 및 성능 향상 기법

2017년 8월

서울대학교 대학원

전기·컴퓨터공학부

신 연 철

Abstract

Video multicast, streaming real-time videos via multicast, over wireless local area network (WLAN) has been considered a promising solution to share common venue-specific videos. By virtue of the nature of the wireless broadcast medium, video multicast basically enables scale-free video delivery, i.e., it can deliver a common video with the fixed amount of wireless resource regardless of the number of receivers. However, video multicast has not been widely enjoyed in our lives due to three major challenges: (1) power saving-related problem, (2) low reliability and efficiency, and (3) limited coverage.

In this dissertation, we consider three research topics, i.e., (1) identification of practical issues with multicast power saving, (2) physical (PHY) rate and forward erasure correction code (FEC) rate adaptation over a single-hop network, and (3) multi-hop multicast, which deal with the three major challenges, respectively.

Firstly, video multicast needs to be reliably delivered to power-saving stations, given that many portable devices are battery-powered. Accordingly, we investigate the impact of multicast power saving, and address two practical issues related with the multicast power saving. From the measurement with several commercial WLAN devices, we observe that many devices are not standard compliant, thus making video multicast performance severely degraded. We categorize such standard incompliant malfunctions that can result in significant packet losses. We also figure out a coexistence problem between video multicast and voice over Internet protocol (VoIP) when video receivers runs in power saving mode (PSM). The standard-compliant power save delivery of multicast deteriorates the VoIP performance in the same WLAN. We analyze the VoIP packet losses due to the coexistence problem, and propose a new power save delivery scheme to resolve the problem. We further implement the proposed scheme with an open source device driver, and our measurement results demon-

strate that the proposed scheme significantly enhances the VoIP performance without sacrificing the video multicast performance.

Second, multi-PHY rate FEC-applied wireless multicast enables reliable and efficient video multicast with intelligent selection of PHY rate and FEC rate. The optimal PHY/FEC rates depend on the cause of the packet losses. However, previous approaches select the PHY/FEC rates by considering only channel errors even when interference is also a major source of packet losses. We propose InFRA, an interference-aware PHY/FEC rate adaptation framework that (1) infers the cause of the packet losses based on received signal strength indicator (RSSI) and cyclic redundancy check (CRC) error notifications, and (2) determines the PHY/FEC rates based on the cause of packet losses. Our prototype implementation with off-the-shelf chipsets demonstrates that InFRA enhances the multicast delivery under various network scenarios. InFRA enables 2.3x and 1.8x more nodes to achieve a target video packet loss rate with a contention interferer and a hidden interferer, respectively, compared with the state-of-the-art PHY/FEC rate adaptation scheme. To the best of our knowledge, InFRA is the first work to take the impact of interference into account for the PHY/FEC rate adaptation.

Finally, collaborative relaying that enables selected receiver nodes to relay the received packets from source node to other nodes enhances service coverage, reliability, and efficiency of video multicast. The intelligent selection of sender nodes (source and relays) and their transmission parameters (PHY rate and the number of packets to send) is the key to optimize the performance. We propose EV-CAST, an interference and energy-aware video multicast system using collaborative relays, which entails online network management based on interference-aware link characterization, an algorithm for joint determination of sender nodes and transmission parameters, and polling-based relay protocol. In order to select most appropriate set of the relay nodes, EV-CAST considers interference, battery status, and spatial reuse, as well as other factors accumulated over last decades. Our prototype-based measurement results

demonstrate that EV-CAST outperforms the state-of-the-art video multicast schemes.

In summary, from Chapter 2 to Chapter 4, the aforementioned three pieces of the research work, i.e., identification of power saving-related practical issues, InFRA for interference-resilient single-hop multicast, and EV-CAST for efficient multi-hop multicast, will be presented, respectively.

keywords: video multicast, WLAN, multicast power saving, PHY/FEC rate adaptation, multi-hop multicast.

student number: 2010-20828

Contents

List of Tables

List of Figures

Chapter 1

Introduction

1.1 Video Multicast over WLAN

Facing the explosion of mobile multimedia traffic, video multicast, i.e., streaming real-time video via multicast, over wireless local area network (WLAN) has been considered a promising solution to share common venue-specific videos, e.g., live lecture videos in smart classrooms, live broadcast videos in smart stadiums, and informative videos in smart conference halls or museums. By virtue of the nature of the wireless broadcast medium, video multicast basically enables scale-free video delivery, i.e., it can deliver a common video with the fixed amount of wireless resource regardless of the number of receivers.

However, video multicast has not been widely enjoyed in our lives due to three major challenges: (1) power saving-related problems, (2) low reliability and efficiency, and (3) limited coverage.

Firstly, power saving operation, which is essential for battery-powered WLAN devices, should be carefully implemented in commercial devices in terms of interoperability, since many packets can be lost if access point (AP) sends when stations (STAs) turn off the radio interface. However, WiFi alliance, in charge of the interoperability test of commercial WLAN devices, does not test whether each device fol-

lows the multicast power saving operations defined in IEEE 802.11 standard [1], which implies that multicast performance can be severely degraded due to the limited inter-operability. Besides, according to IEEE 802.11 standard, AP sends multicast packets to STAs in PSM before transmitting any unicast packets, which incurs a serious coexistence problem. Second, IEEE 802.11 standard had no retransmission mechanism for multicast packets for avoiding the acknowledgement (ACK) explosion problem until a few years ago, and newly defined multicast retransmission mechanisms [2] have not been widely deployed. In relation to the lack of retransmission mechanisms, multicast packets are typically transmitted using the most robust physical (PHY) rate in order to serve the receivers with low channel quality, which requires large airtime. Therefore, video multicast has been regarded unreliable and inefficient. Finally, the transmission range of WLAN is typically not large enough to cover all the area of places such as large auditoriums and sports stadiums.

In order to clarify and overcome the aforementioned challenges, this dissertation addresses three technical issues. 1) The power saving operation is essential since most WLAN devices are battery-powered, and the inter-operability for the power saving operation is the major concern. Turning off the radio interface, which is an indispensable operation for power saving, might incur packet losses when AP sends packets while a STA turns the radio interface off. The power saving operation for multicast is different from that for unicast, but there is no in-depth examination on commercial devices. Therefore, investigation of the power saving operation of commercial devices clarifies the inter-operability issue in multicast power saving. Another important issue is coexistence with other applications, since the power saving operation for multicast affects the other applications such as voice over Internet protocol (VoIP). Since the power saving delivery of AP is enabled when at least one STA operates in PSM, the problem resulted from the power saving is non-trivial.

2) There have been many schemes to improve reliability and efficiency, which are chronical problems of video multicast. Among them, forward erasure correction

(FEC), which generates parity packets from the original packets to enable receivers to recover the original packets with the parity packets, is one of the well-known reliability enhancement schemes. On the other hand, multi-PHY rate multicast, which utilizes a higher PHY rate, is a representative solution for the efficiency enhancement. With the intelligent selection of PHY and FEC rates, multi-PHY rate FEC-applied multicast, which exploits a higher PHY rate after applying FEC, can improve both reliability and efficiency. The optimal PHY/FEC rates depend on the cause of the packet losses, but previous approaches select the PHY/FEC rates by considering only channel errors even when interference is also a major source of packet losses. Differentiating the cause of packet losses is non-trivial problem for multicst, since existing loss differentiation schemes relying on ACK or request-to-send/clear-to-send (RTS/CTS), which is suited for unicast, cannot be applied for multicast because ACK and RTS/CTS are not available for multicast.

3) In order to extend the coverage, collaborative relaying approaches, where some receiver nodes relay the received packets from the source node to other nodes, have been considered. In addition to the wider coverage, collaborative relaying has potential to enhance both reliability and efficiency. With the collaborative relaying, if the source node transmits at a higher data rate instead of a low data rate and the relay nodes relay the packets at a higher data rate as well, the overall efficiency can be improved. In collaborative relaying, one major concern is the energy consumption of the relay nodes. Furthermore, video streaming application worsens the situation since watching video itself consumes lots of energy, and the energy consumption is directly associated with the total service time of video multicast. Accordingly, the choice of the relay nodes should take into account the battery level as well as the charging status, i.e., the battery is being charged or not. Another important factor is exploiting spatial reuse that enables two relay nodes to transmit simultaneously, thus enhancing the efficiency. Furthermore, interference should also be considered for the selection of relay nodes. Therefore, it is very difficult to develop an elaborate multi-hop multicast system that

considers the three factors as well as the factors accumulated over past years in this field.

1.2 Overview of Existing Approaches

There exists a considerable body of research available in the literature that attempt to investigate the multicast power saving and enhance the multicast performance. Existing approaches can be classified into three categories: (1) multicast power saving, (2) reliability and efficiency enhancement, and (3) coverage extension.

1.2.1 Multicast Power Saving

There are several studies on the video multicast for power-saving stations. In [3], He *et al.* investigated the impact of beacon/DTIM periods and background traffic on the power consumption. In [4], Hiraguri *et al.* analyzed the influence of the multicast traffic on power consumption, and proposed a scheme to reduce the power consumption by modifying the traffic indication map (TIM) element. In [5], Lee *et al.* proposed an AP-side solution to resolve the side-effects of the multicast power save delivery by preventing the multicast STAs from running in the PSM.

Although those studies made beneficial observations on the power saving operation for video multicast, none of them addresses the inter-operability and the coexistence issue with VoIP traffic.

1.2.2 Reliability and Efficiency Enhancement

PHY/FEC Rate Adaptation for Multicast

Alay *et al.* [6] proposed to determine the optimal PHY/FEC rates that maximize the video bitrate. Based on the packet loss rate (PLR) feedback from the receiver with the lowest PLR, AP determines whether to increase/decrease/keep its PHY rate. With PLR estimation and an off-line PLR versus the optimal FEC rate table, X-Wing [7]

determines the PHY rate achieving the maximum estimated throughput of the receiver with the lowest APLR. X-Wing assumes that PLR decreases by 5% as it decreases PHY rate by one step. Bulut *et al.* [8] proposed optimal PHY/FEC rate selection with IEEE 802.11n multiple input multiple output (MIMO) mode selection between spatial multiplexing (SM) and space time block code (STBC). According to the current 802.11 standard, however, multicast packets should be sent via legacy PHY rates, i.e., 802.11a PHY rates, and current off-the-shelf devices also utilize the legacy PHY rates for multicast. None of the above approaches addresses the impact of interference on the multi-rate FEC-applied multicast, and hence, their PHY/FEC rate adaptation does not consider interference.

Wireless Video Transmission

Softcast [9] proposed a joint channel and source coding for scalable video streaming. The key idea of SoftCast is to enable the linear relationship between the pixel values and the transmitted signal by exploiting analog video coding and real-valued modulation. Parcast [10] enhanced Softcast with a design well-suited for MIMO-OFDM WLAN. Flexcast [11] modifies MPEG4 codec and incorporate rateless coding for video streaming. These schemes require no feedback on wireless channel status, and the received video quality is automatically adjusted depending on the channel quality of each receiver. However, they require heavy modification to video codec and PHY layer. Futhermore, channel quality agnostic video transmission is vulnerable to interference, as high signal strength due to interference can be misinterpreted as a high pixel value.

1.2.3 Coverage Extension

Collaborative Relay over WLAN

Lin *et al.* [12] proposed a relay-based video multicast system, which allocates the channel time and selects PHY rate of each relay nodes. By applying Scalable video

coding (SVC) [13], a video is encoded into a base layer and multiple enhancement layers, and AP sends the packets of the base layer using a robust PHY rate while relay nodes send the packets of the enhancement layers using higher PHY rates.

PeerCast [14] proposed that AP selects a higher PHY rate to deliver a batch of packets to the majority of STAs, and a suitable subset of these STAs relay the packets. Peercast proposes the power-controlled ACK mechanism which requires the STAs to transmit the ACK frames simultaneously at the transmit power ensuring the received signal strengths of AP are the same, which enables the AP to estimate the number of clients receiving packets successfully.

Alay *et al.* [15] proposed a two-hop relay multicast system using FEC. The users are divided into two groups in a way that receivers in Group 1 have better average channel quality than those in Group 2. The selected receivers among Group 1 relay the packets to Group 2. The system computes the optimum system parameters, including relay selection, user partition, transmission rates, and FEC rates, and transmission time scheduling. Besides, the authors consider directional antenna to enhance the efficiency.

Opportunistic Routing

Opportunistic routing (OR), where all the neighboring nodes of a sender node have opportunities to relay each packet instead of designating the fixed next-hop node, has been utilized for multi-hop multicast. For achieving high scalability and resolving the "crying baby" problem in the multicast scenario, Pacifier [16] proposes a tree-based OR and round-robin scheduling-based batch transmission. Uflood [17] identifies the major factors in selection of forwarders (relay nodes) and proposes the distributed forwarder selection algorithm that concerns the proposed factors. Uflood is the first work that enables the multi-rate multicast OR.While aforementioned OR schemes (for unicast and multicast) target on applications requiring 100 % reliability such as file transfer, ViMOR [18] proposes a multicast OR scheme suited for the video streaming. With the philosophy of total denial of acknowledgement, ViMOR enables every video

frame to be delivered before its deadline.

However, none of existing multi-hop multicast schemes considers interference, battery status, and spatial reuse.

1.3 Main Contributions

1.3.1 Practical Issues with Multicast Power Saving

We identify the two practical issues with multicast power saving. First of all, we identify the various malfunctions of commercial WLAN devices on both AP and STA sides. Secondly, we claim that there is a serious coexistence problem between video multicast and VoIP traffic where the former incurs large delay to the latter. We analyze the packet losses due to the coexistence problem, and propose a candidate solution. The proposed scheme based on intra-access category (AC) strict priority can resolve the problem with a simple protocol modification. Instead of giving strictly higher priority to multicast packets over unicast packets regardless of AC, we propose to limit the strict priority of multicast traffic only within the same AC. Our prototype-based measurement results verify that the proposed scheme effectively resolves the coexistence problem.

In summary, we claim the following contributions in this work.

- We report the malfunctions of both commercial AP and STA devices based on the extensive measurement.
- We identify the coexistence problem between video multicast and VoIP by both measurement and analysis.
- We propose the intra-AC strict priority based multicast power saving delivery that resolves the coexistence problem.
- We implement the proposed scheme with an open source WLAN device driver, and empirically demonstrate that the proposed scheme resolves the coexistence

problem.

1.3.2 Interference-aware PHY/FEC Rate Adaptation

In order to optimize the PHY/FEC rates depending on the cause of packet losses, we propose InFRA, an interference-aware PHY/FEC rate adaptation framework for the multi-rate FEC-applied wireless multicast system. In InFRA, each STA periodically requests desired PHY/FEC rates, and the AP chooses the best PHY/FEC rates based on the requests from multiple STAs. InFRA diagnoses the cause of packet losses using received signal strength indicator (RSSI) and cyclic redundancy check (CRC) error notifications, which are both available in the standard. If a packet is lost, we infer it as due to the poor channel quality when an average RSSI of the associated batch is lower than a PHY rate-dependent threshold. Otherwise, we infer it as due to interference. We further classify the losses from interference depending on whether the CRC error notification exists.

Based on that, InFRA determines appropriate PHY/FEC rates to minimize the air-time consumption while meeting various performance requirements, e.g., the fraction of nodes satisfying the target video packet loss rate. When packet losses occur due to poor channel quality, InFRA decreases PHY rate while when packet losses happen due to interference, InFRA determines whether to decrease PHY rate or FEC rate based on the interfering signal strength and the number of packet losses. We implement InFRA with an open-source WLAN device driver, and evaluate the performance under various scenarios.

In summary, we claim the following contributions in this work.

- We investigate the impact of interference on multi-rate FEC-applied multicast, and empirically verify the importance of interference-aware PHY/FEC rate selection.

- We propose a standard-compliant loss differentiation scheme for multicast based

on RSSI and CRC error notifications.

- We propose an interference-aware PHY/FEC rate adaptation framework, InFRA, which selects the optimal PHY/FEC rates depending on the cause of packet losses.

- We propose a feedback protocol to support large scale video multicast, which requires minimal overhead while enabling fast adaptation.

- We implement InFRA with an open-source WLAN device driver, and our measurement results with off-the-shelf devices demonstrate that InFRA improves the performance significantly, especially when the interference is the major source of the packet losses.

1.3.3 Energy-aware Multi-hop Multicast

We propose EV-CAST, a multi-hop video multicast system that considers battery status, interference, and spatial reuse. We focus on two-hop networks where destination nodes are one-hop or two-hops away from the source node, since most indoor auditoriums can be covered by two-hop transmission. Moreover, video streaming over more than three-hops is inappropriate due to large delay and bandwidth limitation. EV-CAST involves (1) an algorithm for joint determination of sender nodes and their transmission parameters (PHY rate and the number of forwarding packets), (2) online network management, and (3) polling-based relay protocol. As a kind of tree-based OR, EV-CAST constructs a two-hop multicast tree and leverages it for opportunistic overhearing. A novel centralized algorithm determines sender nodes and their transmission parameters by taking into account various factors including battery status and spatial reuse as well as factors reported up-to-date. The chosen relay nodes are scheduled to exploit the spatial reuse with avoiding collisions among relay nodes.

We implement EV-CAST with an open-source WLAN device driver and comparatively evaluate the performance of EV-CAST with existing schemes in a large-scale

testbed. Our measurement results demonstrate that EV-CAST outperforms the state-of-the-art schemes.

Our contributions are summarized as followings.

- We propose EV-CAST, the first practical video multicast protocol that simultaneously address both challenges: It maximizes the number of served nodes while maximizing the total service time by offering significant improvements over a state-of-the-art protocol.

- We present the design of EV-CAST, which is well-suited for video multicast over two-hop network. The main components, i.e., the novel algorithm that jointly determines the sender nodes and their transmission parameters, online network management, and polling-based relay protocols, are integrated harmonically.

- We propose a novel algorithm that jointly determines the set of sender nodes and their transmission resource. The algorithm is designed based on the principles not only accumulated over past years in this field, but also newly addressed in this chapter. To the best of our knowledge, it is the first relay selection for video multicast that concerns interference, battery status, and spatial reuse.

- We present the prototype implementation of EV-CAST and evaluate the performance in a large-scale testbed. Our measurement results demonstrate that EV-CAST serves larger number of nodes with a smaller airtime.

1.4 Organization of the Dissertation

The rest of the dissertation is organized as follows.

Chapter 2 presents identification of practical issues with multicast power saving. The measurement results with various commercial WLAN devices are presented along with the identified malfunctions. After that, identification of the coexistence problem via measurement and analysis is provided. Then, the design of the proposed scheme

is presented, and the performance of the proposed scheme is evaluated with the measurement.

Chapter 3 figures out the impact of interference on multi-rate FEC-applied multicast with a measurement study. Then, the detailed design of InFRA including architecture and operations of both AP and STA sides is provided. The performance of InFRA is evaluated via measurements under various scenarios.

Chapter 4 presents the design of EV-CAST. The philosophies to select relay nodes are firstly discussed. Based on them, the detailed design of EV-CAST including network management, key algorithms, and relay transmission, is presented. The performance of EV-CAST is evaluated via measurements under various scenario in an NGO-owned wireless testbed, imec w-iLab.t testbed.

Finally, Chapter 5 concludes the dissertation with the summary of contributions and discussion of the future research directions.

Chapter 2

Practical Issues with Multicast Power Saving

2.1 Introduction

During the last 10 years or so, IEEE 802.11 [19] WLAN has been popular for wireless access network by virtue of its high data rate and relatively low cost. As the data rate of WLANs increases, the video streaming service is becoming one of main applications over WLANs today. Given that many portable devices are battery-powered while video quality relies on the reliable delivery of video traffic, video multicast frames need to be *reliably* delivered to *power-saving* stations.

The IEEE 802.11 allows multicast receivers to enable the power management while receiving multicast traffic. For the power save delivery of multicast frames, AP buffers all multicast packets when at least one STA associated with it operates in PSM. The buffered multicast packets are transmitted after delivery traffic indication map (DTIM) beacons periodically transmitted every DTIM period, which is determined as an integer multiple of the beacon interval. Then, the power-saving STAs wake up and receive all the buffered multicast packets.

In this chapter, we empirically analyze the video multicast operation in the aspects that whether commercial WiFi devices operate as defined in the standard. In order to investigate the issue, commercial WiFi devices are tested for both cases when the

power management option of the STA is enabled and disabled. With respect to the standard-compliance issue, our experimental results show that all the devices which have been used in this experiments are non-compliant with the standard when the STA enables the power management functionality. Moreover, such noncompliance disturbs the communication and causes significant losses.

Moreover, according to the IEEE 802.11 standard (Clause 11.2.3.4, [1]), when an AP transmits the buffered multicast packets after a DTIM beacon, the AP has to transmit all the buffered multicast packets before transmitting any unicast packet, including VoIP packets. Therefore, when VoIP coexists with video multicast, such strictly higher priority of the buffered multicast results in significantly long pause of the VoIP, thus heavily degrading the call quality. This problem, although it is rooted in the standard, may possibly cause disruption of time-critical conversational voice service. Moreover, it is against the common belief that voice traffic should have higher priority than video traffic.

The contributions of this chapter are summarized as follows. We first report various kinds of standard-incompliant malfunctions of commercial WLAN devices, which make the performance of video multicast to power-saving receivers unacceptably poor. Second, we report the coexistence problem with the voice over Internt protocol (VoIP) via measurement and analysis. Third, we propose a simple solution to resolve the coexistence problem, and verify that the performance gain via prototype-based measurement.

The rest of this chapter is organized as follows. We first present the multicast and power management operation of IEEE 802.11. Then, we present the undesirable video multicast operations of commercial WLAN devices. After that, we address the coexistence problem with the VoIP applications. Finally, we conclude the chapter.

2.2 Multicast & Power Management Operation in IEEE 802.11

The legacy 802.11 medium access control (MAC) operations of the multicast are defined quite differently from those of the unicast. First, multicast frames do not use MAC-layer automatic repeat request (ARQ), i.e., there is no retransmission, and request-to-send (RTS)/clear-to-send (CTS) exchange cannot be used. Accordingly, the failed frames due to the collision or the channel error cannot be recovered, thus making multicast inherently unreliable. Second, multicast frames are transmitted at a data rate in the basic service set (BSS) basic rate set, which is generally low in order to allow even poorly-connected users to receive frames correctly. The usage of the low data rate limits available video source rate. As the maximum data rate goes up to 600 Mbps with today's 802.11n, the data rate gap between unicast and multicast increases significantly.

Today, most battery-powered portable devices including smartphones, tablet PCs, and laptops support the WLAN access, so an energy efficient operation is required to WLAN. To this end, IEEE 802.11 standard defines a power management (PM) operation, which operates differently according to the transmission methods, i.e., unicast and multicast. For the PM operation, two power management modes, namely, power saving mode (PSM) and active mode (AM) are defined. A STA in PSM toggles between two different power states, namely, (1) *awake* state in which the STA can transmit or receive signals and (2) *doze* state in which the STA turns off the radio components so that the STA cannot sense signals. On the other hand, a STA in AM always runs in *awake* state.

For unicast service, an access point (AP) buffers all frames destined to a STA in PSM, and informs the presence of the buffered frame via the traffic indication map (TIM) element in beacon frames. STAs in PSM wake up (i.e., switch from *doze* state to *awake* state) periodically to receive beacons.[1] Then, if an *awake* STA recognizes the

[1] According to the standard, a STA in PSM does not need to wake up at every beacon transmission time. When to wake up is actually an implementation issue, and there is normally a tradeoff relationship

existence of a buffered frame addressed to itself, the STA transmits a power save (PS)-poll frame in order to request the delivery of that frame, otherwise, it goes to *doze* state again. If more frames destined to the STA are still buffered, the AP sets *More Data* bit in the MAC header. Upon receiving a frame whose *More Data* bit is set to one, the STA should stay *awake*.

For multicast service, the AP also buffers multicast frames when at least one STA associated with it operates in PSM, even if all the receivers of the multicast frames are working in AM. The buffered multicast frames are transmitted immediately after delivery TIM (DTIM) beacons, which are special beacons.[2] In order to announce the existence of the multicast frames, the AP sets an indication bit in the DTIM beacon frame to one.

To transmit the buffered frames, the following rules are used: (1) the AP should transmit the buffered multicast frames before transmitting any unicast frame; and (2) the AP should continue to transmit the multicast frames until all the buffered multicast frames are sent. For the following transmission the *More Data* bit is also used. In fact, the AP may not be able to deliver all the buffered frames within a beacon interval following the DTIM beacon. We refer to such a situation as *delivery overflow*, and according to the second rule, in the *delivery overflow* case, the AP should continue to transmit the multicast frames by setting the indication bit to one even in the non-DTIM beacons. At the STA side, a STA, after a DTIM beacon, should remain *awake* until receiving all the multicast frames, i.e., until receiving a frame whose *More Data* bit is set to zero or the beacon frame in which the indication bit is set to zero.

2.3 Inter-operability Issue

In this section, we extend our previous work [20] by experimenting with a larger set

between the energy saving and the delay performance depending on the wake-up period.

[2]DTIM beacons are transmitted every "DTIM periods" as shown in Fig. 2.1a.

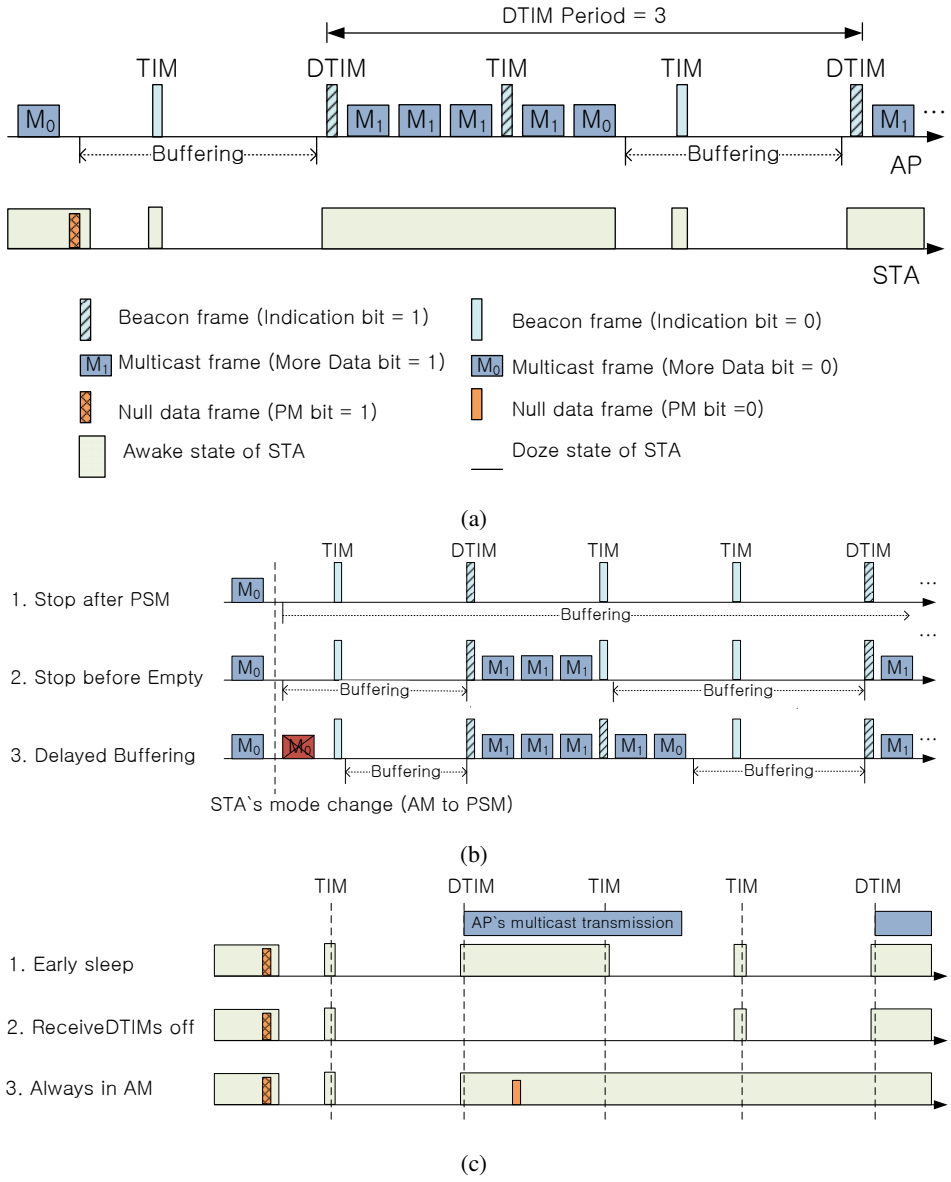

Figure 2.1: Standard compliant operation and various malfunctions of both AP and STA: (a) standard compliant power management operation for multicast service, (b) malfunctions of AP, and (c) malfunctions of STA.

Table 2.1: Summary of experimental results.

End-to-end delivery ratio (PSNR)		Apple AP	Cisco AP	Cybertan AP	Mmctech AP	Malfunction of STA
Cisco STA	PM_OFF	99.5 % (35.5 dB)	99.5 % (36 dB)	85.3 % (19.2 dB)	98.9 % (34.6 dB)	Always in AM
	PM_ON	99.1 % (35.3 dB)	99.7 % (36.7 dB)	85.3 % (18.5 dB)	98.6 % (33.4 dB)	
Intel STA	PM_OFF	95.4 % (27.2 dB)	97.8 % (31.9 dB)	83.5 % (17.5 dB)	96.6 % (30 dB)	Early Sleep
	PM_ON	71.1 % (14.2 dB)	50.7 % (11.6 dB)	80.2 % (16.3 dB)	1.5 % (7.3 dB)	
RealTek STA	PM_OFF	97.4 % (31.6 dB)	96.0 % (28.9 dB)	83.5 % (18.1 dB)	97.9 % (32 dB)	ReceiveDTIMs off
	PM_ON	12.4 % (8.2 dB)	94.9 % (27.3 dB)	81.8 % (17 dB)	5.1 % (7.9 dB)	
Malfunction of AP		Stop before Empty & Delayed Buffering	Delayed Buffering	-	Stop after PSM	

of commercial WLAN devices, and observe that several commercial WLAN devices are not standard-compliant, which makes them inappropriately for video multicast.

2.3.1 Malfunctions of Commercial WLAN Devices

We experimentally examine the video multicast operations of commercial WLAN devices in conjunction with the power management. Four different AP devices and three STA devices, which are widely used, are tested in this experiment:

- Apple: AirPort Extreme Base Station (Apple AP) [21]
- Cisco: AIR-AP1232AG-A-K9 (Cisco AP) [22]
- Mmctech: MW-2060 (Mmctech AP) [23]
- Cybertan: APD-2000 (Cybertan AP) [24]
- Intel: Intel Pro/Wireless 3945 ABG Network Connection (Intel STA, embedded in Lenovo ThinkPad X60s laptop) [25]
- Realtek: 802.11b/g Mini Card Wireless Adapter (Realtek STA, embedded in LG Xnote X110 laptop) [26]
- Cisco: CB21AG (Cisco STA, PCMCIA card) [27]

In our experiments, all the AP devices use the same DTIM period of three beacon intervals. Three APs (MmcTech, Apple, and Cisco) use 2 Mbps physical (PHY) layer data rate for multicast, while Cybertan AP uses 1 Mbps due to the limitation of the configuration. For this test, a video clip (416x240 resolution, MPEG-4 codec, 800 kbps, 30 fps) is streamed via multicast. We analyze the operation by comparing the list of the packets at the transmitter, receiver, and in the air. The detailed experimental setup is described in [20].

Through the examination, it turns out that the experimental devices show various malfunctions when the PM operation is enabled. It should be noted that most of today's WLAN devices enable the PM operation by default, and hence, the malfunctions are easily observed in real environments. Fig. 2.1 illustrates the standard compliant operation and abnormal operations which we find by the experiments where an AP serves video multicast to a PM-enabled STA. In Fig. 2.1a, a null data frame whose PM bit is one is sent to notify its AP that the STA switches to PSM. As mentioned earlier, the standard compliant operation specifies that upon the reception of such a frame, the AP should start buffering multicast frames, and then transmit all the buffered multicast frames after a DTIM. Then, STAs should operate compliantly to receive all the multicast frames. Nevertheless, the commercial WLAN devices, both the APs and the STAs, malfunction in different ways.

The malfunctions of the APs are categorized in three cases as shown in Fig. 2.1b. First, in *Stop after PSM* case, the AP never transmits when a STA notifies that it switches to PSM. As the whole multicast transmission is delayed until all the STAs return to AM, *Stop after PSM* causes significant delay as well as packet losses due to the buffer overflow. Second, in *Stop before Empty*, the AP stops the multicast transmission when *delivery overflow* occurs. Such an operation utilizes only $1/(DTIM\ period)$ of wireless resources, and hence, it may cause packet losses resulting from insufficient resources. Third, *Delayed Buffering* is defined that the AP cannot buffer multicast frames as soon as a STA switches to PSM. Although *Delayed Buffering* leads to packet losses,

the impact is less serious especially when there are numerous STAs, since it is rare that all the STAs run in AM. Based on the above explanations, these three operations are standard-incompliant.

Fig. 2.1c describes undesirable operations of STAs. An *Early Sleep* STA goes to sleep after receiving multicast frames during only a single beacon period after a DTIM beacon, even when buffered multicast frames continue to be sent after a subsequent non-DTIM beacon. Accordingly, an *Early Sleep* STA loses multicast packets in the *delivery overflow* situation. *ReceiveDTIMs off* indicates that a STA does not wake up to receive every DTIM beacon, as a result, the STA misses packets after the skipped DTIM beacons. In the standard, the *ReceiveDTIMs* parameter indicates whether the corresponding STA always wakes up to receive DTIM beacons. Therefore, in order for a STA to successfully receive a multicast service, it is recommended to turn the *ReceiveDTIMs* on.

In *Always in AM* case, on the other hand, the STA mostly runs in AM after one multicast frame is received. Note that when a STA enables the PM functionality, the STA toggles between AM and PSM. Specifically, a PM-enabled STA starts to run in PSM after not receiving any frame for an predefined *inactivity time*. Likewise, a PM-enabled STA returns to AM when specific amount of packets are received. Under such an operation, the STA with *Always in AM* returns to AM as soon as a single frame is received, and hence, an *Always in AM* STA looks as if it is always in AM. In this case, it is difficult to achieve efficient power management, though the STA can receive all the multicast frames. Even if the later two cases, i.e., *ReceiveDTIMs off* and *Always in AM*, are standard-compliant, they are also undesirable for the aforementioned reasons.

Note that above-mentioned malfunctions negatively affect the video multicast service in various ways. A *Stop after PSM* AP does not provide a video service at all, and for a *Stop before Empty* AP, the available wireless resource might not be enough to support high quality videos. A *Delayed Buffering* AP drops several packets, thus degrading the video quality. An *Early Sleep* STA losses packets when a high qual-

ity video is subscribed, i.e., when *delivery overflow* occurs, and a *ReceiveDTIMs off* STA losses packets intermittently, thereby the received video quality is degraded. An *Always in AM* STA is able to receive all video packets so that good video quality is expected at the cost of more energy consumption.

2.3.2 Performance Evaluation

The end-to-end delivery ratio, PSNR, and the corresponding malfunctions of the commercial WLAN devices are summarized in Table 2.1. The PSNR is a widely used video quality metric, and a higher PSNR indicates better video quality. Apparently, packet losses decrease the PSNR.[3] When the STAs disable the PM functionality (PM_OFF), the end-to-end delivery ratio is over 95 % and the PSNR is over 27 except for the Cybertan AP. Using 1 Mbps PHY rate for multicast, the Cybertan AP cannot fully deliver the 800 kbps video due to protocol overheads. On the other hand, the end-to-end delivery ratio decreases in many cases when the STAs enable the PM functionality (PM_ON), accordingly the PSNR decreases severely. However, in the Cisco STA case, the ratio is almost the same as the PM_OFF case due to the *Always in AM* characteristic of the Cisco STA.

Now, we discuss the results of the other two STA devices, i.e., Intel and Realtek STAs, with respect to the interaction with each AP. Firstly, when the two types of STAs communicate with the Cybertan AP, the end-to-end delivery ratios and the PSNRs of the PM_ON case are slightly smaller than those of the PM_OFF case. In fact, based on our close examination, the Cybertan AP is the only standard-compliant AP device out of our experimental group. That indicates that the degradation with the PM_ON case results from the malfunctions of the two STAs. However, the reason why the degradation is relatively small is that Intel and Realtek STAs mostly run in AM even if their PM is enabled, because the Cybertan AP transmits packets with 1 Mbps PHY

[3]The maximum PSNR of the used video clip is 37.8 dB, and typically, the PSNR under 25 dB is considered unacceptable.

rate, thus almost fully utilizing the air time, and hence, not allowing the STAs to go to PSM.

On the other hand, other three APs have malfunctions as shown in Table 2.1. With the *Stop before Empty & Delayed Buffering* malfunctions, the Apple AP drops many packets. Especially when the Realtek STA is served, the problem is worsened dramatically because the STA does not receive every DTIM beacon. Also, the Cisco AP loses packets due to *Delayed Buffering*. With the Intel STA, the Cisco AP additionally loses packets owing to the fact that Intel STA switches to *doze* state after non-DTIM beacon, while the Cisco AP transmits the buffered frames at that time. With the Realtek STA, a large number of packets are received, since the *inactivity time* of the Realtek STA is relatively long, not allowing the STA to run in PSM. In the Mmctech AP case, the AP never sends multicast frames after a STA starts to run in PSM, so the number of the transmitted frames is extremely small, thus severely lowering the PSNR.

From these observations, many unexpected and undesirable malfunctions which degrade video quality are detected in several commercial devices. Therefore, standard-compliant operations are necessary as the minimum requirement for satisfactory video multicast service.

2.4 Coexistence Problem of Video Multicast and VoIP

2.4.1 Problem Statement

As stated above, setting strictly higher priority to the buffered multicast might degrade the VoIP performance, even though VoIP should generally be serviced with the highest priority. The logical basis of giving the highest priority to the buffered multicast is that most multicast traffic is lightly loaded and used for the management purpose. However, different from light management multicast traffic, video multicast requires large bandwidth, thus delaying the VoIP traffic heavily.

Fig. 2.2 describes an example scenario of the coexistence problem where video

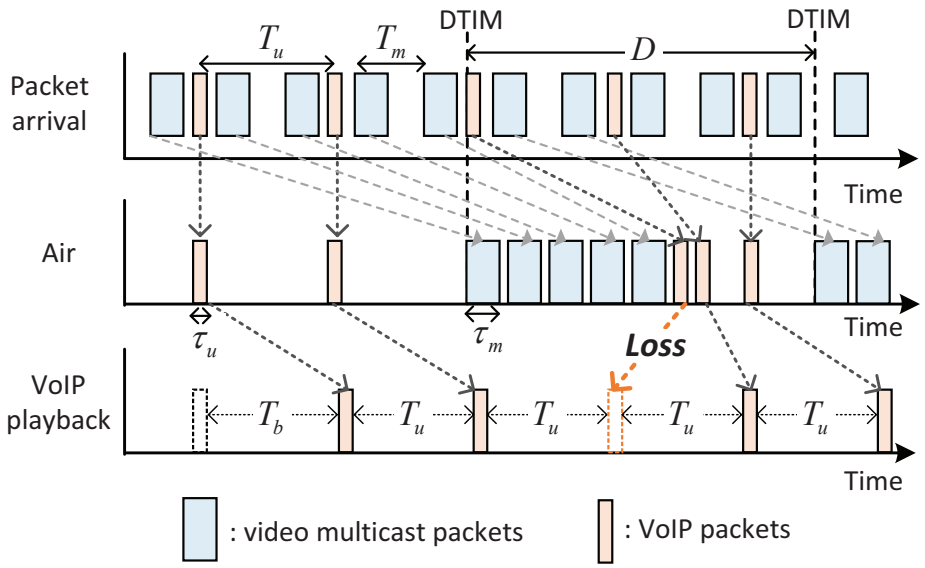

Figure 2.2: Example scenario of the coexistence problem.

multicast traffic and VoIP downlink coexist. The figure shows the timelines of the packet arrival at the AP, the wireless transmission, and the VoIP playback. Video multicast and VoIP packets arrive periodically with periods of T_m and T_u, respectively. We assume that the VoIP STA operates in AM since STAs with traffic of a short period, like VoIP, generally operate in AM. Then, each VoIP packet is transmitted to the STA as soon as it arrives before the DTIM. However, after the DTIM, the buffered multicast packets are transmitted while the VoIP packets are deferred to be transmitted. After all the buffered packets are transmitted, the VoIP packets are transmitted. The VoIP packets are periodically played by the de-jitter buffer[4]. If the delay of a VoIP packet due to the buffered multicast is larger than the de-jitter buffer size, T_b, the packet cannot be played and it is lost by the de-jitter buffer. AP buffers the multicast packets as long as at least one STA operates in PSM, even when the power-saving STA does not sub-

[4]For a multimedia service, a de-jitter buffer, which is also called a playback buffer, is used to cope with delay variation. A de-jitter buffer first enqueues a number of packets and then starts to output them with a constant inter-playback interval. A packet received after a due playback time cannot be played, which is equivalent to a packet loss

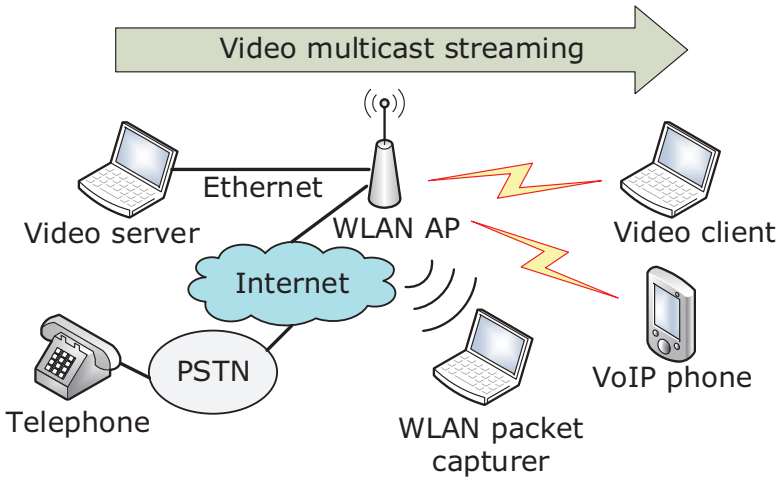

Figure 2.3: Measurement topology.

scribe to the multicast stream in the upper layers. Since STAs without much traffic mostly operate in the PSM, it is common that there is at least one STA operating in PSM. Therefore, the coexistence problem can occur frequently in a real environment.

2.4.2 Problem Identification: A Measurement Study

In order to demonstrate the problem, we set a simple network topology, where a server streams a video clip via multicast, and at the same time, a voice call is initiated between a VoIP phone [28] and a telephone attached to the public switched telephone network (PSTN). Fig. 2.3 shows the measurement topology. We analyze the operation of each device, by capturing the packet traces with a WLAN packet capturer (Airpcap Nx USB adapter). The employed AP is Cisco AIR-AP1232AG-A-K9 (firmware version: 12.3(2) JA2). The video client is a Linux-based laptop (kernel version: 3.5.0-24-generic) with iwlwifi device driver running over a built-in Intel WLAN card, Centrino Advanced-N 6235.

In this measurement, each device is placed about two meters apart from the AP in order to minimize the impact of packet losses due to channel errors. The DTIM

period and PHY rate for multicast packets are configured as 3 and 2 Mbps, respectively. The default PHY rate selection algorithm is used for unicast packets. The video content (416x240 resolution, 800 kbps, 30 fps) is encapsulated with MPEG-2 transport stream (TS). The VoIP traffic is generated using ITU-T G.711 [29] codec, and the packetization interval is set to 20 ms. The video multicast and the VoIP packets are transferred through realtime transport protocol, user datagram protocol, and Internet protocol (RTP/UDP/IP).

Figs. 2.4a and 2.4b show the packet transmission instants of VoIP uplink (VoIP-UL, i.e., from VoIP phone to AP), downlink (VoIP-DL, i.e., from AP to VoIP phone), and video multicast traffic during a 0.5-second time interval for two different power management (PM) modes of the video receiver. When the PM is disabled, a station always runs in the AM, while when the PM is enabled, the station runs in adaptive PSM (A-PSM), which alternate between AM and PSM [30]. In A-PSM, STA which has no unicast packet to send or receive operates mainly in PSM. The PSM only mode was not supported by the employed device.

In Fig. 2.4a, we observe that when the PM of the video receiver is disabled, the points are evenly distributed, which indicate periodic packet transmissions from the employed video multicast and VoIP applications. Since the VoIP packetization interval is 20 ms, about 25 points are drawn during 0.5 second. Some irregular points in the figure might be caused by errors and/or retransmissions. However, different traffic patterns are observed in Fig. 2.4b. We observe that when the PM of the video receiver is enabled, the point patterns become irregular. The periodic pattern of VoIP-UL is maintained, because the VoIP phone contends with the AP independently of the PM mode of the video receiver. On the other hand, since the AP subsequently sends buffered multicast packets after a DTIM beacon, the video traffic shows a bursty traffic pattern. Moreover, the VoIP-DL packets are not observed during the video transmission, and we observe that VoIP-DL packets are transmitted after burst video transmission is ended. Accordingly, the bursty pattern is also observed in VoIP-DL, because

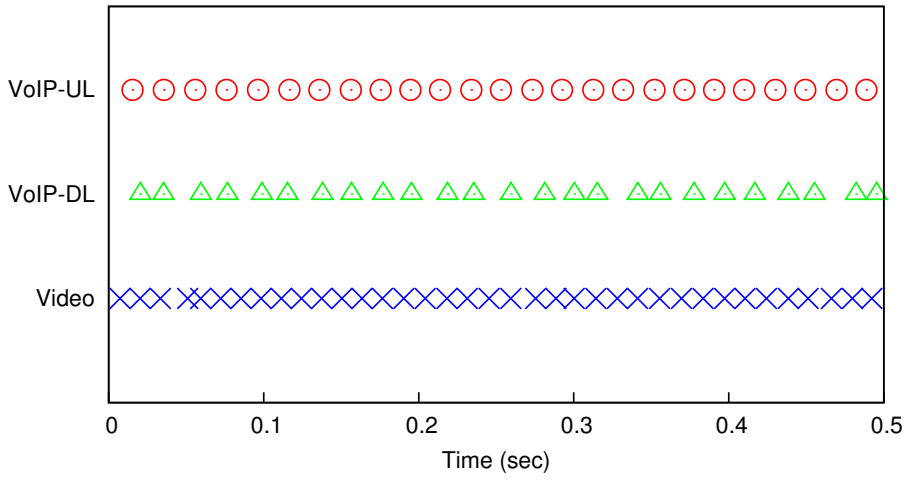

(a)

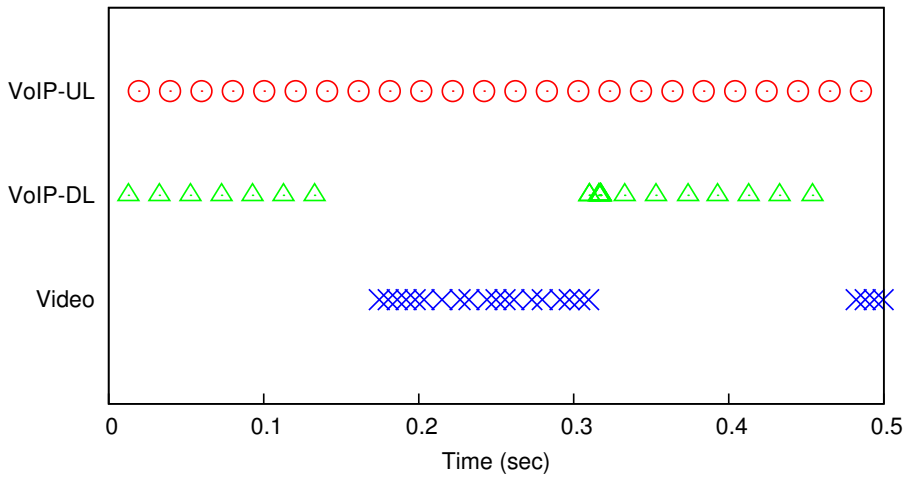

(b)

Figure 2.4: Measurement results: packet transmission instants of VoIP-DL, UL and video: (a) PM is disabled (PM=Off), (b) PM is enabled (PM=On).

Table 2.2: QoS Performance for VoIP

Traffic type	Jitter (ms)	PLR (%)	R-score
VoIP-DL (No Mcast)	0.59	0.13	86.78
VoIP-UL (No Mcast)	0.72	0.14	86.59
VoIP-DL (PM=Off)	4.23	0.19	85.87
VoIP-UL (PM=Off)	3.56	0.26	84.62
VoIP-DL (PM=On)	19.44	2.05	63.58
VoIP-UL (PM=On)	11.78	0.36	82.95

the delayed VoIP packets that arrive during the subsequent multicast transmission are transmitted successively. Therefore, the measured traffic patterns confirm that the VoIP packets are delayed by the transmission of the buffered multicast packets.

We estimate the QoS parameters of the VoIP traffic, i.e., average jitter, packet loss ratio (PLR), and R-score [31], based on the captured packet trace as shown in Table 2.2. R-score is a widely used voice call quality metric, which is calculated by the following simplified equation [32]:

$$R = R_{max} - I_{delay} - I_{loss}, \tag{2.1}$$

where R_{max} is the maximum R-score, and I_{delay} and I_{loss} are impairment factors due to end-to-end delay and packet losses, respectively. The values of the detailed parameters depend on the voice codecs. In general, voice calls with R-score of 80 or above are considered high-quality voice calls. For the R-score calculation, we assume that the wired delay is 35 ms as in [32]. Due to the de-jitter buffer, each playable packet experiences the same end-to-end delay, which is approximately the sum of the wired delay and the de-jitter buffer size (95 ms). In [32], it is reported that the PLR is the dominant factor of R-score when the end-to-end delay is under 150 ms.

For the R-score estimation, we assume that the de-jitter buffer size is 60 ms, and the wired delay is 150 ms. The jitter is calculated according to [33]. Since the wired delay

cannot be measured with our devices, we only measure the delay variation incurred by the wireless network, assuming the constant wired delay. In a real situation, there might be additional jitter due to wired network.

In the PM-enabled downlink case, significant jitter and PLR are measured due to the video multicast, and as a result, we observe R-score lower than 80. Therefore, the call quality is degraded noticeably in practice. Based on this observation, we confirm that video multicast delivery to power-saving stations may severely deteriorate the QoS of the VoIP.

2.4.3 Packet Loss Analysis

With a simple analysis, we derive the average packet loss rate (PLR) of the VoIP packets. For our analysis, we assume an error-free network, i.e., no channel and collision error, with a fixed wired delay. Moreover, all the unicast and multicast packets are assumed to be sent at fixed physical (PHY) rates, R_u and R_m, respectively. Different from the *online delivery policy* in [34] that delivers not only the multicast packets buffered during the previous DTIM period but also the multicast packets arriving while the buffered multicast packets are being transmitted, we assume the *offline delivery policy* that only delivers the buffered multicast packets and buffers the multicast packets arriving in the middle of the current DTIM period. Note that the *offline delivery policy* is implemented in *ath9k* device driver, an open-source WLAN device driver.

Then, when N_m multicast packets are buffered during the previous DTIM period, the time duration for transmitting them successively, δ_m, is expressed as

$$\delta_m = \sum_{j=1}^{N_m} \left(\tau_m + \tau_{BO[BE]}^{(j)} \right), \tag{2.2}$$

where τ_m and $\tau_{BO[BE]}^{(j)}$ are multicast packet transmission time and backoff time of the jth packet whose AC is best effort, respectively. According to the IEEE 802.11 standard, the AC of multicast packets is set to best effort.

t_{dtim} and t_{last} denote the time instances of the current DTIM and the reception

of the last VoIP packet in the previous DTIM period, respectively. We assume that the wireless bandwidth is sufficiently large such that the last VoIP packet in the previous DTIM period is transmitted without additional delay due to multicast. Then, we assume that the last VoIP packet in the previous DTIM is played at $t_{last} + T_b$.

Then, for the VoIP packets delayed due to the buffered multicast, the due playback time, $t_{play}^{(i)}$, and the reception time, $t_{rx}^{(i)}$, of the ith delayed VoIP packet in the current DTIM period, are expressed as follows:

$$t_{play}^{(i)} = t_{last} + T_b + i \cdot T_u, \tag{2.3}$$

$$t_{rx}^{(i)} = t_{dtim} + \delta_m + \sum_{j=1}^{i} \left(\tau_u + \tau_{BO[VO]}^{(j)} + \tau_{sifs} + \tau_{ack} \right), \tag{2.4}$$

where τ_u, $\tau_{BO[VO]}^{(j)}$, τ_{sifs}, and τ_{ack} are VoIP packet transmission time, backoff time of the jth packet whose AC is voice, short interframe spacing (SIFS), and time duration for ACK transmission, respectively.

Then, we define the waiting time of the ith VoIP packet, $d^{(i)}$, as the time difference of the due playback time from the packet reception time, i.e., $d^{(i)} = t_{play}^{(i)} - t_{rx}^{(i)}$, and assume that the packet is lost if $d^{(i)} < 0$. By taking expectation, we obtain the average waiting time, $\bar{d}^{(i)}$, as:

$$\bar{d}^{(i)} = -T_u/2 + T_b - \bar{\delta}_m + i \left(T_u - \tau_u - \bar{\tau}_{BO[VO]} - \tau_{sifs} - \tau_{ack} \right), \tag{2.5}$$

$$\bar{\delta}_m = \bar{N}_m \cdot \left(\tau_m + \bar{\tau}_{BO[BE]} \right), \tag{2.6}$$

where the variable with the bar indicates the expectation of the random variable. Note that $(t_{dtim} - t_{last})$ follows the uniform distribution $U(0, T_u)$. Then, the expected number of the lost packets, $\bar{N}_l$, is calculated as follows:

$$\bar{N}_l = \left\lfloor \frac{\max\left(T_u/2 + \bar{\delta}_m - T_b, 0\right)}{T_u - \tau_u - \bar{\tau}_{BO[VO]} - \tau_{sifs} - \tau_{ack}} \right\rfloor \tag{2.7}$$

The expected number of the VoIP and video multicast packets during a DTIM period, $\bar{N}_u$ and $\bar{N}_m$, respectively, are expressed as:

$$\bar{N}_u = D/T_u = D \cdot B_u/L_u, \tag{2.8}$$

$$\bar{N}_m = D/T_m = D \cdot B_m/L_m, \tag{2.9}$$

where D is the length of a DTIM period, and B_u and L_u are source rate and payload length of VoIP, respectively, and B_m and L_m are source rate and payload length of video multicast, respectively. Eventually, the expected VoIP packet loss rate, p, is calculated by $p = \bar{N}_l/\bar{N}_u$.

Fig. 2.5 presents the analysis results. We assume an IEEE 802.11n WLAN network that consists of an AP, a VoIP STA in AM, and a multicast STA in PSM. PHY rates are assumed to be fixed to 6, 24, and 65 Mb/s for multicast data, ACK, and VoIP data packets, respectively. Note that multicast packets are typically sent at the most robust legacy PHY rate, i.e., 6 Mb/s in 5 GHz band and 1 Mb/s in 2.4 GHz band. It is assumed that the multicast packets are encapsulated with the MPEG-2 TS format. We also assume that the VoIP codec is G.711 with packetization interval of 20 ms, and the de-jitter buffer size is 60 ms, and both VoIP and multicast packets are transferred through real-time transport protocol, user datagram protocol, and Internet protocol (RTP/UDP/IP). We calculate the PLR for different video source rates and DTIM periods. Furthermore, we estimate R-score according to Eq. 2.1.

Fig. 2.5(a) presents the PLR results. We observe that the PLR decreases as the DTIM period increases and the video source rate increases. The longer the DTIM period and the larger video source rate, the more multicast packets are buffered so that the paused time of the VoIP packets increases. Such a long pause makes the packets to be received after the due playback time, thus incurring significant packet losses at the de-jitter buffer. In Fig. 2.5(b), we observe that the R-score drops to under 80 due to high PLR when DTIM period and video source rate are large. Since it is a common case that DTIM period is set to two or larger and video source rate is larger than 1 Mb/s, the coexistence problem can severely degrade the VoIP quality.

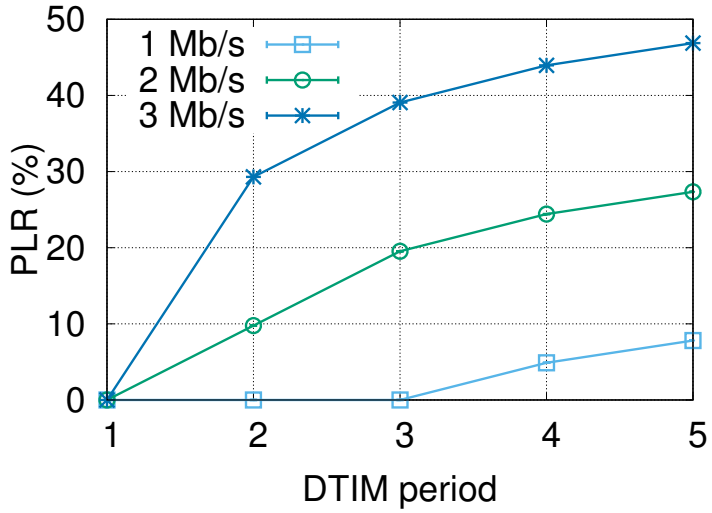

(a)

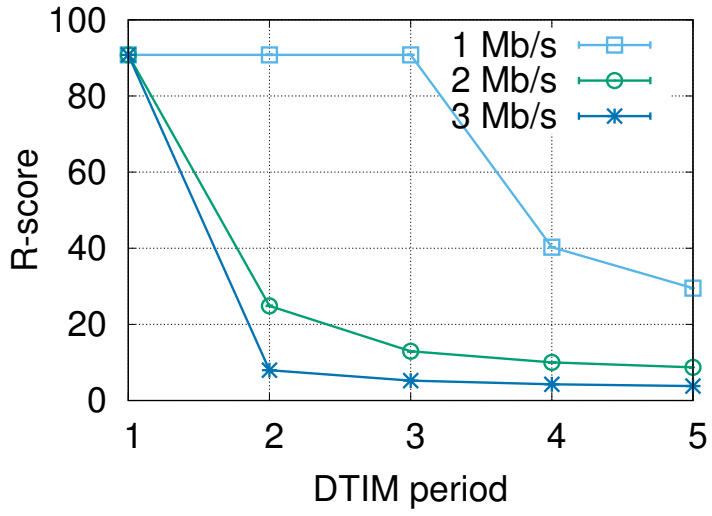

(b)

Figure 2.5: Analysis results: (a) PLR, (b) R-score.

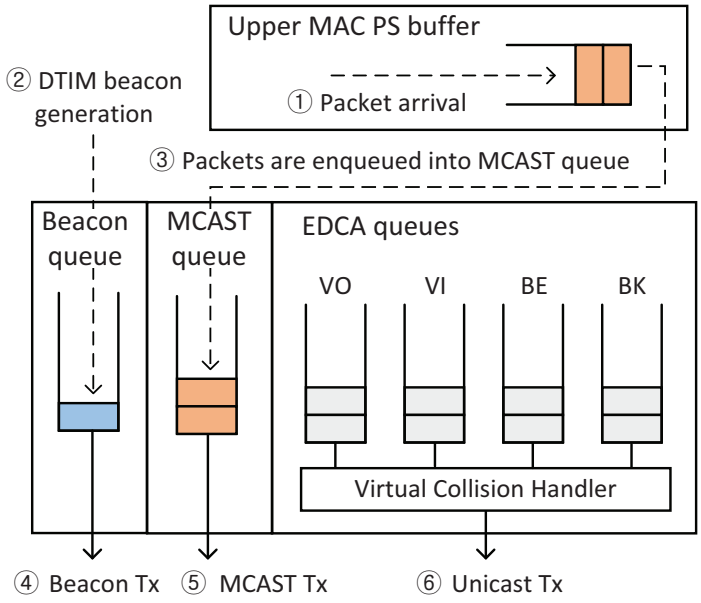

(a)

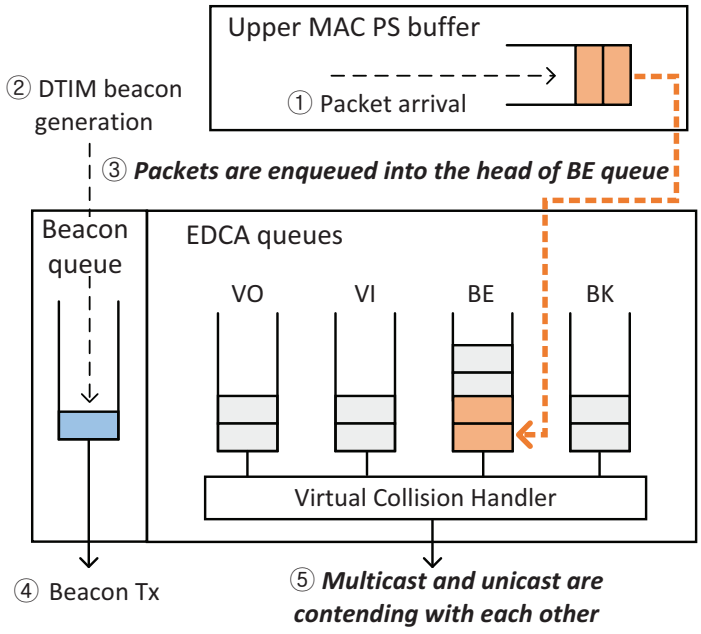

(b)

Figure 2.6: Comparison between 802.11 standard and proposed scheme: (a) 802.11 standard, (b) proposed scheme.

2.4.4 Proposed Scheme

We now propose a new power save delivery scheme to resolve the aforementioned coexistence problem. In contrast to the IEEE 802.11 standard which sets the strictly higher priority to the buffered multicast than other unicast packets irrespective of the AC, we propose that the strict priority of the multicast packets be applied only within the same AC. Specifically, in the proposed scheme, the buffered multicast packets have strictly higher priority than the other packets of the same AC, but contend with the packets of the other ACs according to the enhanced distributed channel access (EDCA) policy [35]. With the EDCA policy, packets from the four different ACs, i.e., in the descending order of priority, voice (VO), video (VI), best effort (BE), and background (BK), contend with each other. By setting different channel access parameters to the four ACs, packets of higher priority AC have higher chance of being transmitted earlier than those of lower priority ACs. According to the standard, multicast packets are regarded as best effort packets, and hence, we propose that all the multicast packets are transmitted before transmitting any best effort unicast packets, while allowing the packets of other ACs (VO, VI, and BK) to contend with multicast packets.

Fig. 2.6 shows the operation flows of the conventional 802.11 scheme and the proposed scheme. We present the conventional operation flow based on the implementation in *ath9k* device driver.[5] There are an upper MAC power save (PS) buffer and six lower MAC hardware queues, namely, a beacon queue, a multicast (MCAST) queue, and four EDCA queues. When packets arrive at the AP, they are buffered into an upper MAC PS buffer. A few milliseconds before a DTIM, the DTIM beacon is generated and enqueued into the beacon queue. After that, in the case of the conventional scheme, the multicast packets are enqueued into the MCAST queue, and after the DTIM beacon is transmitted, the multicast packets are transmitted, and then, other unicast packets are

[5] Although the detailed implementation can be different from the device drivers, the overall flows basically remain the same.

transmitted from the EDCA queues. In the proposed scheme, the buffered multicast packets are enqueued into the head of BE queue instead of the MCAST queue. Then, after the DTIM beacon transmission, the multicast and unicast packets contend with each other. With the proposed scheme, the VoIP packets can be transmitted along with the multicast packets.

Our proposed scheme might degrade the performance of the management multicast traffic in two perspectives: delay and energy consumption of the receivers. However, the increase of delay is expected to be marginal, since VoIP traffic consumes low bandwidth. Moreover, many management multicast packets are not time-critical in that the required delay is in the order of several seconds, and it is quite common that the received management multicast packets are not actually used in applications [36]. Regarding the energy consumption, the amount of energy required to receive a few additional packets is relatively small compared to the energy consumed during the tail time, which is the time to wait before returning to PSM [37]. The impact on the video multicast traffic will be investigated in Section 2.4.5.

We propose to modify the operation of AP because application-based solutions, e.g., modifying video players to prevent WiFi network interface card (NIC) from going to the PSM during video multicast, cannot solve the problem. As stated above, the coexistence issue occurs even when there is only one PSM STA in the network, and the application-based solutions cannot control the power saving mode of other devices not subscribing to the video multicast. Accordingly, the scheme in [5] cannot solve the problem.

2.4.5 Performance Evaluation

Measurement Setup

We implement our proposed scheme with off-the-shelf WLAN chipset by modifying the latest *ath9k* device driver, backport 4.2.6-1. We modify the flow of the packet as in Fig. 2.6(b), and also fix the AP-side malfunctions reported in [38].

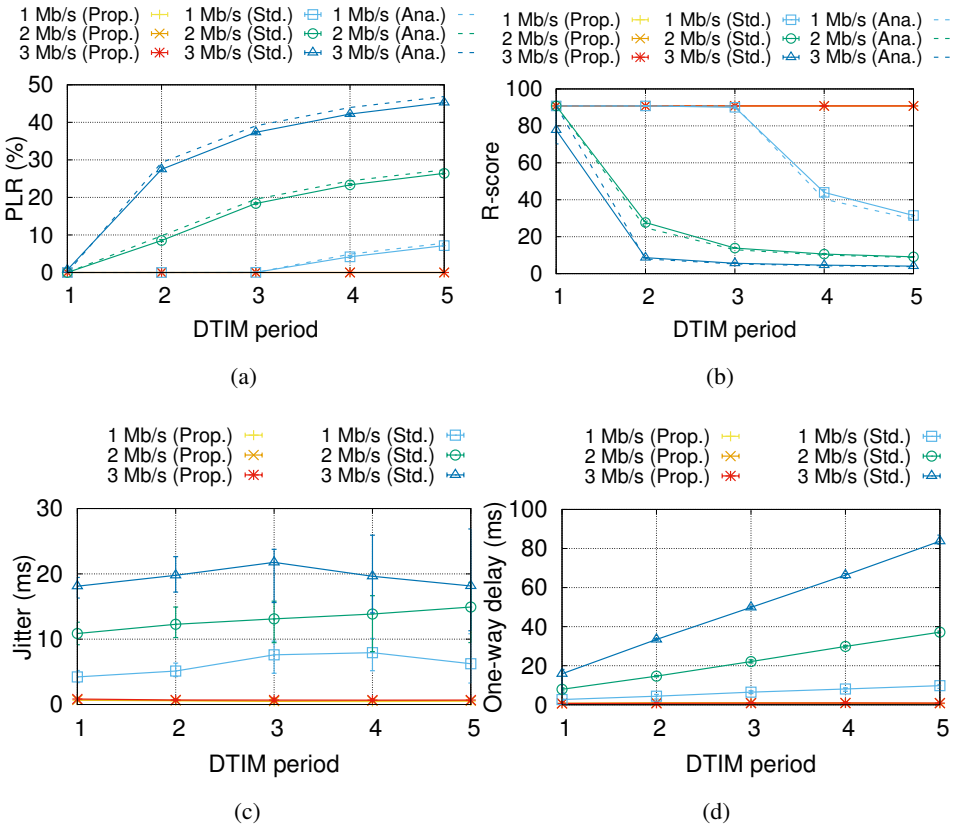

Figure 2.7: VoIP downlink performance: (a) PLR, (b) R-score, (c) jitter, and (d) one-way delay.

We conduct experiments to evaluate the proposed scheme. An AP and two STAs, i.e., a VoIP STA in AM and a video multicast STA in PSM, constitute an IEEE 802.11n WLAN using a channel in 5 GHz band, where all devices are Samsung Ativ Pro (XQ700T1C-F53) equipped with Qualcomm Atheros AR9380 chipsets. Ubuntu 14.04 is installed in the laptops, and the AP is configured with HostApd 2.4 [39]. We place the AP and the STAs close to each other to minimize packet losses due to the channel error. The PHY rate for multicast is set to 6 Mb/s, and the default PHY rate selection algorithm is used for unicast.

We generate video multicast and both uplink and downlink VoIP traffic with Ixia IxChariot 7.30 [40]. The video packets are encapsulated with MPEG-2 TS, and we

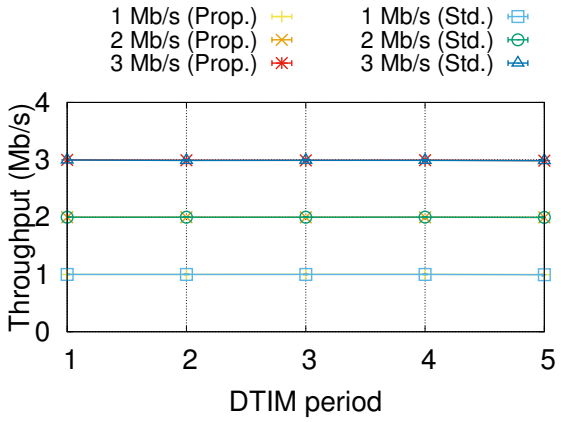

(a)

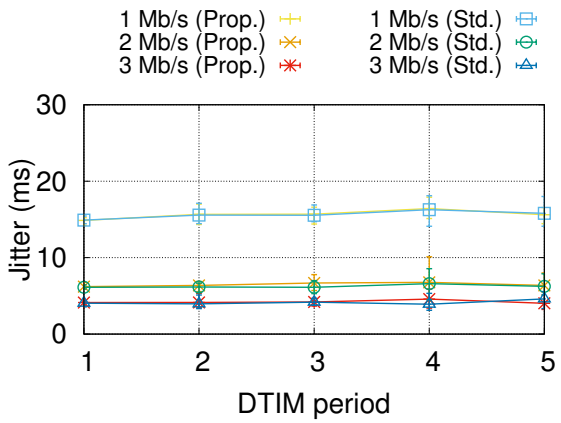

(b)

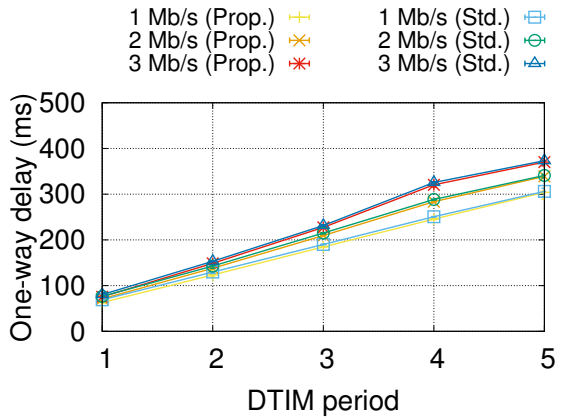

(c)

Figure 2.8: Video multicast performance: (a) throughput, (b) jitter, and (c) one-way delay.

employ G.711 codec with packetization interval of 20 ms for VoIP. Both video and voice packets are transmitted through RTP/UDP/IP.

The following performance metrics are measured: (i) *R-score*, (ii) *PLR*, (iii) *Jitter*, and (iv) *One-way delay*. We evaluate the performance for various video source rates (1, 2, and 3 Mb/s) and DTIM periods (1 to 5). The measurement of 60 seconds is iterated 10 times.

Measurement Results

Fig. 2.7 presents the performance results of the VoIP downlink for various DTIM periods and multicast source rates. For both PLR and R-score results, we also present the analysis results with the dotted lines. The error bars represent the minimum and maximum values. As shown in Fig 2.7(a), when the conventional standard delivery scheme (*Std.*) is employed, the PLR increases and R-score decreases as the DTIM period and video source rate increases as addressed in Section 2.4. We also observe that the analysis results are in good agreement with the measurement results. The reason why the measurement results show slightly lower PLR than the analysis results is that IxChariot occasionally generates VoIP packets later than the packetization interval. Whereas, in the case when DTIM period is 1 and video source rate is 3 Mb/s, a few packets are lost at the jitter buffer because of the long backoff counters, probing packets from other devices, and other overheads, and hence, the measured R-score is lower than the analysis result.

In contrast, the proposed scheme (*Prop.*) achieves R-scores higher than 80 for all the different settings in consideration, since the proposed scheme allows the VoIP downlink traffic to be transmitted with video multicast.

Figs. 2.7(c) and 2.7(d) present the jitter and average one-way delay values before entering the de-jitter buffer, respectively. The jitter is calculated by a weighted moving average of the delay variation according to [33]. We observe that the standard delivery scheme incurs large jitters proportional to the video source rates, while the

proposed scheme achieves much lower jitters. A large delay variation is observed for the first packet after a DTIM beacon, but the other deferred VoIP packets have small delay variations, and hence, the jitter converges to a small value. As the DTIM period increases, both initial delay variation and the number of the deferred VoIP packets increase. Accordingly, the impact of the DTIM period is marginal. For the one-way delay performance, we observe that the standard delivery scheme incurs larger one-way delays as expected, while the proposed scheme achieves much lower delay values.

Although we skip the VoIP uplink results due to the space limitation, we observe that the PLR, jitter, and one-way delay are close to zero for both schemes, regardless of the DTIM periods and video source rates. It is because the VoIP uplink traffic independently contends with the video multicast.

Fig. 2.8 presents the performance results of video multicast. In Fig. 2.8(a), we observe that the throughput values of the proposed scheme and the standard scheme are the same. Since channel quality is good, PLR is almost zero, thus yielding the throughput same as the source rate. In Figs. 2.8(b) and 2.8(c), we observe no noticeable difference between the proposed scheme and the standard scheme in terms of both jitter and one-way delay. Note that the jitter decreases as the video source rate increases, since the jitter converges to a lower value when a larger number of packets are buffered during a DTIM period. As a consequence, our measurement results verify that the proposed scheme improves the VoIP performance, without sacrificing the video multicast performance.

2.5 Summary

To make video multicast service practically attractive, delivering video multicast frames reliably to power-saving receivers is a very important problem. In this chapter, we first have identified the standard incompliance issues of commercial WLAN devices, which makes video multicast delivery to power-saving receivers very unacceptable. Also, we

identified the problem with analysis results. In order to resolve the problem, we have proposed an intra-AC strict priority-based power save delivery scheme and demonstrated that the proposed scheme resolves the coexistence problem effectively. With the proposed scheme, video multicast and VoIP can be enjoyed harmoniously in the same WLAN. As future work, we plan to investigate the impact of video multicast on more diverse types of traffic.

Chapter 3

InFRA: Interference-Aware PHY/FEC Rate Adaptation for Video Multicast over WLAN

3.1 Introduction

With the prevalence of mobile devices such as smartphones and tablets as well as the increase of capacity, the traffic volume of multimedia applications over the IEEE 802.11 wireless local area network (WLAN) has grown explosively during the last decade [41]. As one of the promising solutions for the explosion of multimedia traffic, multicast has attracted the interest from both the research community and industry practitioners, especially when sharing a common venue-specific video to multiple receivers, e.g., live video seminars and lectures in companies and live broadcast in sports stadiums and concert halls. Multicast services, however, have not been widely deployed as multicast over WLAN has inherent low reliability due to the absence of retransmission.[1]

Employing packet-level forward erasure correction (FEC) on multicast is a well-known reliability enhancement method. Each video frame is packetized, and a batch of the packets generate additional parity packets via FEC encoding, thus allowing each

[1] IEEE 802.11aa [2] defines new retransmission protocols for multicast to improve reliability, yet they are not widely-adopted in off-the-shelf chipsets.

receiver to recover lost packets with the parity packets. The FEC rate, i.e., the ratio of the number of original packets (batch size, K) over the total number of original and parity packets (generation size, N), is a key design parameter.

Another challenge of video multicast is low efficiency as the physical (PHY) layer data rate for multicast is typically set to the lowest rate to serve even the user with the worst channel condition. Although multicast PHY rate adaptation allows access point (AP) to use a higher PHY rate depending on the situation, adapting only PHY rate is unreliable due to the lack of the loss recovery mechanism [42]. We believe that applying FEC with multicast PHY rate adaptation can realize reliable and efficient multicast service, with appropriate selection of PHY and FEC rates.

Although lowering either the PHY or FEC rate can reduce the packet losses, the impact could be different depending on the cause of packet losses. Decreasing the PHY rate lowers the required signal-to-interference plus noise ratio (SINR), thus allowing packets to be transmitted successfully even when the channel quality is poor. However, if a packet loss is caused by interference (e.g., collision), decreasing the PHY rate is not helpful [43]. On the other hand, decreasing the FEC rate, i.e., increasing N, enhances reliability, when interference is the dominant factor of packet losses, by increasing the opportunities of accessing the channel without interference. Lowering the FEC rate can be less effective than lowering the PHY rate when many packets are lost due to poor channel quality [6, 14]. Therefore, diagnosing the cause of packet losses enables us to select proper PHY/FEC rates.

We propose InFRA, an interference-aware PHY/FEC rate adaptation framework for the multi-rate FEC-applied wireless multicast system. In InFRA, each station (STA) periodically requests desired PHY/FEC rates, and the AP chooses the best PHY/FEC rates based on the requests from multiple STAs. InFRA diagnoses the cause of packet losses using received signal strength indicator (RSSI) and cyclic redundancy check (CRC) error notifications, which are both available in the standard. If a packet is lost, we infer it as due to the poor channel quality when an average RSSI of the associated batch is

lower than a PHY rate-dependent threshold. Otherwise, we infer it as due to interference. We further classify the losses from interference depending on whether the CRC error notification exists.

Based on that, InFRA determines appropriate PHY/FEC rates to minimize the airtime consumption while meeting various performance requirements, e.g., the fraction of nodes satisfying the target application-layer packet loss rate (APLR).[2] When packet losses occur due to poor channel quality, InFRA decreases PHY rate while when packet losses happen due to interference, InFRA determines whether to decrease PHY rate or FEC rate based on the interfering signal strength and the number of packet losses.

Our key contributions are summarized as follows:

- We investigate the impact of interference on multi-rate FEC-applied multicast, and empirically verify the importance of interference-aware PHY/FEC rate selection.
- We propose a standard-compliant loss differentiation for multicast based on RSSI and CRC error notifications.
- We propose an interference-aware PHY/FEC rate adaptation framework, InFRA, which selects the optimal PHY/FEC rates depending on the cause of packet losses.
- We propose a feedback protocol to support large scale video multicast, which requires minimal overhead while enabling fast adaptation.
- We implement InFRA with an open-source WLAN device driver, and our measurement results with off-the-shelf devices demonstrate that InFRA improves the

[2]We distinguish application-layer PLR, i.e., the PLR after FEC decoding, from the MAC-layer PLR (MPLR), i.e., the PLR before FEC decoding. For brevity, the packet loss and PLR indicate the MAC-layer packet loss and MPLR, respectively, unless noted otherwise.

performance significantly, especially when the interference is the major source of the packet losses.

The remainder of the chapter is organized as follows: we discuss the related work in Section 3.2, and address the impact of interference on multi-rate FEC-applied multicast in Sections 3.3. We provide the detailed design of InFRA and evaluate the performance in Sections 3.4 and 3.5, respectively. Finally, we conclude the chapter in Section 3.6.

3.2 Related Work

3.2.1 Reliable Multicast Protocol

Pseudo-broadcast

Pseudo-broadcast converts multicast frames into unicast frames to a specific receiver, while other receivers overhear the frames in the promiscuous mode. Pseudo-broadcast method takes the advantages of the unicast, such as retransmission and binary exponential backoff.

Medusa [44] determines value of each packet depending on the type of corresponding video frame, and decides the packet scheduling and the PHY rate of each packet. As a transmission rule, it adopts the pseudo-broadcast in order to use an appropriate contention window by the binary exponential backoff.

Dircast [45] proposes a multi-AP video multicast system, where different receivers associated to different APs to watch the same video. It proposes an efficient user association algorithm, and unicast receiver (target receiver) selection scheme for pseudo-broadcast. Additionally for non-target receivers, it adds forward erasure correction (FEC) packets.

Since pseudo-broadcast has knowledge of reception status of only a single target receiver, it cannot guarantee QoS (quality of service) of other receivers.

Leader-based protocol

Leader-based protocol (LBP) selects a receiver as a leader, which sends acknowledgement frame whenever it receives multicast frames correctly, while other non-leader receivers send negative acknowledgement (NACK) frame whenever they fail to receive the multicast frames. Various multicast protocols adopt LBP [46, 47].

As LBP allows NACK from all non-leader receivers and retransmits until all receivers receive correctly, it has very low efficiency due to frequent retransmissions when there are many receivers.

Feedback-based protocol

Research communities have proposed various feedback-based multicast protocols by developing efficient feedback schemes. REMP [48] proposed a multicast protocol with IEEE 802.11n aggregate MPDU (A-MPDU), where the feedback is delivered via block ACK. After receiving A-MPDU consisting of multple multicast frames from AP, a leader node sends modified block ACK (same as the original block except for the addition of SNR field), while other nodes send NACK unless they receives all MPDUs correctly. If AP receives NAK or corrupted feedback, it re-selects the leader node based on SNR. Kim *et al.* [49] proposed orthogonal frequency division multiple access (OFDMA)-based multicast ACK (OMACK), where each receiver transmits 1 or -1 representing ACK or NACK on a uniquely assigned subcarrier. IEEE 802.11 standard also defines multicast feedback protocols. IEEE 802.11aa amendment [2] defines groupcast with retries (GCR) with block ACK, where a set of selected receivers sends feedback via block ACK after receiving block ACK request from AP.

Forward error correction (FEC)

FEC is another type of reliability enhancement. By generating parity packets, the sender enables receivers to recover lost packets using those parity packets [50]. FEC-based protocol guarantees the delay requirements, since the delay is bounded by the

FEC rate, unlike other ARQ-based protocols. For this reason, FEC-based protocol are widely used for multicast over WLAN [6, 7, 51–54]. Besides, (enhanced) multimedia broadcast multicast services ((e)MBMS) in cellular network also employs this approach [55].

Combination of different mechanisms

Some work employs a combination of different mechanisms, e.g., psuedo-broadcast with infrequent reports from other receivers [56], psuedo-broadcast with FEC [45], and feedback-based retransmission with FEC [57].

3.2.2 PHY/FEC rate adaptation for multicast service

PHY rate adaptation

MUDRA [42] and AMUSE [58] present a multicast rate adaptation algorithm which is designed to support hundreds of users in crowded venues. They define the feedback protocols for large scale multicast, and based on them, heuristic multicast rate adaptation algorithms are proposed.

The authors of [59] define a QoE model considering buffering ratio (ratio of time amount for rebuffering event over total playback time) and average bitrate, and propose a link adaptation scheme that determines MCS (modulation and coding scheme) and retry limit for GCR-block ACK.

CDRA [60] makes criteria to detect collision based on RSSI and packet loss ratio (PLR). AP detects collision periodically, and adjusts PHY rate only when collision is not detected.

FEC rate adaptation

Nafaa *et al.* [51] proposes an adaptive FEC mechanism considering packet loss pattern. Using mean burst loss length, i.e., the number of consecutive packet losses, and mean

inter-loss distance, i.e., the number of packets between packet loss events, the number of original packets per block (k) and the number of encoded packets (n) are determined.

Lee *et al.* [53] optimize k, n, and packet length with consideration of packet loss probability, bandwidth, and deadline of video frame for real-time video.

PHY/FEC Rate Adaptation for Multicast

Alay *et al.* [6] proposed to determine the optimal PHY/FEC rates that maximize the video bitrate. Based on the PLR fed back from the the receiver with the lowest PLR, AP determines whether to increase/decrease/keep its PHY rate. When the AP increases or decreases the PHY rate, it chooses the FEC rate as a predetermined value. If the AP keeps the current PHY rate, it chooses the FEC rate based on the current PLR value. With PLR estimation and an off-line PLR versus the optimal FEC rate table, X-Wing [7] determines the PHY rate achieving the maximum estimated throughput of the receiver with the lowest APLR. X-Wing assumes that PLR decreases by 5% as it decreases PHY rate by one step. Bulut *et al.* [8] proposed optimal PHY/FEC rate selection with IEEE 802.11n MIMO mode selection. According to the current 802.11 standard, however, multicast packets should be sent via legacy PHY rates, i.e., 802.11a PHY rates, and current off-the-shelf devices also utilize the legacy PHY rates for multicast.

None of the above approaches addresses the impact of interference on the multi-rate FEC-applied multicast, and hence, their PHY/FEC rate adaptation does not consider interference.

3.2.3 Wireless Video Transmission

Softcast [9] proposed a joint channel and source coding for scalable video streaming. The key idea of SoftCast is to enable the linear relationship between the pixel values and the transmitted signal by exploiting analog video coding and real-valued modulation. Parcast [10] enhanced Softcast with a design well-suited for MIMO-OFDM

WLAN. These schemes require no feedback on wireless channel status, and the received video quality is automatically adjusted depending on the channel quality of each receiver. However, they require heavy modification to video codec and PHY layer. Futhermore, channel quality agnostic video transmission is vulnerable to interference, as high signal strength due to interference can be misinterpreted as a high pixel value.

3.2.4 Wireless Loss Differentiation

There are several studies on the differentiation of the cause of packet losses. CARA [43] and RRAA [61] differentiate the channel error and the collision by exploiting the request-to-send/clear-to-send (RTS/CTS) handshake. BLMon [62] and MiRA [63] diagnose the cause of losses by analyzing the aggregate MAC protocol data unit (A-MPDU) and block ACKs. However, such schemes are limited to the unicast service, since RTS/CTS, A-MPDU, and block ACK are not applicable to multicast. COLLIE [64] determines the cause of packet losses by analyzing symbol-level metrics, and REPE [65] detects the collision by sampling RSSI with a high frequency during the packet reception. However, both of them require heavy modification of the PHY layer. CDRA [60] detects collision based on RSSI and PLR, which can be applied to multicast. AP judges the existence of the interference with two fixed RSSI thresholds and a single PLR threshold. However, the criteria is too naive to work properly in a real environment, as the impact of interference is tightly coupled with the PHY rate.

3.3 Impact of Interference on Multi-rate FEC-applied Multicast

Interference from contending nodes or hidden nodes is a major source of packet losses in WLAN. In fact, various existing studies have shown that WLAN performance is highly affected by interference. A recent study [42] shows that interference causes burst packet losses intermittently in a large scale multicast network. Therefore, it is

important to investigate the impact of the interference on PHY/FEC rate decision.

3.3.1 Measurement Setup

In order to investigate the impact of the interference on PHY/FEC rate decision, we conduct a simple experiment. Our measurement setup consists of four nodes: one AP, one STA, and two interferers (I1 and I2), equipped with Qualcomm Atheros AR9380 chipsets. The AP and the interferers are configured by Hostapd-2.5 [39]. In an auditorium with the layout shown in Fig. 3.1(a), we measure average APLR by varying the location of the STA and the interference type. The AP transmits FEC-encoded packets via multicast, where the employed FEC code is random linear network code (RLNC) [66] and the batch size (K) is fixed to 10. The determination of K will be discussed in Section 3.4.6. APLR is measured for three different combinations of (PHY rate, N): (i) initial setup (36 Mb/s, 12), (ii) PHY rate decrease (24 Mb/s, 12), and (iii) FEC rate decrease (36 Mb/s, 18). The two combinations, i.e., (24 Mb/s, 12) and (36 Mb/s, 18), incur similar airtime usages. The interferers broadcast the packets back-to-back using PHY rate of 6 Mb/s.

3.3.2 Measurement Results

Fig. 3.1(b) shows the average APLR for different scenarios. When the STA is located at Loc1 and all the interferers are disabled, all the three combinations work well. As the STA moves farther to Loc2, the initial setup, (36 Mb/s, 12), suffers from significant packet losses. Comparing the two possible options, i.e., decreasing PHY rate or FEC rate, we observe that decreasing PHY rate is more effective. On the other hand, when interference I1 is activated and the STA is at Loc1, decreasing PHY rate does not improve reliability. Since the packet losses are due to the nearby interferer, SINR becomes much lower than the required SINR for the decreased PHY rate, and hence, decreasing PHY rate increases the airtime only. On the other hand, decreasing the FEC rate increases the opportunities of accessing the channel without collision, thus

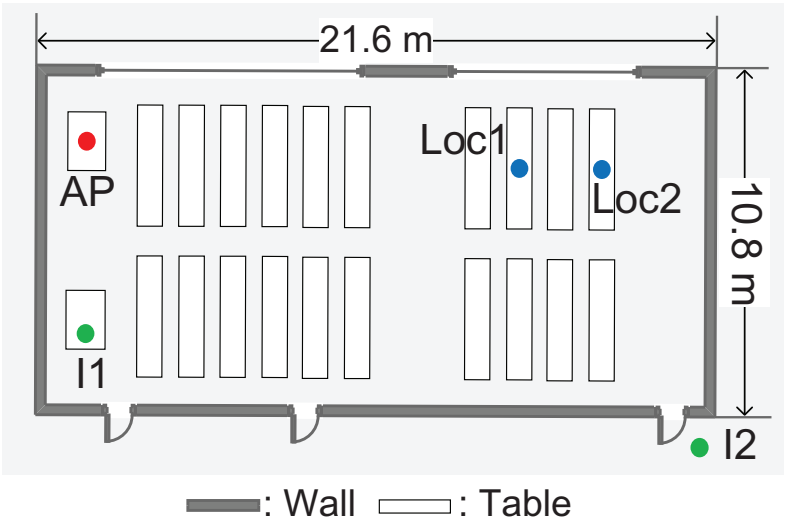

(a) Measurement topology.

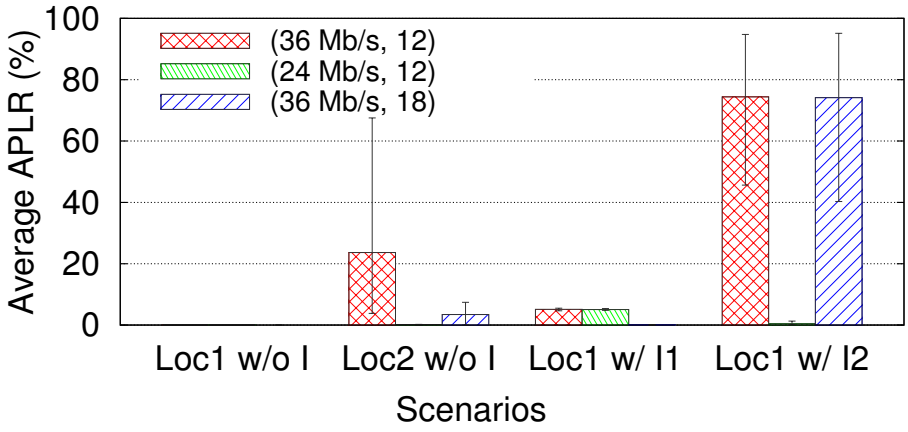

(b) Average packet loss rate.

Figure 3.1: Preliminary measurement results.

reducing the packet losses.

For the last scenario, where the STA is at Loc1 and interference I2 is activated, the interferer and the AP are hidden from each other, and hence, APLR increases significantly with the initial setup. In this case, decreasing PHY rate reduces the packet losses significantly as the interfering signal strength is so low that decreasing PHY rate enables the STA to successfully receive packets even with the interference (i.e., the capture effect [67]). Whereas, decreasing FEC rate fails to decrease the APLR, since the burst losses due to hidden interference exceed the loss recovery capability of the FEC. From this measurement study, we verify that the effects of PHY and FEC rates are different from each other, and interference should be considered when determining PHY/FEC rates.

3.4 InFRA: Interference-aware PHY/FEC Rate Adaptation Framework

3.4.1 Network Model and Objective

We consider an infrastructure mode WLAN that consists of an AP and multiple associated STAs. We assume low mobility of the STAs, e.g., the majority of users are seated and watching a common video. We consider real-time transport protocol/user datagram protocol (RTP/UDP)-based video streaming and the video packets are packetized as MPEG-2 TS (transport stream) format, which is a typical protocol for video multicast.

Our objective is to develop an interference-aware PHY/FEC rate adaptation framework for multi-rate FEC-applied multicast to minimize the airtime consumption while satisfying the following requirements.

- **Service level agreements (SLAs):** Given target APLR, S ($= 1\%$ [68]), and a node satisfaction ratio (NSR) threshold X (e.g., $X = 95\%$), InFRA aims at guaranteeing that at least X of the nodes experience APLR below S. The

number of allowed unsatisfied nodes, U, is then determined by $U = \lfloor (1-X)Y \rfloor$, where Y is the number of total nodes. Since the user satisfaction is not linearly proportional to the APLR, e.g., typically the APLR below 1% is considered unacceptable for video streaming, the objective based on the target APLR is more practical.

- **Scalability:** Protocol overhead should be minimized to support a large number of receivers.

- **Fast recovery:** When SLA is not satisfied, immediate re-selection of PHY/FEC rates should be conducted.

3.4.2 Overall Architecture

We present an overview of InFRA architecture. Fig. 3.2 describes the overall architecture of InFRA, where the data flow and the internal information exchange are presented. We implement InFRA in the MAC-layer of both the AP and the STA with the modification of the off-the-shelf device driver. It is possible to implement InFRA of STA-side in a user space by using an application programming interface (API) to obtain the RSSI and CRC error notifications, as in Wireshark [69].

We adopt a request-based approach where each STA determines and reports the locally optimal PHY/FEC rates and AP chooses the network-wide PHY/FEC rates. This contrasts a centralized approach where the AP determines the optimal PHY/FEC rates based on the channel quality reports from STAs. Since interference relationship (interfering nodes and the signal strength) is heterogeneous for different receivers, we distribute the computation load to multiple receivers to support a large number of receivers.

In order to meet the APLR requirement, our design tries to find the PHY/FEC rates ensuring that the decoding failure ratio (DFR) is less than or equal to S (=1%).[3] Accordingly, each STA needs to receive at least 100 batches to measure the DFR of

[3]The rationale behind this is that 1) our framework should be transparent to the FEC codes including

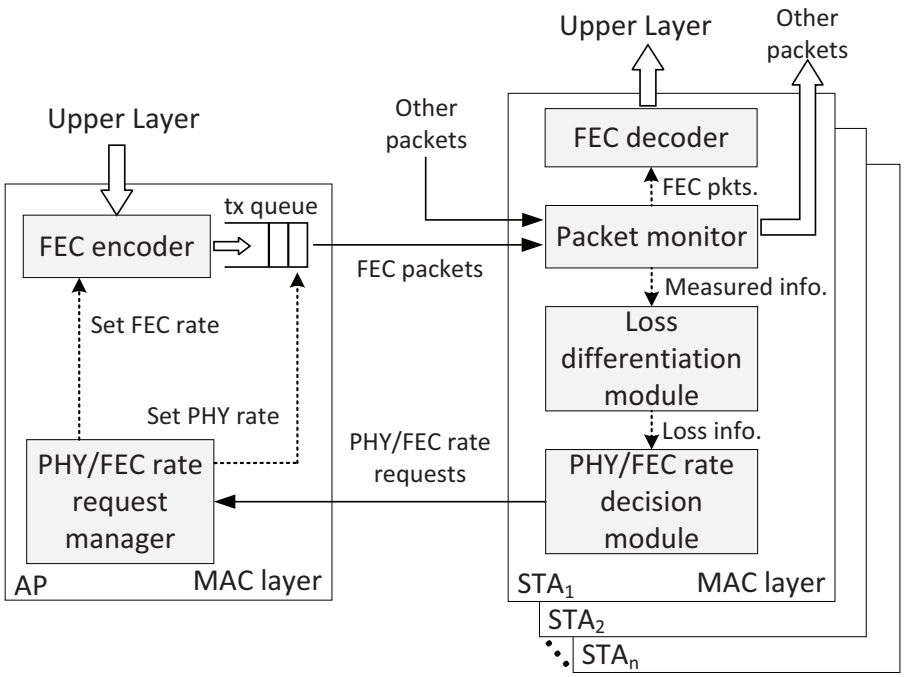

Figure 3.2: Overview of InFRA architecture.

1%, so it basically requests the PHY/FEC rates every 100 batches. Although such a long request period is less responsive, it is more stable since higher PHY/FEC rates are tried based on long-term statistics, which avoids frequent trials that might incur the packet losses. Moreover, it requires lower feedback overhead, which is beneficial for multicast. To support fast recovery, we make each STA send a request immediately when it fails to meet the target DFR, i.e., it fails to decode two batches out of the latest 100 batches.

AP-side Modules

The AP-side components are FEC encoder and PHY/FEC rate request manager. The FEC encoder generates N encoded packets per K packets. We control the FEC rate

non-systematic codes where the APLR is the same as the DFR, and 2) it is more conservative in the case of the systematic codes in that the APLR requirement is satisfied if the DFR requirement is satisfied.

by controlling N, while fixing K. The PHY/FEC rate request manager collects the requests of PHY/FEC rates from STAs and determines whether the SLA is satisfied. It also determines the PHY/FEC rates to achieve the network-wide objective in Section 3.4.1, and the determined parameters are input to the FEC encoder and the transmit packet queue.

STA-side Modules

The STA-side components are FEC decoder, packet monitor, loss differentiation module, and PHY/FEC rate decision module. The FEC decoder gathers FEC-encoded packets and decodes them if possible. The decoded K original packets in a batch are then delivered to the upper layers. The packet monitor inspects the packet flow, and observes the existence of interfering nodes, and also measures the input values for the loss differentiation module that diagnoses the cause of measured packet losses. Specifically, it infers the portion of losses due to channel error and interference, which are used for determining PHY/FEC rates to request. The PHY/FEC rate decision module determines the best PHY/FEC rates and requests the determined parameters.

3.4.3 FEC Scheme

For FEC, we employ RLNC [66], which is a type of fountain codes (also called rateless codes). RLNC is simple yet erasure-resilient, and is widely used in many applications such as video streaming, cloud storage, and opportunistic routing [70]. We employ RLNC, but our design is transparent to the type of FEC codec, i.e., other FEC schemes such as Raptor [71] and Luby Transform (LT) codes [72] can also be used.

RLNC encodes a packet by taking a linear combination of K original packets with random coefficients. In the same way, RLNC can generate an arbitrary number of encoded packets.[4] Upon receiving K linearly independent packets, each receiver

[4]We employ a systematic approach that transmits K original packets and $N - K$ encoded packets rather than transmitting only N encoded packets. In addition to low complexity, a systematic code reduces

decodes and restores the original packets via matrix inversion.

In our scheme, each RLNC packet has a header including a batch ID, the generation size, a sequence number in the batch, and K encoding coefficients, and hence, each receiver can identify the packet loss using the sequence number.

3.4.4 STA-side Operation

Packet Monitor

The packet monitor measures the information used for loss differentiation by examining the incoming packets. The measured values are average RSSI from AP ($\overline{\gamma}_A$), current PHY rate of the batch (R_{cur}), current generation size of the batch (N_{cur}), the number of packet losses in the batch (L), the number of CRC errors (C), and the maximum RSSI of weak interference (γ_w), where the definition of weak interference is presented in the next subsection. Since FEC-encoded packets in a batch have the same length and are transmitted at the same PHY rate, we can infer whether a CRC-error packet is an FEC-encoded packet by examining the LENGTH and RATE elements in the SIGNAL field.[5] γ_w is the maximum RSSI value from the interfering nodes satisfying $\overline{\gamma}_A - \gamma_w \geq \delta(R_{min})$, where $\delta(R_{min})$ is the RSSI threshold for the minimum PHY rate. Whenever a packet with a new batch ID arrives, the packet monitor inputs the measured values to the loss differentiation module.

Loss Differentiation Module

The purpose of the loss differentiation module is to diagnose the cause of multicast packet losses in a standard-compliant manner. Since ACK, RTS/CTS, and A-MPDU

APLR because it allows the received original packets to be salvaged when decoding fails.

[5] In order to provide the information for demodulation, the SIGNAL field in the PLCP (physical layer convergence procedure) header, transmitted at the minimum PHY rate, includes LENGTH and RATE elements indicating the length of the packet and the PHY rate used for the remaining part of the packet, respectively.

based schemes are not applicable to multicast, InFRA utilizes RSSI and CRC error notifications, which are both available at WLAN receivers.

Loss Differentiation Metrics: RSSI is a per-packet measure of the received signal strength (RSS), and is available at every WLAN device. In most device drivers including ath9k, RSSI is a measure of signal power above the noise floor. Therefore, RSSI is equivalent to the SNR in the absence of interference, and hence, is proportional to the packet delivery ratio (PDR). However, PDR drops while RSSI increases when there is interference. When a packet with a low RSSI is lost, we can infer that it is due to channel error. In contrast, when a packet with a high RSSI is lost, we can infer that it is due to interference. Accordingly, RSSI can be used as a metric to determine the cause of packet losses, i.e., channel error or interference.

We conduct experiments to investigate the RSSI characteristics of FEC-encoded multicast packets. We apply the FEC with $K = 10$ and $N = 20$, and the coded packets are transmitted at different PHY rates (6 Mb/s to 54 Mb/s). We move along a predetermined path at a walking speed (about 0.5 m/s) and measure the standard deviation of RSSI in a batch and RSSI deviation of CRC-error packets, i.e., RSSI of CRC-error packet minus the average RSSI of the associated batch.

Fig. 3.3(a) shows the distribution of standard deviation of RSSI values in a batch. We observe that above 90% of batches show the standard deviation of under 1 (dB), and thus the RSSI variation in a batch is quite small. Fig. 3.3(b) shows the distribution of RSSI deviation of CRC-error packets, and most RSSI deviations are observed from -1 to 1. RSSI variation is low because the transmission time of a batch is smaller than the coherence time.[6] Therefore, we utilize the average RSSI of a batch as a metric to distinguish between the channel error loss and the interference loss. Another reason for adopting the average RSSI, not the individual RSSI, is that RSSI cannot be obtained

[6]The coherence time with 0.5 m/s at 5.8 GHz is about 43.5 ms according to Clarke's model [73], and the maximum batch transmission time with 6 Mb/s is 41.3 ms. In fact, as we limit the maximum N to 13 for 6 Mb/s as addressed later, the actual maximum batch transmission time in InFRA is smaller than 27 ms.

for lost packets without CRC error notifications, e.g., due to preamble losses.

In Section 3.3, we verified that decreasing PHY rate can be effective depending on the interfering signal strength. To this end, we define two types of interference: weak and strong interferences. Weak interference is defined as interference whose RSSI is smaller than the RSSI of the target packet by at least $\delta(R_{min})$ so that decreasing the PHY rate enables successful packet reception due to the capture effect. We define strong interference as interference whose RSSI is higher than the RSSI of the target packet minus $\delta(R_{min})$ so that decreasing the PHY rate does not enable the packet reception. When a packet is lost due to weak interference, the SIGNAL field transmitted at the minimum PHY rate is correctly received, but the CRC check fails. Then, if we decrease the PHY rate to the minimum PHY rate, packet losses due to weak interference can be prevented. Accordingly, we infer that a loss due to weak interference generates the CRC error notification, while a loss due to strong interference does not.

Our approach: We classify a total of L losses into l_{ch}, l_s and l_w, which denote the number of losses due to channel error, strong interference, and weak interference, respectively. Our algorithm examines the average RSSI ($\overline{\gamma}_A$), and if the average RSSI is smaller than the RSSI threshold of the current PHY rate, $\delta\left(R_{cur}\right)$, all L losses are considered due to channel error.

The RSSI threshold is defined as the minimum RSSI required to ensure that PLR is lower than a target PLR, ρ (we choose $\rho = 0.1$ as in [74]), with a nominal packet length. Although a packet of a low RSSI might be lost due to interference, we regard it as the channel error since low RSSI implies the possibility of the channel error. In contrast, if the average RSSI is greater than or equal to the RSSI threshold, all L losses are inferred due to interference. As mentioned above, we determine that C and $(L - C)$ losses are considered due to weak interference and due to strong interference, respectively.

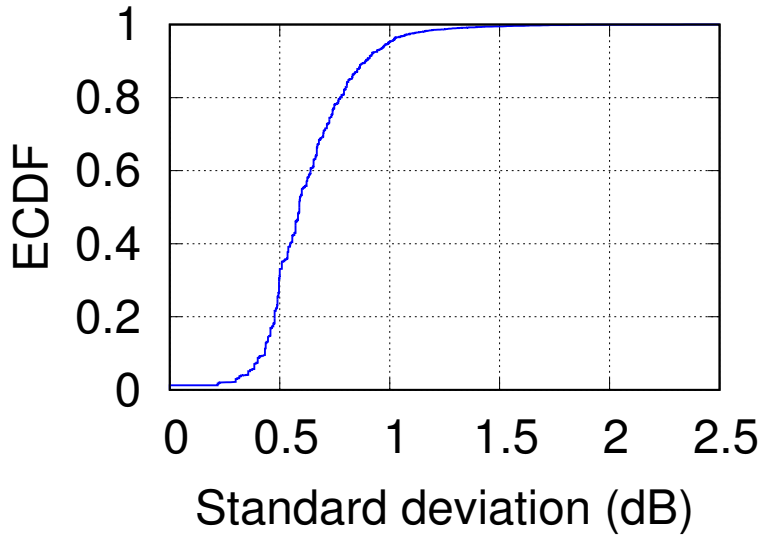

(a)

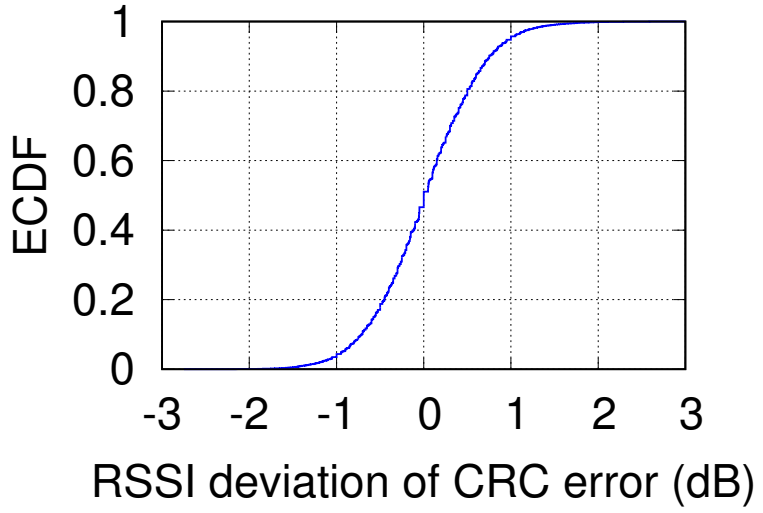

(b)

Figure 3.3: RSSI characteristics of the FEC-encoded multicast packets.

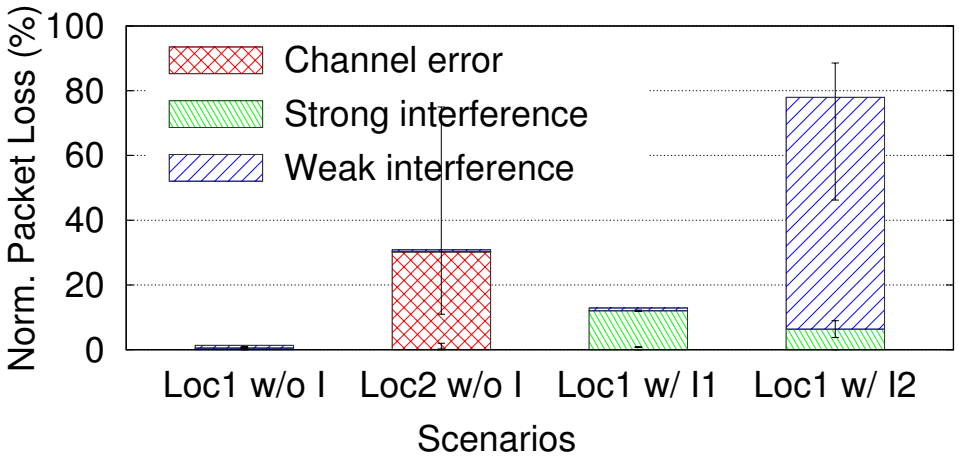

Figure 3.4: Loss differentiation results in the preliminary measurement.

The differentiation process are expressed in (3.1).

$$(l_{ch}, l_s, l_w) = \begin{cases} (L, 0, 0), & \text{if } \overline{\gamma}_A < \delta\left(R_{cur}\right), \\ (0, L - C, C), & \text{otherwise.} \end{cases} \tag{3.1}$$

Fig. 3.4 presents the loss differentiation results of the STA in the measurement in Section 3.3, with the initial setup, (36 Mb/s, 12). The number of losses are normalized by the number of total transmitted packets. When the STA is located at Loc2 without interference (Loc2 w/o I), our loss differentiation module regards the most losses as the channel error losses due to the low RSSI. When interference I1 is activated, which is closer to the AP (Loc1 w/ I1), the loss differentiation module then determines that the losses are due to the strong interference, since CRC error notifications are rarely observed. In the case of (Loc2 w/ I2), most losses incur the CRC error notifications, thus classified as the weak interference losses. Note that some packets are lost without CRC error notification when the preamble detection fails due to interference. Through this reult, we verify that the loss differentiation module diagnoses the cause of the packet losses appropriately.

PHY/FEC Rate Decision Module

We define *RN pair* as a pair of PHY rate R and generation size N, which is denoted by $Q = (R, N)$ or Q for brevity. Each STA calculates the batch-level optimal *RN pair*, Q^{bat} for every batch, and based on that, each STA determines the *RN pair* to request, Q^{req}.

As discussed above, we consider two aspects to determine R: (i) RSSI from the AP and (ii) the capture effect when there is weak interference. To this end, we define two types of *RN pair*: (i) *RN pair* whose R is determined by the RSSI from AP, called channel-oriented *RN pair*, $\hat{Q} = (R_{ch}, N_{ch})$, where R_{ch} and N_{ch} are called channel-oriented R and N, and (ii) *RN pair* whose R is determined by the condition to induce the capture effect, called capture-inducing *RN pair*, $\tilde{Q} = (R_{cap}, N_{cap})$, where R_{cap} and N_{cap} are called capture-inducing R and N.

Determination of batch-level optimal Q: For a batch, each STA calculates two batch-level *RN pairs*, i.e., $\hat{Q}^{bat}$ and $\tilde{Q}^{bat}$. Algorithm 1 provides the formal description of the process. For the channel loss case (lines 1−8), i.e., if $\overline{\gamma}_A < \delta(R_{cur})$, only $\hat{Q}^{bat}$ is returned, since there is no weak interference loss. If the target PLR (ρ) is not satisfied by R_{cur} (line 2), R_{ch} is determined by the GETRATE function that finds the maximum R whose RSSI threshold is smaller than the input RSSI. As a result, we set the PHY rate ensuring that PLR is smaller than ρ by channel error. The estimated number of channel error losses for the new PHY rate, l'_{ch}, is then conservatively assumed to be $\lceil \rho N_{cur} \rceil$. Otherwise, R_{ch} and l'_{ch} remain to be the current values. N_{ch} is determined as the minimum N satisfying the following inequality:

$$N \cdot \frac{N_{cur} - l'_{ch}}{N_{cur}} \geq K. \tag{3.2}$$

We add a constant ϵ ($\epsilon = 1$) to handle unexpected losses.

For the interference loss case (lines 9−24), i.e., if $\overline{\gamma}_A \geq \delta(R_{cur})$, we increase the PHY rate when the RSSI is high enough to support a higher PHY rate. For a conservative design, we increase R_{ch} only to the next higher PHY rate than R_{cur} in

Algorithm 1 Determination of batch-level *RN pairs*

Require: $\overline{\gamma}_A, l_{ch}, l_s, l_w, R_{cur}, N_{cur}, \gamma_w$

Ensure: $\hat{Q}^{bat}, \tilde{Q}^{bat}$

if $\overline{\gamma}_A < \delta(R_{cur})$ **then** ▷ Channel loss
  if $l_{ch}/N_{cur} > \rho$ **then**
    $R_{ch} \leftarrow \text{GETRATE}(\overline{\gamma}_A), l'_{ch} \leftarrow \lceil \rho N_{cur} \rceil$
  else
    $R_{ch} \leftarrow R_{cur}, l'_{ch} \leftarrow l_{ch}$
  end if
  $N_{ch} \leftarrow \left\lceil K \frac{N_{cur}}{N_{cur} - l'_{ch}} \right\rceil + \epsilon$
  $\hat{Q}^{bat} \leftarrow (R_{ch}, N_{ch}), \tilde{Q}^{bat} \leftarrow \varnothing$
else ▷ Interference loss
  if PRI condition is satisfied **then**
    $R_{ch} \leftarrow R^{+}_{cur}, l'_{ch} \leftarrow \lceil \rho N_{cur} \rceil$
  else
    $R_{ch} \leftarrow R_{cur}, l'_{ch} \leftarrow 0$
  end if
  if $l_w == 0$ **then** ▷ Strong interference only
    $N_{ch} \leftarrow \left\lceil K \frac{N_{cur}}{N_{cur} - l'_{ch} - l_s} \right\rceil + \epsilon$
    $\hat{Q}^{bat} \leftarrow (R_{ch}, N_{ch}), \tilde{Q}^{bat} \leftarrow \varnothing$
  else ▷ Weak interference
    $N_{ch} \leftarrow \left\lceil K \frac{N_{cur}}{N_{cur} - l'_{ch} - l_s - l_w} \right\rceil + \epsilon$
    $R_{cap} \leftarrow \text{GETRATE}(\overline{\gamma}_A - \gamma_w)$
    $N_{cap} \leftarrow \left\lceil K \frac{N_{cur}}{N_{cur} - l_s} \right\rceil + \epsilon$
    $\hat{Q}^{bat} \leftarrow (R_{ch}, N_{ch}), \tilde{Q}^{bat} \leftarrow (R_{cap}, N_{cap})$
  end if
end if

function GETRATE(γ)
  Find out rate R s. t. $\delta(R) \leq \gamma < \delta(R^{+})$
  return R
end function

the rate set, R^{+}_{cur}, as long as the conditions for PHY rate increase (PRI) are satisfied (line 10). In addition to the RSSI condition ($\overline{\gamma}_A \geq \delta(R^{+}_{cur})$), we adopt a history-based mechanism to avoid the failure due to impetuous PHY rate increase. When FEC decoding fails twice before receiving the latest 100 batches, InFRA records the failed PHY rate, R_{fail}, and limits the PHY rate under R_{fail} for a window (100 batches), which is doubled whenever it further fails to decode two batches before receiving 100 batches at R_{fail}.

If all losses are due to strong interference, N_{ch} are determined in a similar way to the channel loss case except for considering l_s (line 16), thus the algorithm returns $\hat{Q}^{bat}$ only. On the other hand, if some portion of the losses are due to weak interference, the algorithm returns another *RN pair*, $\tilde{Q}^{bat} = (R_{cap}, N_{cap})$, as well as $\hat{Q}^{bat}$. R_{cap} is determined by the RSSI difference between the maximum weak interference (γ_w) to induce the capture effect. Note that the increase of RSSI due to weak interference is marginal since the signal strength of the weak interference is much smaller than RSSI from the AP (smaller by at least 8 dB). Therefore, the RSSI difference is assumed to be the same as the signal-to-interference ratio (SIR). Although there is a report that SIR threshold is lower than the SNR threshold [75], we use the same threshold values for the channel error case (line 3) for the sake of simple and conservative operations.

We assume that weak interference losses will be removed with R_{cap}, as R_{cap} is determined by considering the maximum weak interference. Since R_{cap} is inherently lower than R_{ch}, the expected number of channel errors is assumed to be zero. We then determine N_{cap} by considering l_s only (line 21).

Update of R and N: We find $\hat{Q}^{req}$ and $\tilde{Q}^{req}$ satisfying at least 99 batches out of the latest 100 batches. For this purpose, in addition to keeping track of the most conservative parameters (minimum R and maximum N) from Q^{bat}'s, we also update the second minimum R and the second maximum N. We take the second minimum and maximum values into account to avoid over-provisioning due to the most conservative parameters, since the determination of Q^{bat} is based on conservative estimation of

channel error and adoption of ϵ.

The minimum and the second minimum R's (R_{ch}^{min}, R_{ch}^{2ndmin}, R_{cap}^{min}, and R_{cap}^{2ndmin}) and the maximum and the second maximum N's (N_{ch}^{max}, N_{ch}^{2ndmax}, N_{cap}^{max}, and N_{cap}^{2ndmax}) are updated for every batch. When more than one batch return the same maximum N, the second maximum N is set to the maximum value. The same rule is applied to R.

PHY/FEC rate request: Depending on the type of the request, i.e., a regular or an event-driven request, $\hat{Q}^{req}$ and $\tilde{Q}^{req}$ are determined in different ways. For $\hat{Q}^{req}$, in the case of the regular request, we compare the required airtime of the following two Q's: $(R_{ch}^{min}, N_{ch}^{2ndmax})$ and $(R_{ch}^{2ndmin}, N_{ch}^{max})$. Note that both Q's guarantee the DFR requirement that allows decoding failure of the maximum one batch out of the latest 100 batches, as decoding of all the batches are expected to be successful except for the single batch that could be satisfied by $(R_{ch}^{min}, N_{ch}^{max})$.

Among the two candidates, Q requiring less airtime is chosen. Similarly, we determine $\tilde{Q}^{req}$ requiring less airtime among $(R_{cap}^{min}, N_{cap}^{2ndmax})$ and $(R_{cap}^{2ndmin}, N_{cap}^{max})$. When a STA sends an event-driven request, the STA requests the most conservative parameters: $\hat{Q}^{req} = (R_{ch}^{min}, N_{ch}^{max})$ and $\tilde{Q}^{req} = (R_{cap}^{min}, N_{cap}^{max})$. The PHY/FEC rate request messages are sent via unicast. In order to alleviate the congestion and contention, each STA defers a random interval from 0 to T_r before the request.

3.4.5 AP-side Operation

Based on the PHY/FEC requests from STAs, AP finds the network-wide *RN pair*, $Q^{net} = (R^{net}, N^{net})$ satisfying at least X (=95%) of the receivers (at least $Y - U$ receivers). AP re-selects Q^{net} upon receiving event-driven requests from more than U receivers or after sending the latest 100 batches and waiting additional T_r. Q requiring the least airtime is selected among four candidates: $(R_{ch,Y-U}, N_{ch,1})$, $(R_{ch,Y}, N_{ch,U+1})$, $(R_{cap,Y-U}, N_{cap,1})$, and $(R_{cap,Y}, N_{cap,U+1})$, where the second subscription value means the descending order in each parameter, e.g., if $Y = 20$ and $U = 1$, $R_{ch,Y-U}$ means the 19th largest (2nd-minimum) value in R_{ch}'s and $N_{cap,U+1}$ means the 2nd maxi-

Table 3.1: Default RSSI threshold and maximum generation size.

R (Mb/s)	6	12	18	24	36	48	54
$\delta(R)$ (dB)	8	11	14	17	20	23	26
N_{max}	13	24	34	42	55	65	69

mum value in N_{cap}'s. For the same reason as in the previous subsection, all the four candidate Q's satisfy the NSR requirement.

We limit N^{net} to a maximum generation size, N_{max}, dependent on R^{net}, considering the delay and the bandwidth as detailed below.

3.4.6 Practical Issues

RSSI Threshold Calibration

It is known that the RSSI-PDR relationship differs depending on the devices [76]. To overcome this, we develop an on-line calibration of the RSSI thresholds on top of the default RSSI thresholds obtained from our off-line measurements (Table 3.1). Note that we skip the 9 Mb/s due to its inferior performance to 12 Mb/s as in the IEEE 802.11n standard [1]. Whenever receiving the measured results from the packet monitor, the calibration module records the number of received packets and lost packets according to the measured average RSSI. The measured RSSI values are indexed relatively to the current RSSI threshold for a given PHY rate. When the sample is gathered sufficiently, the calibration module updates the RSSI threshold based on the measurement. To remove the effect of interference, the data are recorded only when interference is not detected.

FEC Parameters (K and N_{max})

We determine K and N_{max} by considering the delay and the bandwidth, while existing schemes determine them arbitrarily, e.g., $K = 100$ and $N_{max} = 300$ in [7]. Such a

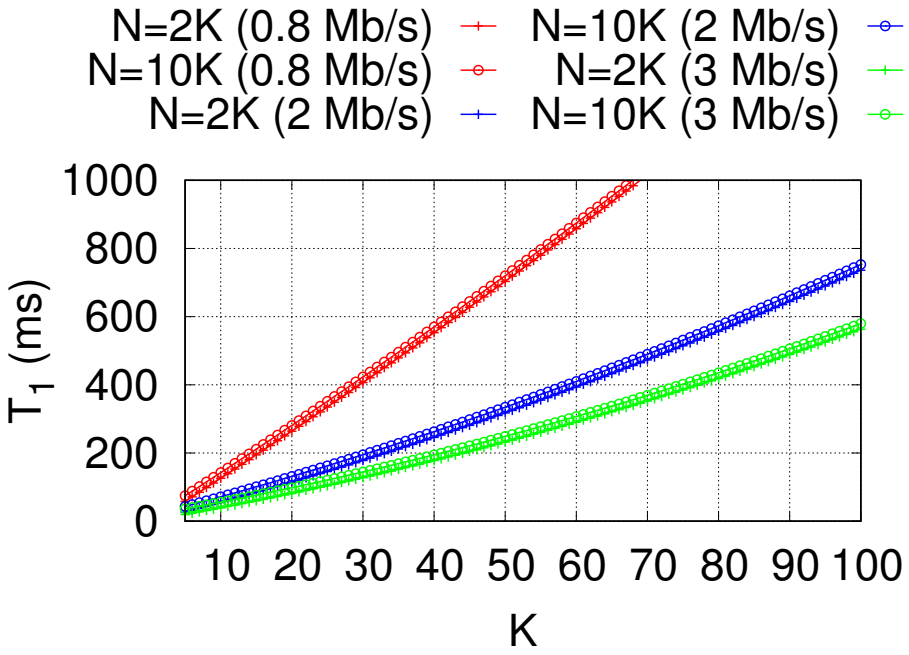

Figure 3.5: Delay and maximum N with respect to K.

large K value incurs a large buffering delay at the FEC encoder, as the encoder waits for K packets to arrive. Whereas, N_{max}/K is related to the throughput and should be limited by the wireless bandwidth.

We determine K and N_{max} by considering the delay and the bandwidth, while most of the existing schemes determine them arbitrarily, e.g., $K = 100$ and $N_{max} = 300$ in [7]. The delay incurred by FEC-applied multicast consists of the buffering delay at FEC encoder (T_b), FEC encoding delay (T_e), air delay (T_a), and FEC decoding delay (T_d). We consider the maximum delay of the first packet in a batch, which is denoted by T_1, since the first packet in a batch requires the longest T_b. The maximum T_b is expressed by $T_b = (K-1)\lambda/B_{src}$, where λ is the nominal application packet length (= 1328 B) and B_{src} is the video source rate. The air delay is maximized when the FEC decoding is performed after receiving N_{max}-th packets, so it is modeled as $T_a = N_{max} \cdot \tau(R, \lambda)$, where $\tau(R, \lambda)$ denotes the tx time of a single packet, a function

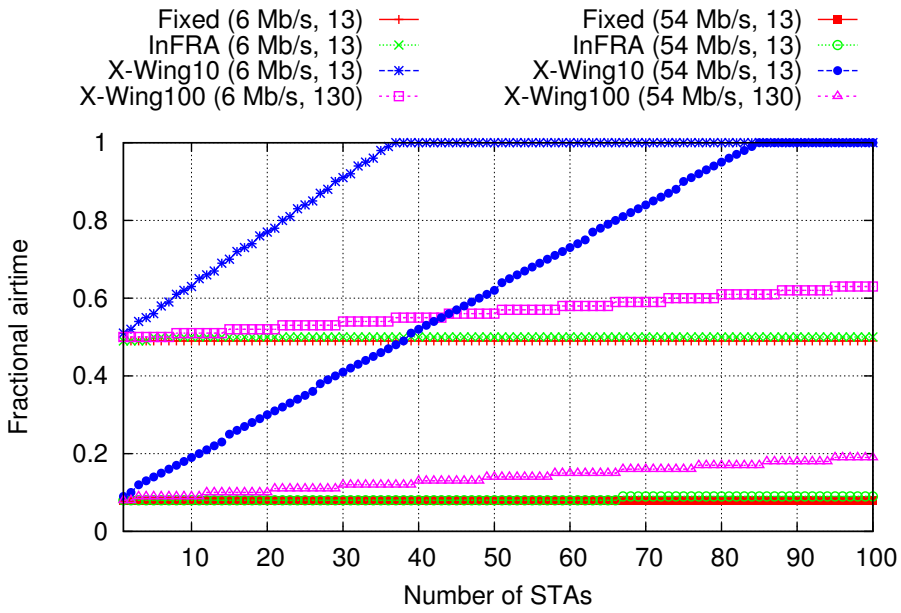

Figure 3.6: Fractional airtime analysis results.

of the PHY rate, R, and λ.[7] The encoding and decoding delays are modeled by our measurement results as $T_e = 0.037N$ and $T_d = 0.02K^2 + 0.125K$, respectively. Fig. 3.4.6 shows the delay and maximum generation size with respect to K, and we observe that the batch size K is dominant factor to the delay, and a large K value such as 100 is inappropriate to the real-time streaming. Assuming the range of video bitrates in consideration is from 1 to 3 Mb/s, we choose K as 10, which requires maximum buffering delay of about 100 ms, and N_{max} for each PHY rate as in Table 3.1, requiring 80% of the total wireless bandwidth.

Feedback overhead

In order to achieve high scalability, we basically employ a long-term feedback (once every 100 batches), on the other hand, other schemes like X-Wing adopt per-batch feedback. In order to compare the scalability, we conduct a simple numerical analysis

[7] We skip the actual equation due to space limitation, but the equation is rather straightforward.

Table 3.2: Notation and parameter values used in experiments.

Symbol	Definition	Exp. Val.
K	Batch size	10
S	Target APLR	1%
X	Target node satisfaction ratio	95%
Y	Number of total receivers	20
U	Number of allowed unsatisfied receivers	1
T_r	Maximum request deferring time	200 ms

of airtime consumption. We assume an ideal situation where no collisions and channel error take place, thus providing optimistic results. We assume that unicast feedback packets are sent at 802.11n PHY rate whose MCS is the same as that of the multicast packets, and the traffic rate is 2 Mb/s, where the payload size of each packet is set to 1,328 bytes.[8] We compare the performance of InFRA with two versions of X-Wing, i.e., X-Wing10 ($K = 10$) and X-Wing100 ($K = 100$), and the fixed PHY/FEC rate schemes without feedback.

Fig. 3.6 presents the analysis results. Although the analysis yields the optimistic results, per-batch feedback of X-Wing requires significant airtime while InFRA requires little additional overhead. While increasing K can reduce the overhead, it incurs the considerable delay as addressed in Section 3.4.6. More efficient design of feedback protocol to further reduce the overhead is our future work.

3.5 Performance Evaluation

We comparatively evaluate the performance of InFRA under various scenarios. We have implemented InFRA by modifying the latest ath9k device driver, backport 4.2.6-1.

[8]We skip the actual equations due to space limitation, but the analysis is rather straightforward.

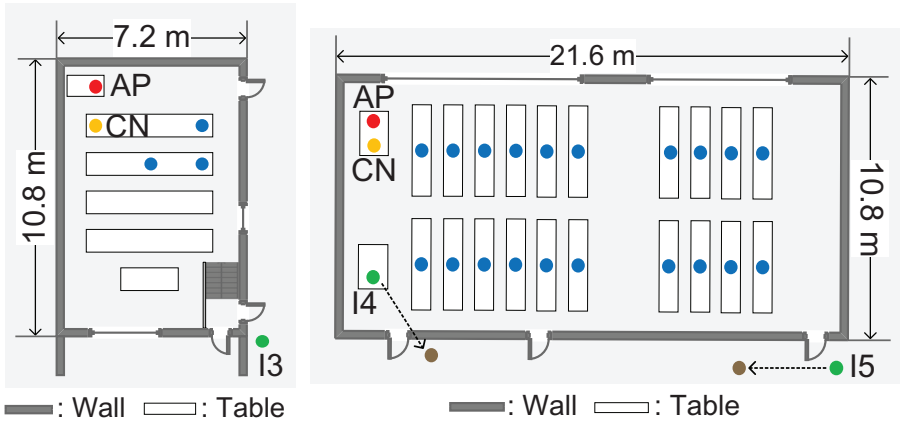

(a) Classroom (b) Auditorium

Figure 3.7: Measurement topology.

3.5.1 Measurement Setup

We conduct our experiments in two different places: (1) a classroom and (2) an auditorium, where both the floor plans are shown in Fig. 3.7. The AP and multiple STAs (3 and 20 for the small and large-scale experiments, respectively) constitute a WLAN using a channel in 5 GHz band, not occupied by other pre-deployed APs. HP-ProBook-450-G2 with AR9380 chipset is configured as the AP by using Hostapd, and the same type of laptops are used for STAs, where 17 and 3 STAs are equipped with AR9380 and AR9462, respectively. Ubuntu 14.04 is installed in the laptops. A STA is configured as a capturing node (CN) with the monitor mode to measure the airtime. We use the parameter values listed in Table 3.2, and the following performance metrics are measured: (i) *APLR*, (ii) *NSR*, i.e., the fraction of nodes that satisfy target APLR, (iii) *Fractional airtime*, i.e., the fraction of airtime occupancy by multicast sessions, and (iv) *Peak signal to noise ratio (PSNR)*, a widely-adopted video quality metric [77].

We compare InFRA with the following schemes:

(1) *Fixed PHY/FEC rates:* various combinations of R and N. We evaluate the fixed schemes for all possible combinations of R (= 6, 12, 18, 24, 36, 48, and 54 Mb/s) and N (= 13, 15, 20, and 25).

(2) *X-Wing* [7]: a modified version for fair comparison. The original X-Wing employs the bounded LT code with $K = 100$ and $N_{max} = 300$, and the target APLR S is set to 10%. In order to eliminate the effect from the difference of the FEC schemes and the target values, we employ the RLNC with $K = 10$ and $N_{max} = 30$, and set S to 1%.

3.5.2 Small Scale Evaluation

In order to investigate the detailed operation of InFRA, we conduct small-scale experiments where three STAs are associated with an AP and a hidden interferer (I3) exists, as presented in Fig. 3.7(a). We generate constant bit rate (CBR) traffic of 2 Mb/s from the AP to STAs using Iperf 2.0.5 with fixed packet length of 1,328 bytes according to the standard MPEG-2 TS with RTP packet format. We evaluate the performance of InFRA and X-Wing under three different scenarios: (i) no interference, (ii) regular interference (CBR of 1.5 Mb/s), and (iii) burst interference (periodic on-off pattern whose on and off durations are 0.5 s and 2.5 s, respectively). The MPDU size and the PHY rate of the interferer are set to 1,400 bytes and 6 Mb/s, respectively.

Fig. 3.8 presents the snapshots on how InFRA and X-Wing select the PHY rate and the generation size, (R, N), under different scenarios. When there is no interference (Figs. 3.8(a) and 3.8(d)), InFRA chooses 48 Mb/s continuously since it determines R based on long-term statistics while keeping N small enough to handle intermittent losses. X-Wing oscillates between 48 and 54 Mb/s, thus losing some packets. X-Wing sets N to 10 whenever all the receivers decode a batch, but such an aggressive protection cannot prevent packet losses in advance. When regular interference is generated (Figs. 3.8(b) and 3.8(e)), both InFRA and X-Wing increase N as it is more efficient than decreasing R. In the burst interference case (Figs. 3.8(c) and 3.8(f)), when the burst losses exceed the loss recovery capability of FEC, InFRA decreases R while X-Wing keeps losing packets as it has no mechanism to handle burst losses due to interference. We observe that InFRA increases the interval between the trials to the higher PHY rate by the history-based mechanism.

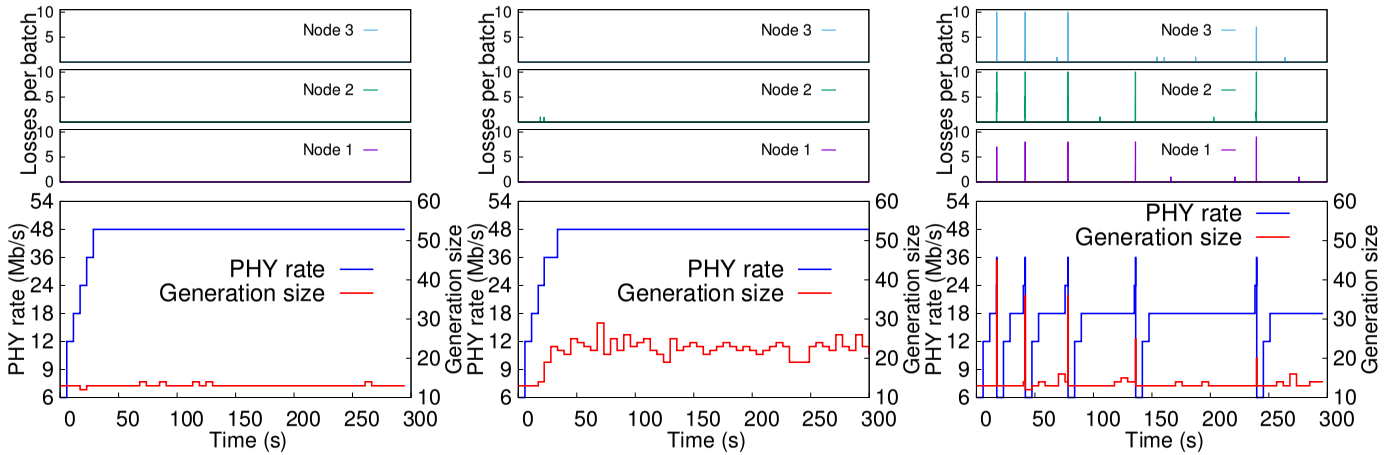

(a) InFRA w/o I. (b) InFRA w/ regular I. (c) InFRA w/ burst I.

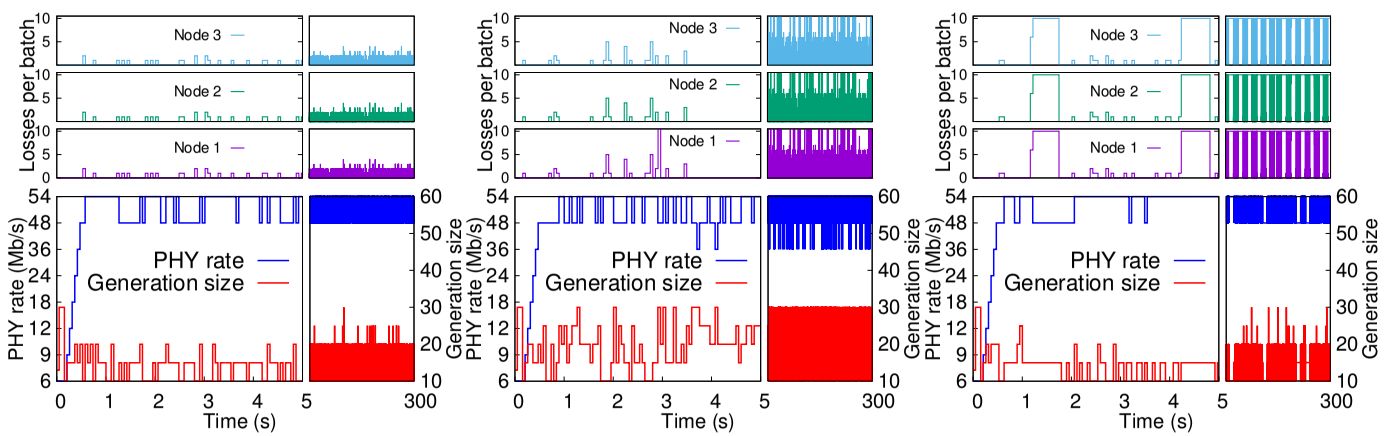

(d) X-Wing w/o I. (e) X-Wing w/ regular I. (f) X-Wing w/ burst I.

Figure 3.8: Transition of Packet losses per batch, PHY rate, and generation size under different scenarios.

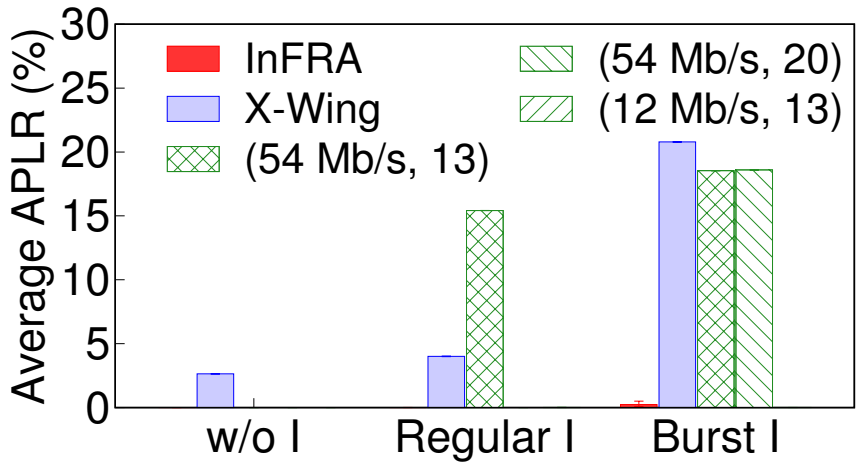

(a) Average APLR.

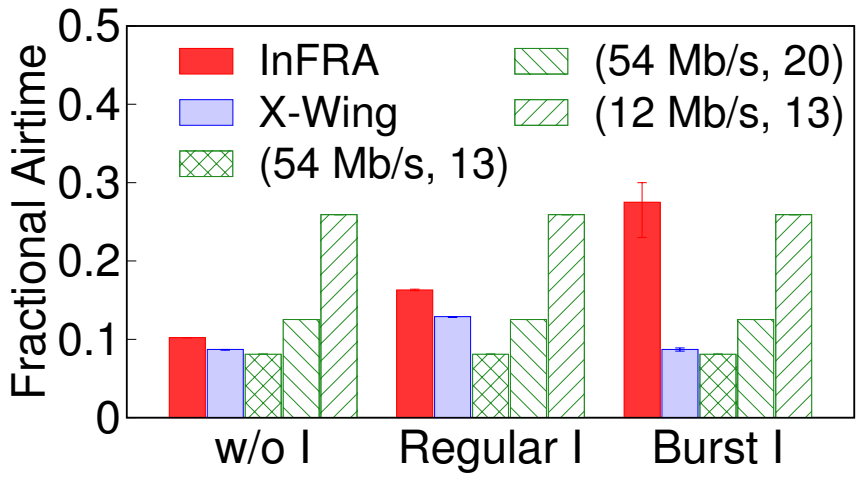

(b) Fractional airtime.

Figure 3.9: Average APLR and fractional airtime for each small-scale scenario.

Fig. 3.9 presents the average APLR and the fractional airtime. We compare the performance with the three fixed parameters: (54 Mb/s, 13), (54 Mb/s, 20), and (12 Mb/s, 13), the best fixed parameters for scenarios 1, 2, and 3, respectively. In Fig. 3.9(a), we observe that many packets are lost due to burst interference except for InFRA and (12 Mb/s, 13). Note that different nodes experience a similar level of losses. As shown in Fig. 3.9, the best fixed parameter varies depending on the scenarios, and InFRA meets the APLR requirement and consumes slightly longer airtime than the best fixed parameters under all the scenarios. On the other hand, X-Wing fails to meet the APLR requirement for the aforementioned reasons.

3.5.3 Large Scale Evaluation

We evaluate the performance with 20 STAs in the auditorium shown in Fig. 3.7(b). With streaming a real video clip (1280x720 resolution, MPEG-4 codec, 2 Mb/s, 5 min), we measure the performance for the various source rates of the interference. The other settings of the interference are the same as in Section 3.5.2.

Fig. 3.10 presents the NSR and the fractional airtime with respect to the interference source rates. InFRA achieves the target NSR (=95%) while requiring a similar airtime to the best fixed parameters. In the case of X-Wing, NSR decreases as the interference source rate increases, and some nodes with good channel quality receive the packets with the hidden interference, thus yielding larger NSRs than those with the contention interference. In average, InFRA achieves 2.3x and 1.8x higher NSR than X-Wing with interference I4 and I5, respectively. With the contending node, the amount of packet loss is smaller than that with the hidden node, and hence, the required airtime is less than the hidden interference case.

Fig. 3.11 presents the PSNR values across the receivers and the breakdown of the fractional airtime under the selected three scenarios: (i) no interference, (ii) contention interference (CBR of 4 Mb/s), and (iii) hidden interference (CBR of 4 Mb/s). Besides X-Wing, we compare InFRA with the selected fixed parameters, (36Mb/s, 13) and

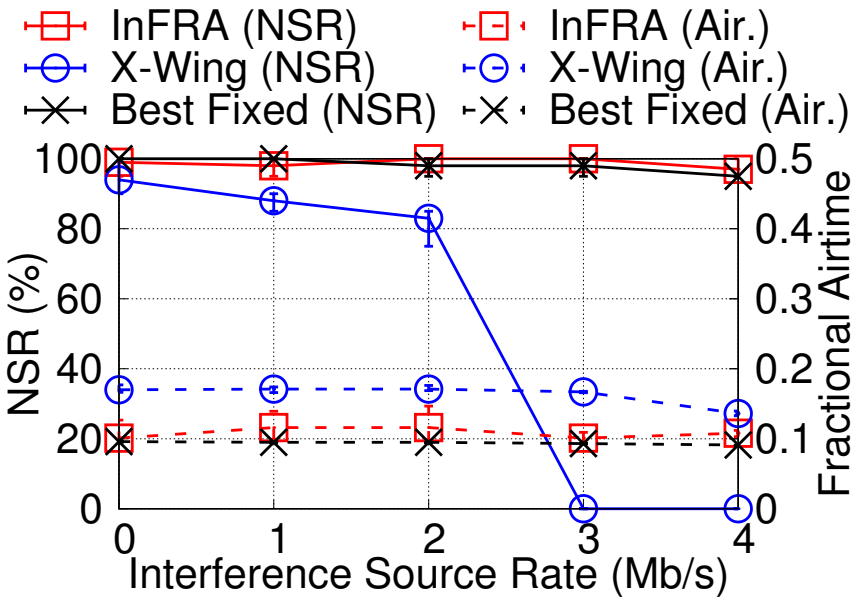

(a) w/ I4.

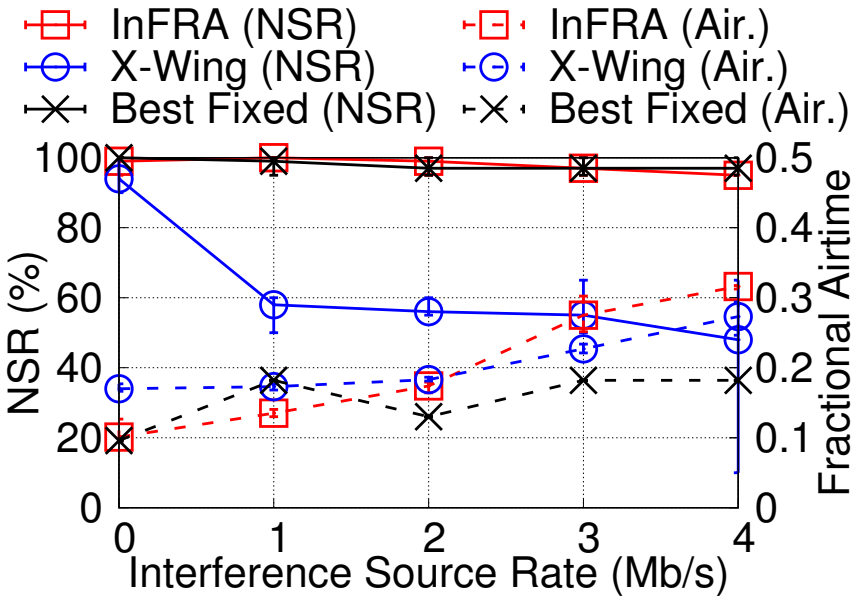

(b) w/ I5.

Figure 3.10: NSR and fractional airtime w.r.t. source rate of interference.

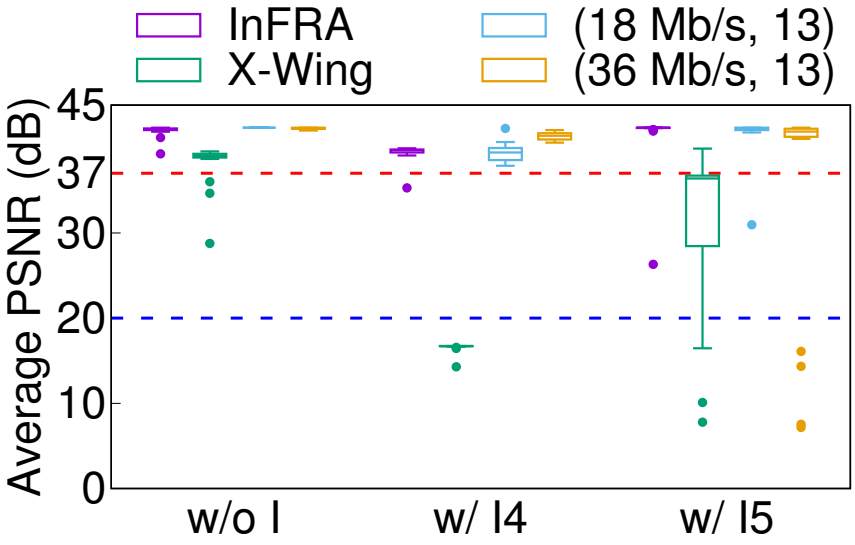

(a) Average PSNR.

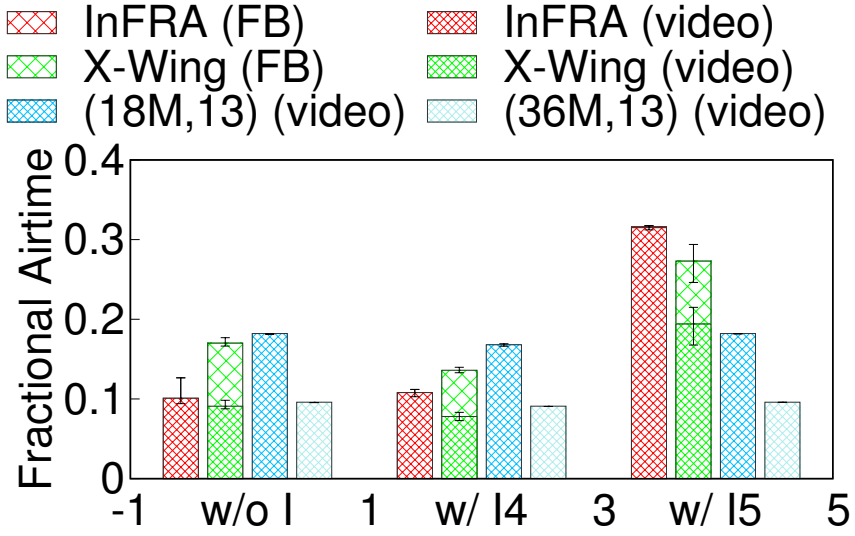

(b) Fractional airtime.

Figure 3.11: Average PSNR and fractional airtime for each large-scale scenario. The box plot describes the median (line within the box), inter-quartile range (upper and lower borders of the box), maximum and minimum values within in 1.5 inter-quartile range (whiskers), and the outliers (circles).

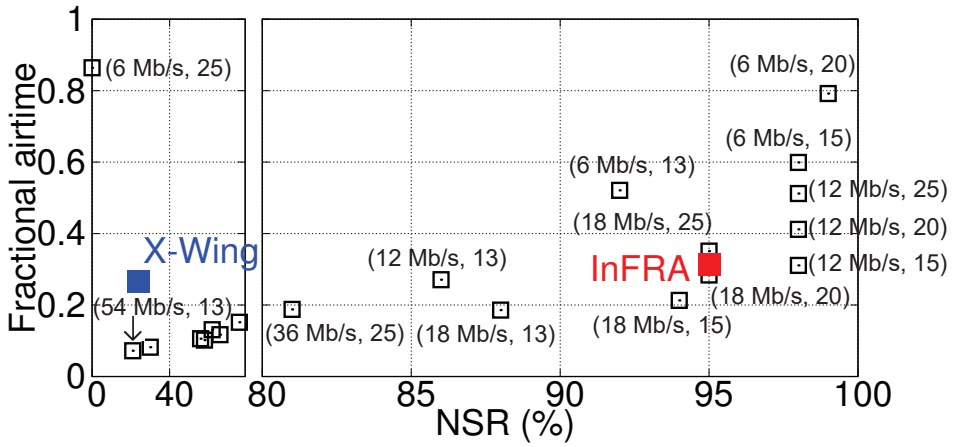

Figure 3.12: NSR and fractional airtime under interference with YouTube traffic.

(18Mb/s, 13), which are the best for scenarios 1 and 2, and scenario 3, respectively.

In Fig. 3.11(a), PSNR values of 20, 25, 31, and 37 are mapped to mean opinion score (MOS) of 2 (poor), 3, 4, and 5 (excellent), respectively [77]. InFRA provides the excellent-quality of video to at least 19 receivers, while some receivers are poorly served with X-Wing. In Fig. 3.11(b), we present the portion of feedback (FB) packets. InFRA requires to send the feedback (PHY/FEC rate request) once every 100 batches, while X-Wing sends three feedback packets every batch. Accordingly, X-Wing incurs much larger feedback overhead than InFRA. In the case of X-Wing with interference I4, the feedback overhead decreases as some feedback packets collide with the interference packets. Note that in scenario 3, InFRA requires large airtime since it chooses a low PHY rate due to the conservative selection of PHY rate in the weak interference case. Designing more efficient PHY rate selection with the weak interference is our future work.

We finally evaluate the performance when the interference traffic is real YouTube traffic. Both interference I4 and I5 are activated, where each interferer streams a YouTube video (1280x720p resolution and 1.2 Mb/s [78]) to a closely located STA, as shown in Fig. 3.7(b). Fig. 3.12 presents the NSR and the fractional airtime of InFRA and all

the comparison schemes. In this figure, the performance improves as the point goes toward the bottom right direction. We observe that InFRA achieves the performance similar to the best fixed PHY/FEC scheme under the real environment.

3.6 Summary

We proposed InFRA to differentiate the selection of PHY/FEC rates along with the cause of packet losses. On top of the classification of interference, our standard-compliant loss differentiation mechanism diagnoses the cause of packet losses based on RSSI and CRC error notifications. The elaborate framework of the PHY/FEC rate decision enables efficient and interference-resilient multicast service with minimal overhead. From extensive evaluation with prototype implementation, we demonstrate that InFRA enhances the multicast delivery, achieving 2.3x and 1.8x higher NSR with a contention interferer and a hidden interferer, respectively, compared with the state-of-the-art PHY/FEC rate adaptation scheme.

Chapter 4

EV-CAST: Interference and Energy-aware Video Multicast Exploiting Collaborative Relays

4.1 Introduction

Wireless multicast has been considered an attractive solution especially when sharing common data with multiple receivers, since it utilizes inherent broadcast nature of wireless channel. A major application of multicast is streaming real-time video to multiple receivers, e.g., sharing a screen with multiple students in a classroom and broadcasting live events to audience in a sports stadium or a concert hall. Along with the increasing popularity of unicast-based video streaming, the interest in video streaming via multicast, so called video multicast, has been increasing as well.

In large auditoriums or sports stadiums, a single sender (an access point in the infrastructure mode and a source node in the ad-hoc mode) can hardly cover the whole coverage. Furthermore, extension of coverage can provide better experience to audience, e.g., according to [79], over 50% of users are more willing to leave their seats if they can view all of the action with their devices in other places such as concession areas. Therefore, collaborative relaying approach that enables some receiver nodes to relay the packets from the source node to other nodes has been considered to enhance

the coverage without additional deployment of infrastructure.

Most collaborative relaying schemes employ intra-flow network coding (NC) [66]. With NC, the source node generates N encoded packets for each batch of K original packets by taking linear combination of the original packets with random coefficients. K and N are called batch size and generation size, respectively. Then, relay nodes re-encode the packets and transmit them. Even though the relay nodes fail to decode the original packets, they can re-encode the received packets by taking linear combination of the received packets. By exploiting the possibility of reception over unfavorable links thanks to the broadcast nature, the reliability and relay gain are enhanced significantly.

In collaborative relaying, one major challenge is determining sender nodes, i.e., source and relay nodes, and their transmission parameters (TPs), i.e., physical (PHY) rate and generation size.[1] In determining relay nodes, the current battery level of nodes should be considered. While nodes with high battery level are willing to relay, other nodes with low battery level are not. As mobile battery chargers become more popular, it is not uncommon for mobile nodes to be charged. Accordingly, the charging status, i.e., whether a node is charged or not, should be considered as well. Another important factor is the spatial reuse. If we choose spatially reusable nodes, nodes that can transmit simultaneously without interfering with each other, we can provide video multicast more efficiently.

On the other hand, in determining TPs of sender nodes, interference should be considered carefully. In [80], the impact of the interference on the selection of TPs is addressed in a single-hop network. For multi-hop multicast networks, more heterogeneous interference can deteriorate the performance, thus making the problem more complex.

In this paper, we propose EV-CAST, a video multicast protocol that exploits collaborative relaying. EV-CAST entails an elaborate design fitted for video streaming

[1] If the network size is sufficiently small, the source node might be the only sender node.

over two-hop network that concerns 1) joint determination of sender nodes and their TPs, 2) online network management, and 3) polling-based relay protocol.

As a kind of tree-based multicast, EV-CAST constructs a two-hop multicast tree for opportunistic overhearing. Extending the framework in [80] to multi-hop networks, we propose an interference-aware link characterization, and all the links on the tree are characterized based on that. After that, a novel centralized algorithm determines sender nodes and their TPs by taking into account various factors including battery status and spatial reuse as well as the factors reported up-to-date. Chosen relay nodes are scheduled to transmit with consideration of spatial reusability. The link and battery state measurement is conducted online and updated periodically with relatively low overhead.

We implement EV-CAST in Linux device driver and comparatively evaluate the performance of EV-CAST with existing schemes in imec w-ilab.t testbed [81]. Our measurement results demonstrate that EV-CAST achieves significantly better performance than state-of-the-art schemes.

Our contributions are summarized as follows.

- We propose EV-CAST, a practical video multicast protocol exploiting collaborative relaying, which is well-suited for two-hop multicast networks. The main components, i.e., the novel joint sender nodes and their TPs selection algorithm, online network management based on interference-aware link characterization, and polling-based relay protocol, are integrated harmoniously.

- We propose an interference-aware link characterization for multi-hop networks. Depending on the cause of packet losses, i.e., channel error or interference, we determine desirable TPs of each link not only from sender nodes but also from non-sender nodes.

- We propose a novel algorithm that jointly determines sender nodes and their TPs. The algorithm is designed based on the principles not only accumulated

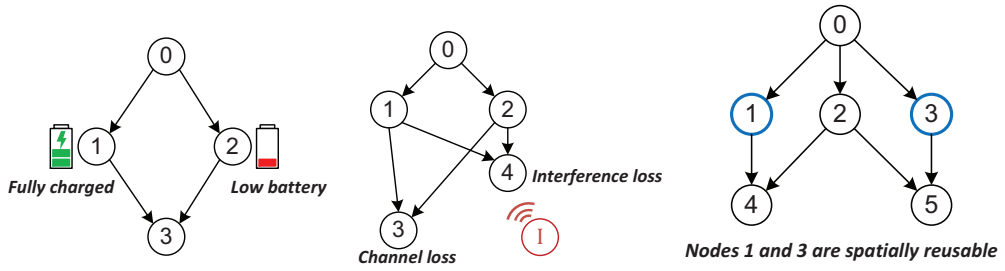

(a) (b) (c)

Figure 4.1: Various factors for selecting relay nodes and resource: (a) battery status, (b) interference, and (c) spatial reusability

over the past years, but also newly addressed in this paper. To our best knowledge, it is the first multicast relay selection work that concerns battery status, interference, and spatial reuse.

- We present the prototype implementation of EV-CAST and evaluate the performance in imec w-ilab.t testbed. Our experiment results demonstrate that EV-CAST outperforms the state-of-the-art video multicast schemes.

The rest of the paper is organized as follows: In Section 4.2, we discuss the philosophies for the relay nodes and their transmission parameter selection. In Sections 4.3 and 4.4, we present the detailed design of EV-CAST and evaluate the performance. We discuss the related work in Section 4.5, and finally conclude this paper in Section 4.6.

4.2 Factors for Sender Node and Transmission Parameter Selection

In two-hop multicast network, the major concern is the selection of sender nodes and their TPs. There have been various studies that address the factors to be considered, e.g., packet delivery rate (PDR), expected transmission time (ETT), number of neighbors, etc. In addition to them, we take three key factors into account: (1) battery status,

(2) interference, and (3) spatial reusability. Note that some factors which necessitate the batch-level feedback such as packet reception correlation in [17] is not considered in this work.

Fig. 4.1 describes the newly addressed factors. Each circle indicates a node while index zero is assigned to the source node. Fig. 4.1a shows an example where a source node has two neighbor nodes, i.e., relay candidates, having different battery status. While node 1's battery is fully charged, the remaining battery of node 2 is low. Since the relaying functionality involves additional energy consumption, the remaining battery is directly related with the duration of relaying. Moreover, we also consider the charging status, i.e., whether the battery of a node is being charged or not. It may be reasonable to select a node charging its battery even though its current battery level is low. As portable battery chargers become popular, it is common that even mobile nodes can be charged.

Fig. 4.1b presents an example when there exists an interfering node (node I). Two two-hop nodes, i.e., nodes 3 and 4, experience packet losses due to the different causes, i.e., interference and low channel quality. In [80], it is reported that the optimal TPs depends on the cause of packet losses, and diagnosing the cause of packet losses enables an interference-resilient video multicast. Therefore, we take the interference into account for the sender node and TP selection.

Fig. 4.1c presents an example when the spatial reuse, i.e, concurrent transmission of two or more nodes, is available. In order to serve nodes 4 and 5, if nodes 1 and 3 are selected as relays, which are not neighbor with each other and do not share any common neighbor nodes except for the source node, concurrent transmission is possible, thus reducing the airtime resource. In this work, we consider such a pair of nodes that can transmit simultaneously, which is called SRP (spatially reusable pair).

4.3 EV-CAST: Interference and Energy-aware Multicast Exploiting Collaborative Relays

In order to provide a high-quality video to many users for a long time, we develop EV-CAST, an interference and energy-aware video multicast system exploiting collaborative relay. The design of EV-CAST follows the philosophy of tree-based schemes as in [**?**, 16]. Unlike belt-based schemes such as MORE, where all nodes can operate as relay [17, 82], tree-based schemes allow only selected nodes to relay packets, while receiver nodes can receive packets from any relay nodes due to the broadcast nature. We note that such receiving from any relay nodes, called opportunistic reception, has been exploited to enhance PDR in some of the first multi-hop multicast protocols (e.g., ODMRP [83]). In [**?**], it is verified that tree-based schemes are more suitable for real-time video streaming than belt-based schemes.

4.3.1 Network Model and Objective

We mainly consider an ad-hoc mode WLAN that consists of a single source and multiple destinations.[2] Although it might not achieve the full potential, we can also apply EV-CAST framework to the infrastructure mode to enhance the reliability and efficiency as mentioned above. We assume low mobility of the destination nodes, e.g., the majority of users are seated and watching a common video. We consider real-time transport protocol/user datagram protocol (RTP/UDP)-based video streaming and the video packets are packetized as MPEG-2 transport stream (TS) format [88], which is a widely-employed protocol for video multicast.

Our primary objective is maximizing node satisfaction ratio (NSR), which is defined as the fraction of nodes watching videos with target application-layer PLR (APLR).[3]

[2] Although ad-hoc network with smartphones is not widely utilized yet, smartphone ad-hoc network (SPAN) has attracted an interest from research community and industry practitioners, where geocommunity-based video multicast is one of the promising applications [84–87].

[3] We distinguish application-layer PLR, i.e., PLR after NC decoding, from the MAC-layer PLR

When NSR is higher than a target NSR, e.g., 95%, we aim to maximize the video multicast service time. Moreover, we aim at developing a system that requires minimal overheads in order to support a large number of destination nodes.

4.3.2 Overview

EV-CAST consists of three main components: 1) network management, 2) interference and energy-aware sender nodes and their TPs selection (INFER) algorithm, and 3) relay-assisted video transmission. Source node constructs a topology map with maximum two hops from itself by gathering the link state information of all possible links in the network (network management). Based on the topology map updated during runtime, the source node determines a set of sender nodes, including the source and relay nodes, and their TPs by running INFER algorithm. Then, the selected relay nodes, if they exist, forward the packets received from the source node after re-encoding them (relay-assisted video transmission). In the rest of this section, we provide the detailed description of the three main components.

4.3.3 Network Management

As in [**?**], we employ a centralized relay selection in that the source node is in charge of determining relay nodes. Since the relay nodes are determined based on a global topology map, it generally selects more efficient relays than distributed relay selection schemes based on only local information. Although the centralized relay selection scheme has the drawback of large computational complexity, it is affordable for two-hop network. Another major challenge is how to construct and update the global topology map.

(MPLR), i.e., the PLR before NC decoding. For brevity, the packet loss and PLR indicate the MAC-layer packet loss and MPLR, respectively, unless specified otherwise. In this work, we set the target APLR to 1% [68].

Construction of global topology map

In order to construct a global topology map, the source and one-hop nodes periodically send short multicast packets, called *probing packets*. Initially, the source node sends the probing packets. Nodes receiving the probing packets from the source node, called one-hop nodes, also send the probing packets to discover two-hop nodes. We define two-hop nodes as nodes that receive the probing packets only from the one-hop node(s). In order to inform the local link state information to the source node, each destination node has a parent node to which it sends the link state information. The source node is the parent node of all one-hop nodes, while each two-hop node sets the parent node to the one-hop node having the highest received signal strength indicator (RSSI). Each destination node sends feedback packets to its parent node by unicast, conveying its battery status and link state information for each downstream link from its neighboring one-hop or source node. One-hop nodes relay the feedback packet to the source whenever receiving it from two-hop nodes.

Interference-aware link characterization

In most multi-hop multicast schemes, a link from node i to j is characterized by PLR, but the PLR-based link characterization is unable to differentiate the cause of packet losses, i.e., whether loss is due to low RSSI or interference. Instead of reporting just PLR, in InFRA [80], each receiver differentiates the cause of losses and requests favorable PHY rate, R, and the generation size, N, depending on the differentiated loss statistics. Since InFRA only considers single-hop network, we extend this concept to multi-hop network.

In InFRA, each receiver diagnoses the cause of the packet losses for each batch, based on RSSI and cyclic redundancy check (CRC) error notification. When l_t packets are lost in a batch, each receiver classifies them into l_c, l_s and l_w, representing the number of losses due to channel error, strong interference, and weak interference,

respectively. The classification is expressed as

$$(l_c, l_s, l_w) = \begin{cases} (l_t, 0, 0), & \text{if } \overline{\gamma} < \delta\left(R_{cur}\right), \\ (0, l_t - c, c), & \text{otherwise,} \end{cases} \tag{4.1}$$

where $\overline{\gamma}$ is the average RSSI from the sender (AP in InFRA), R_{cur} is the current PHY rate of the sender, $\delta\left(R_{cur}\right)$ is the RSSI threshold ensuring target PLR (ρ) at PHY rate R_{cur}, and c is the number of CRC error notifications during the batch reception.

From the loss differentiation result, each receiver determines two pairs of R and N, so-called RN pairs, depending on the criteria for determining PHY rate. PHY rate is normally determined by RSSI, but in some cases when there exist weak interference signals using a lower PHY rate to induce the capture effect [67] is more efficient. To this end, two RN pairs, i.e., channel quality-oriented RN pair, (R_{ch}, N_{ch}), and capture inducing RN pair, (R_{cap}, N_{cap}), are determined.

Then, a link from AP is characterized by $\mathbf{q} = (R_{ch}, N_{ch}, R_{cap}, N_{cap})$, which implies that the decoding will be successful if the AP sends N_{ch} encoded packets at R_{ch} or sends N_{cap} encoded packets at R_{cap}. From the requested RN pairs from multiple receivers, the AP determines the most appropriate RN pair. See [80] for more details.

We generalize this concept to multi-hop networks by characterizing any link from node i to node j by $\mathbf{q}^{(ij)} = (R_{ch}^{(ij)}, N_{ch}^{(ij)}, R_{cap}^{(ij)}, N_{cap}^{(ij)})$, which is also called interference-aware link state parameters (ILP). In contrast to InFRA where AP is the only sender, each node in EV-CAST determines $\mathbf{q}$'s for not only current senders but also possible senders, i.e., all neighboring one-hop and source nodes. Accordingly, we propose link characterization methods for sender nodes and non-sender nodes, respectively. ILPs for sender nodes are determined similarly to as in InFRA but in a simpler way to reduce complexity. For non-sender nodes, since loss statistics are not available, we conservatively estimate $\mathbf{q}$ with RSSI of their probing packets by assuming the maximum interference losses of neighboring sender nodes.

Algorithm 2 determines ILP for a sending neighbor node. For sender node i, node j keeps track of the current PHY rate, $R_{cur}^{(i)}$, generation size, $N_{cur}^{(i)}$, the average RSSI per

batch, $\gamma^{(i)}$, and loss parameters, $l_{t,max}^{(i)}$, $l_{c,max}^{(i)}$, $l_{i,max}^{(i)}$, and $l_{s,max}^{(i)}$, which are maximum number of total losses, channel losses, interference losses, and strong interference losses per batch, respectively. Additionally, if decoding of a batch fails, the failed PHY rate, $R_{fail}^{(i)}$, is recorded in order to avoid the frequent trial of PHY rate increase. PHY rate increase to $R_{fail}^{(i)}$ is tried only when the success counter, $c_s^{(i)}$, which is raised by one whenever decoding is successful, reaches the success window, $w_s^{(i)}$, which is doubled whenever decoding fails. From now on, for brevity, we present aforementioned parameters without superscripts representing nodes unless they are necessary.

We aim at finding R_{ch} as the maximum PHY rate ensuring PLR due to channel loss is smaller than a target value, ρ. When there is no channel loss, it is checked whether it is possible to increase PHY rate. If the condition of PHY rate increase is satisfied (line 4), R_{ch} is set to the next higher PHY rate than R_{cur} in the rate set, R_{cur}^{+}. When there are small channel losses whose ratio ($l_{c,max}/N_{cur}$) is smaller than ρ, R_{ch} is set to the current PHY rate. Otherwise, R_{ch} is determined by GETRATE function. If the result is greater than or equal to the current PHY rate, PHY rate is set to the next lower PHY rate than R_{cur}, i.e., R_{cur}^{-} (lines 15−19). N_{ch} is determined such that the channel and interference losses can be recovered. If R_{ch} is equal to R_{cur}, we use the maximum total losses, $l_{t,max}$. Otherwise, we determine N_{ch} by assuming the maximum interference losses, $l_{i,max}$, and target channel errors of ρN_{cur}. We add ϵ to handle additional unexpected losses.

Different from [80], where R_{cap} is determined by measuring interference signal strength, we set R_{cap} to the PHY rate Δ-step lower than R_{ch}. Since we consider multihop network where multiple senders exist necessarily, it is difficult to separate the interference from the target senders, and hence, we employ a simple capture-inducing rate decrease step, Δ, which is empirically set to three in this work. Finally, N_{cap} is determined such that the strong interference losses can be recovered, assuming that R_{cap} is robust enough not to cause channel loss or weak interference loss. (line 27).

Algorithm 3 presents the procedure of determining the ILP for a non-sending

Algorithm 2 Determination of ILP for a sending neighbor

Require: $\overline{\gamma}, l_{t,max}, l_{c,max}, l_{i,max}, l_{s,max}, R_{cur}, N_{cur}, R_{fail}, c_s, w_s$

Ensure: $R_{ch}, N_{ch}, R_{cap}, N_{cap}$

if $l_{c,max} == 0$ **then** ▷ Determining R_{ch}
  if GETRATE($\overline{\gamma}$) $> R_{cur}$ **then**
    if $\left(R_{cur}^{+} < R_{fail}\right) || \left(R_{cur}^{+} == R_{fail} \&\& c_s == w_s\right)$ **then**
      $R_{ch} \leftarrow R_{cur}^{+}$
    else
      $R_{ch} \leftarrow R_{cur}$
    end if
  else
    $R_{ch} \leftarrow R_{cur}$
  end if
else if $l_{c,max}/N_{cur} < \rho$ **then**
  $R_{ch} \leftarrow R_{cur}$
else
  if $R \geq R_{cur}$ **then**
    $R_{ch} \leftarrow R_{cur}^{-}$
  else
    $R_{ch} \leftarrow$ GETRATE($\overline{\gamma}$)
  end if
end if
if $R_{ch} \neq R_{cur}$ **then** ▷ Determining N_{ch}
  $N_{ch} \leftarrow \left\lceil K \frac{N_{cur}}{(1-\rho)N_{cur} - l_{i,max}} \right\rceil + \epsilon$
else
  $N_{ch} \leftarrow \left\lceil K \frac{N_{cur}}{N_{cur} - l_{t,max}} \right\rceil + \epsilon$
end if
$R_{cap} \leftarrow R_{ch} - \Delta$ ▷ Determining R_{cap}
$N_{cap} \leftarrow \left\lceil K \frac{N_{cur}}{N_{cur} - l_{s,max}} \right\rceil + \epsilon$ ▷ Determining N_{cap}

function GETRATE(γ)
  Find out rate R s. t. $\delta(R) \leq \gamma < \delta(R^{+})$
  return R
end function

Algorithm 3 Determination of ILP for a non-sending neighbor

Require: $\overline{\gamma}, R_{cur}^{net}, l_{i,max}^{net}, l_{s,max}^{net}$

Ensure: $R_{ch}, N_{ch}, R_{cap}, N_{cap}$

1: **if** GETRATE$(\overline{\gamma}) > R_{cur}^{net}$ **then** ▷ Determining R_{ch}

2: $\quad R_{ch} \leftarrow R_{cur}^{net^+}$

3: **else**

4: $\quad R_{ch} \leftarrow$ GETRATE$(\overline{\gamma})$

5: **end if**

6: $N_{ch} \leftarrow \left\lceil K \frac{N_{cur}}{(1-\rho)N_{cur} - l_{i,max}^{net}} \right\rceil + \epsilon$ ▷ Determining N_{ch}

7: $R_{cap} \leftarrow R_{ch} - \Delta$ ▷ Determining R_{cap}

8: $N_{cap} \leftarrow \left\lceil K \frac{N_{cur}}{N_{cur} - l_{s,max}^{net}} \right\rceil + \epsilon$ ▷ Determining N_{cap}

neighbor node. Besides the average RSSI of the probing packets from non-sending nodes, $\overline{\gamma}$, we extract some parameters, R_{cur}^{net}, $l_{i,max}^{net}$, and $l_{s,max}^{net}$, which are maximum R_{cur}, $l_{i,max}$, and $l_{s,max}$ among neighboring sender nodes, respectively. We conservatively assume as many interference losses as the maximum interference losses among neighboring sender nodes. Then, R_{ch} is determined by GETRATE function. If the result is higher than R_{cur}^{net}, R_{ch} is set to $R_{cur}^{net^+}$. We limit R_{ch} to $R_{cur}^{net^+}$ in order to increase the PHY rate gradually. Other parameters such as N_{ch}, R_{cap}, and N_{cap} are determined as in Algorithm 2. We avoid the unnecessarily frequent changes of sender nodes with such a conservative design.

Feedback timing

In [**?**], it is reported that per-batch feedback and retransmission schemes like MORE are not suitable for video streaming since they increase the end-to-end delay and even lead to the freeze of video. Instead, we employ a feedback mechanism that combines long-term feedback for regular update and event-driven feedback for fast recovery when target APLR is not satisfied.

Each destination node regularly sends feedback packets in a long-term period. Furthermore, we adapt the feedback period of the regular feedback in order to reduce feedback overheads. The regular feedback period depends on the node's priority: higher

priority nodes continuously use the minimum feedback period, λ_{min},[4] while lower priority nodes double the feedback period whenever it sends the regular feedback two times until it reaches the maximum period, λ_{max}. Higher priority nodes are relays and target nodes, which will be stated in the next section.

We additionally employ an event-driven feedback mechanism to handle the situation that fails to achieve the target APLR. If a node fails to decode two batches before receiving 100 batches, it immediately sends a feedback in an event-driven manner. In this case, the node resets the feedback period to λ_{min}.

4.3.4 Interference and Energy-aware Sender Nodes and Transmission Parameter Selection (INFER) Algorithm

Estimation of the number of innovative packets

For a link from node i to j with $\mathbf{q}^{(ij)} = \left(R_{ch}^{(ij)}, N_{ch}^{(ij)}, R_{cap}^{(ij)}, N_{cap}^{(ij)}\right)$, we assume that node j can decode batches if node i sends packets with $\left(R_{ch}^{(ij)}, N_{ch}^{(ij)}\right)$ or $\left(R_{cap}^{(ij)}, N_{cap}^{(ij)}\right)$. Namely, it is assumed that node j can receive K *innovative packets*, i.e., packets with linearly independent encoding coefficients, from node i if node i sends $N_{ch}^{(ij)}$ packets at $R_{ch}^{(ij)}$ or sends $N_{cap}^{(ij)}$ packets at $R_{cap}^{(ij)}$. Besides, another node (e.g., node k) can receive some packets from node i thanks to the opportunistic listening property, which should be estimated for determining a set of sender nodes and their TPs.

For this purpose, we now define an estimation function, $H(r, n, \mathbf{q})$, which estimates the number of *innovative packets* that a destination node will receive from a sender node with $\mathbf{q}$ when the sender sends n packets at r. The estimation function is

[4] We set λ_{min} to 100 batches in this work, since at least 100 batches are needed to make sure whether the 1% of target APLR is satisfied or not.

defined as

$$H(r,n,\mathbf{q}) = \begin{cases} \min\left(\left\lfloor n \cdot \frac{K}{N_{cap}} \right\rfloor, K\right), & \text{if } r \leq R_{cap}, \\ \min\left(\left\lfloor n \cdot \frac{K}{N_{ch}} \right\rfloor, K\right), & \text{else if } r \leq R_{ch}, \\ 0, & \text{otherwise.} \end{cases} \tag{4.2}$$

The estimation function is interpreted as, for example, if r is lower than or equal to R_{cap}, only N_{cap} is required to provide K innovative packets, but if n (lower than N_{cap}) packets are transmitted, then the packets will be received with the success ratio of K/N_{cap}.

Utility function

INFER algorithm iteratively finds the best set of sender nodes and their TPs that maximize a utility function. We denote a triplet of sender node index, PHY rate, and generation size, by $Q = (I, R, N)$, which is called IRN, and a set π of IRNs, which is called IRN assignment unit (IU), is determined in every round. In order to serve a two-hop node, the source node needs to determine the best one-hop node to relay and its (R, N), and the source node also needs to determine its own (R, N) to serve the one-hop node. Therefore, source node's (R, N) is dependent on the IRN of the one-hop node. Moreover, if the one-hop node is spatially reusable with another one-hop node, it should also be considered to determine the source node's (R, N).

For this reason, we choose at most three IRNs in a round, which is denoted by $\pi = \{Q_0, Q_1, Q_2\}$, where Q_0, Q_1, and Q_2 are IRNs for the source node, the target one-hop node (also called primary relay), and selected SRP node (also called secondary relay), respectively. There are five types of IU: 1) IRN of the source node only ($Q_1 = Q_2 = \varnothing$), 2) IRN of a primary relay only ($Q_0 = Q_2 = \varnothing$), 3) IRNs of the source and a primary relay node ($Q_2 = \varnothing$), 4) IRNs of a primary relay and a secondary relay ($Q_0 = \varnothing$), 5) IRNs of the source, a primary relay, and a secondary relay.

For an IU π, a utility $U(\pi)$ is defined as the ratio of benefit function $B(\pi)$ to cost

function $C(\pi)$:

$$U(\pi) = B(\pi)/C(\pi), \tag{4.3}$$

where $B(\pi)$ is the number of nodes *newly served* by π and $C(\pi)$ is the weighted sum of the airtime required by π. *Served* node is defined as a node whose expected number of the received innovative packets is equal to the original batch size (K). Through multiple rounds, the estimated number of innovative packets increases thanks to the opportunistic listening, and when the number eventually becomes K, this node is referred to be *newly served*.

We define the energy factor to take the battery status into account for the cost function. The energy factor of node i, denoted by E_i, is defined as

$$E_i = \omega^{c_i} e_i, \tag{4.4}$$

where ω (≥ 1) is a constant weight associated with the charging status c, which is 1 if node i is being charged or 0 otherwise, and e_i is the remaining battery of node i in percentage. $T(R, N)$ is the estimated transmission time when transmitting N packets at R:

$$T(R, N) = N \cdot \left\{ \frac{L_m + L_h}{R} + \tau_O \right\} + \tau_{poll}, \tag{4.5}$$

where 1) L_m is the nominal multicast packet length (1328 B with MPEG-2 TS format), 2) L_h is the total length of headers including RTP/UDP/IP/LLC/MAC headers as well as the EV-CAST data packet header indicating K, N, sequence number, and the encoding coefficients, 3) τ_O is the time duration for other overheads including preamble, PHY header, and the backoff, and 4) τ_{poll} is the time duration for relay polling, which will be addressed later.

Considering the airtime and spatial reusability as well as the energy factor, we develop the cost function as follows.

$$C(\pi) = F(Q_0) + \alpha(Q_1, Q_2) \left\{ F(Q_1) + F(Q_2) \right\}, \tag{4.6}$$

where

$$F(Q) = \begin{cases} \frac{T(R_Q, N_Q)}{E_{I_Q}}, & \text{if } Q \neq \varnothing, \\ 0, & \text{otherwise}, \end{cases} \tag{4.7}$$

and $\alpha(Q_1, Q_2)$, a discount factor for the spatial reuse, is given by

$$\alpha(Q_1, Q_2) = \frac{\max\left(T(R_{Q_1}, N_{Q_1}), T(R_{Q_2}, N_{Q_2})\right)}{T(R_{Q_1}, N_{Q_1}) + T(R_{Q_2}, N_{Q_2})}. \tag{4.8}$$

Note that I_Q, R_Q, and N_Q denote node index, PHY rate, and generation size associated to Q, respectively. Since a spatially reusable pair can transmit simultaneously, we encourage to select type-4 and 5 IUs by adopting the discount factor. As the difference of the transmission time between two senders decreases, relative time for simultaneous transmission to the total time increases, and hence, we design the discount factor to be proportional to the transmission time difference.

The utility function captures the considerations in Section 4.2. The utility function favors IUs that increase the number of served nodes. Also, it favors IUs having lower airtime and the nodes charging their batteries and having higher remaining battery level. Furthermore, it favors spatially reusable relays with higher spatial reuse gain.

By searching the best IU to serve each possible destination node, ether one-hop or two-hop, it finds the optimal IU in each round, where the destination node maximizing the utility function is called *target node*. As rounds are repeated, new IUs are selected, thus increasing both the number of the served nodes and the required airtime. Accordingly, the algorithm is finished until all nodes are served or no more airtime is available. Note that the problem determining the set of nodes to be served, similar to the conventional admission control problem addressed in [89], is inherently solved.

IRN adjustment

Although such a round-based selection has an advantage of inherent admission control, it might select redundant IRNs, thus necessitating adjustment of IRNs.

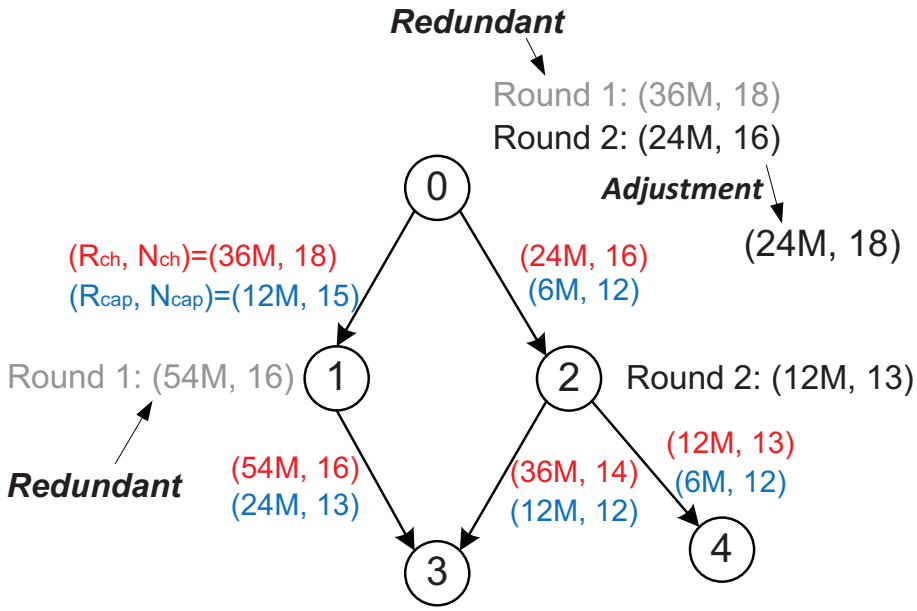

Figure 4.2: Example of IRN adjustment.

Fig. 4.2 depicts an illustrative example of redundant IRNs and necessity of the IRN adjustment. We assume that all nodes' energy factors are 100. In round 1, type 3 IU, $\pi_{\mathbf{1}} = \{(0, 36 \text{ Mb/s}, 18), (1, 54 \text{ Mb/s}, 16)\}$ is selected for node 3 (target node). Note that $B(\pi_{\mathbf{1}})$ is 2 (nodes 1 and 3), and $C(\pi_{\mathbf{1}})$ is $F(36M, 18) + F(54M, 16) = 91 + 64 = 155$, thus resulting in $U(\pi_{\mathbf{1}})$ of 0.0129. After that, $\pi_{\mathbf{2}} = \{(0, 24 \text{ Mb/s}, 16), (2, 12 \text{ Mb/s}, 13)\}$ is selected to serve node 4, where $B(\pi_{\mathbf{2}}) = 2$ (nodes 2 and 4), $C(\pi_{\mathbf{2}}) = 253$, and $U(\pi_{\mathbf{2}}) = 0.0079$. Although $\pi_{\mathbf{1}}$ is selected due to its higher utility, $\pi_{\mathbf{2}}$ makes many transmissions assigned by $\pi_{\mathbf{1}}$ redundant. Therefore, we need an adjustment process to remove the firstly assigned IRNs and increase N_{Q_0} of $\pi_{\mathbf{2}}$ by 2 as shown in the figure. In this case, the adjustment is conducted at the same node, so it is called intra-node adjustment. On the other hand, Q_1 of $\pi_{\mathbf{1}}$ is replaced by IRN for node 2, ans such adjustment between different nodes is called inter-node adjustment.

Motivated by this, we propose an IRN adjustment algorithm, which consists of two phases: source node's intra-node adjustment and relay nodes' inter-node adjust-

Algorithm 4 IRN adjustment

Require: Set of IRNs $\mathbf{\Pi} = \{Q^{(1)}, Q^{(2)}, ..., Q^{(N)}\}$, Set of nodes served by node i $\mathbf{S_i}$, Link matrix $\mathbf{\Psi}$

Ensure: Set of adjusted IRNs $\mathbf{\Pi_{adj}}$

Initialization:

$\mathbf{\Pi_{src}} = \{Q^{(i)} | I^{(i)} = 0, i = 1, ..., N\}$, ▷ $Q^{(i)} = (I^{(i)}, R^{(i)}, N^{(i)})$

$\mathbf{\Pi_{relay}} = \mathbf{\Pi} \setminus \mathbf{\Pi_{src}}, \mathbf{\Pi_{adj}} = \varnothing, \mathbf{D} = \varnothing$

Source adjustment:

$R_a = \min \left\{ R^{(i)} | Q^{(i)} \in \mathbf{\Pi_{src}} \right\}$ ▷ Adjusted R

$N_a = \min \left\{ N | H(R_a, N, \mathbf{q}^{(0j)}) = K, n \in S_{src} \right\}$ ▷ Adjusted N

$\mathbf{\Pi_{adj}} \leftarrow \mathbf{\Pi_{adj}} \cup (0, R_a, N_a)$

Relay adjustment:

Sort $\mathbf{\Pi_{relay}}$ in the increasing order of R_Q

for all $Q^{(j)} \in \mathbf{\Pi_{relay}}$ **do**

  $N_a = \min \left\{ N | H(R^{(j)}, N, \mathbf{q}^{(I^{(j)} n)}) = K, n \in \mathbf{S_j} \right\}$

  if $N_a > 0$ **then**

    $\mathbf{\Pi_{adj}} \leftarrow \mathbf{\Pi_{adj}} \cup (I^{(j)}, R^{(j)}, N_a)$

  end if

end for

ment. Intra-node adjustment of relay nodes is inherently conducted during inter-node adjustment.

Algorithm 4 provides procedure of IRN adjustment. Firstly, we separate IRNs of the source node and find the set of nodes served by the source node, $\mathbf{S_0}$. For source adjustment, we choose the minimum PHY rate among the assigned PHY rates, and find N ensuring the estimated number of innovative packets is K for all nodes in $\mathbf{S_{src}}$. For the relay adjustment, we sort IRNs in the increasing order of PHY rate. Since packets with a lower PHY rate can be received by more nodes, we adjust IRNs from that with the lowest PHY rate to that with the highest PHY rate. Similarly, after determining the set of nodes served by the selected relay node, $\mathbf{S_j}$, we determine the adjusted N, N_a, ensuring that all nodes in $\mathbf{S_i}$ are served by $(R^{(j)}, N_a)$.

Finally, the overall process of INFER algorithm is provided in Algorithm 5.

Algorithm 5 INFER algorithm

Require: $\mathbf{D}$ (set of destination nodes), $\mathbf{\Psi}$ (link matrix)

Ensure: $\mathbf{\Pi}$ (set of IRNs)

Initialization:

$\mathbf{\Pi} \leftarrow \varnothing, \mathbf{S} \leftarrow \varnothing, \mathbf{C} \leftarrow \mathbf{D}$
while 1 **do**
  $u^* \leftarrow 0, \pi^* \leftarrow 0, \mathbf{s}^* \leftarrow \phi$
  for $i \in \mathbf{C}$ **do**
    $\{\pi, u_\pi, \mathbf{s}_\pi\} \leftarrow FindBestIU(i)$
    if $u_\pi > u^*$ **then**
      $\pi^* \leftarrow \pi, u^* \leftarrow u_\pi, \mathbf{s}^* \leftarrow \mathbf{s}_\pi$
    end if
  end for
  $\mathbf{\Pi} \leftarrow \mathbf{\Pi} \cup \pi, \mathbf{S} \leftarrow \mathbf{S} \cup \mathbf{s}^*, \mathbf{C} \leftarrow \mathbf{C} \setminus \mathbf{s}^*$
  $\mathbf{\Pi} \leftarrow IRNadjustment(\mathbf{\Pi})$
  if $CalculateAirtime(\mathbf{\Pi}) > T_{available}$ **then**
    return $\mathbf{\Pi_{prev}}$
  else if $C == \varnothing$ **then**
    return $\mathbf{\Pi}$
  else
    $\mathbf{\Pi_{prev}} \leftarrow \mathbf{\Pi}$
  end if
end while

4.3.5 Assignment, Polling, and Re-selection of Relays

Relay assignment

By INFER algorithm, the source node determines the set of relay nodes along with their TPs and target nodes. Then, the source node sends *RelaySetup* packet to the selected relay nodes via unicast, which includes R, N, and the list of the target nodes. Upon receiving *RelaySetup*, a destination node sets up the relay parameters and sends *TargetNotification* packets to the target nodes via unicast. As in Section 4.3.3, until the source node re-selects relays and target nodes, they send regular feedback packets with

the fixed minimum interval, λ_{min}.

Relay polling

Since EV-CAST has no batch-level acknowledgement and retransmission, frequent collisions between the source and relay nodes or between relays might result in significant degradation of video quality. In addition, the spatial reuse gain of an SRP can be full utilized only when there are no other transmitting nodes. Accordingly, we employ a polling-based relay protocol where the source node explicitly sends *RelayPolling* packet to enable a relay or an SRP to send. For an SRP, the AP sends two *RelayPolling* packets subsequently to each relay node. A relay node re-encodes the packets from the source node, and transmits them as soon as it receives *RelayPolling* packet. After relaying, the relay node sends *RelayEnd* packet to the source node, and then the source node sends *RelayPolling* packets to another relay or SRP nodes. *RelayEnd* packet conveys the number of innovative packets in a batch, and RelayEnd packet with the number of innovative packets smaller than K is called *Imperfect RelayEnd* packet.

Relay re-selection

Basically, the source node runs INFER algorithm every 100 batches. Additionally, there are two cases when the source node immediately re-selects relay nodes: when it receives 1) event-driven feedback packets from more than $X\%$ of total receivers or 2) *Imperfect RelayEnd* packets twice from the same relay node. We set X to 5% in this work as in [80]. With the regular and event-driven re-selection, EV-CAST enables relay selection adaptive to topology variation with minimal overhead.

4.3.6 Discussion

Protocol overhead

EV-CAST utilizes various types of packets for the network and relay management, i.e., one-hop/two-hop probing, feedback, *RelaySetup*, *TargetNotification*, *RelayPolling*, *RelayEnd*, thus incurring additional protocol overhead. Among them, the transmission of one-hop and two-hop probing packets requires the most airtime. Accordingly, we determine the interval of the probing packets in consideration of the protocol overhead. We assume that a network consists of N_1 one-hop nodes and N_2 two-hop nodes. Out of them, there are N_r and N_t relay and target nodes, respectively. Assuming the worst case where all nodes use the minimum feedback interval of λ_{min}, we provide a simple analysis to evaluate the overhead. We analyze the ratio of airtime for the management packets to a given time duration T. For ease of the analysis, we set T to the time interval for generating λ_{min}-batches. For video source rate of B_{src}, T is determined as $T = L_m \cdot \lambda_{min} \cdot K/B_{src}$, and the total overhead during T, V, can be expressed as follows.

$$V = (N_1 + 1)\frac{T}{T_{probe}}\tau_{probe} + (N_1 + 2N_2)\tau_{fb} + N_r\tau_{rs} + N_t\tau_{tn} + \lambda_{min}N_r\left\{\tau_{rp} + \tau_{re}\right\}, \quad (4.9)$$

where T_{probe} and τ_{probe} are the interval and duration of the probing packets, respectively, and τ_{fb}, τ_{rs}, τ_{tn}, τ_{rp}, and τ_{re} are the time duration of feedback, *RelaySetup*, *TargetNotification*, *RelayPolling*, and *RelayEnd* packet, respectively.

The analysis results are shown in Fig. 4.3. We set N_r to 5 as in [15], and assume that N_2 is $3N_1$ and each of relay and source node has two target nodes. As in Fig. 4.3a, the protocol overhead (V/T) is inversely proportional to T_{probe}, and we observe that the protocol overhead decreases marginally when T_{probe} is larger than 2 seconds. Fig. 4.3b shows the protocol overhead with respect to the number of one-hop

nodes. We observe that the protocol overhead is linearly proportional to the number of one-hop nodes. Based on these results, we set T_{probe} to 2 seconds, thus ensuring the protocol overhead under 5% even when the number of one-hop nodes is 100.

4.4 Evaluation

We comparatively evaluate the performance of EV-CAST under various scenarios. We have implemented EV-CAST by modifying the latest ath9k device driver, backport 4.2.6-1 [90].

4.4.1 Measurement Setup

We conduct our experiments on *w-iLab.t* testbed [81], which is a heterogeneous wireless testbed where programmable WLAN, Bluetooth, LTE nodes are deployed. We use WLAN nodes equipped with a signal attenuator of 20 dB to make two-hop networks, where the floor plan is shown in Fig. 4.4. Each node, blue circle in the figure, is equipped with Qualcomm Atheros AR9280 chipset, where Ubuntu 14.04 is installed. The detailed information of the node is provided in [81]. We configure an ad-hoc network on a channel in 5 GHz band. For the energy consumption evaluation, we employ the energy consumption model in [91], since the WLAN nodes in *w-iLab.t* testbed are always AC-powered. The energy consumption parameters are referred to [92].

We measure the following five performance metrics: 1) *APLR*, 2) *NSR*, i.e., fraction of nodes that satisfy the target APLR, 3) *Fractional airtime*, i.e., fraction of airtime occupancy by multicast sessions, and 4) *Fractional transmit time*, i.e., ratio of time for transmitting packets to the total time, and 5) *network lifetime*, which is defined as time duration from when video multicast service starts until the first node failure due to energy depletion happens.

We compare EV-CAST with the following schemes:

- *Original 802.11*: the lowest PHY rate without NC.

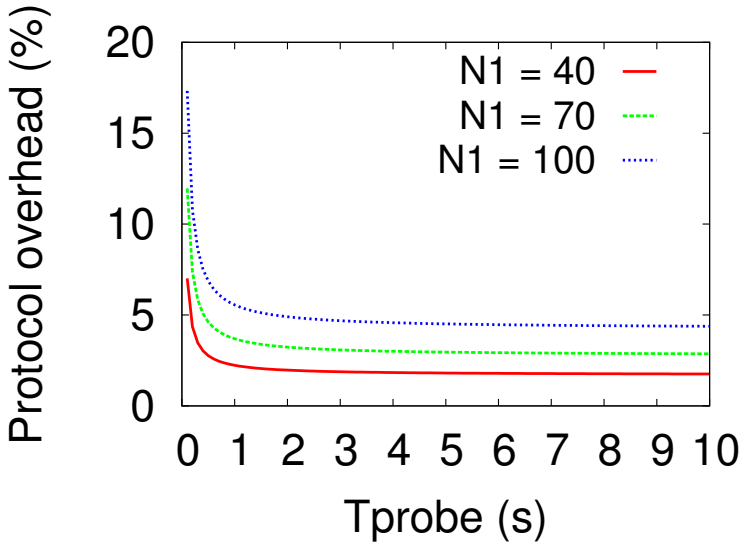

(a)

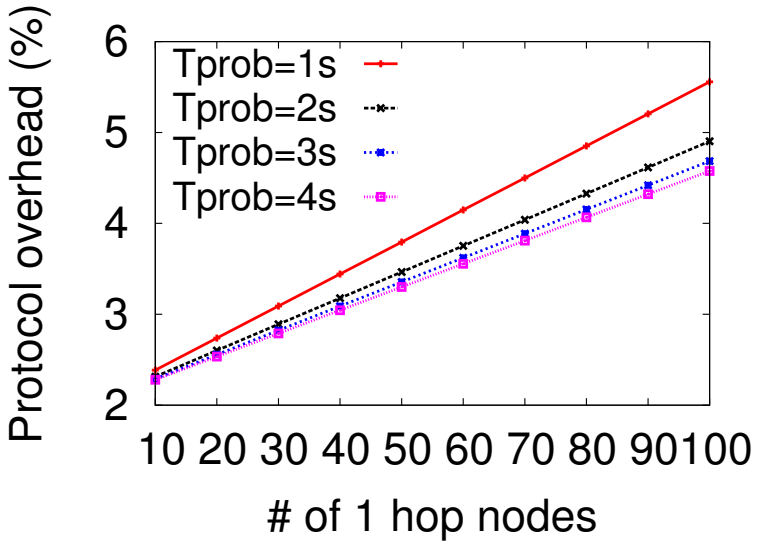

(b)

Figure 4.3: Analysis results: protocol overhead with respect to (a) the probing interval and (b) the number of 1-hop nodes.

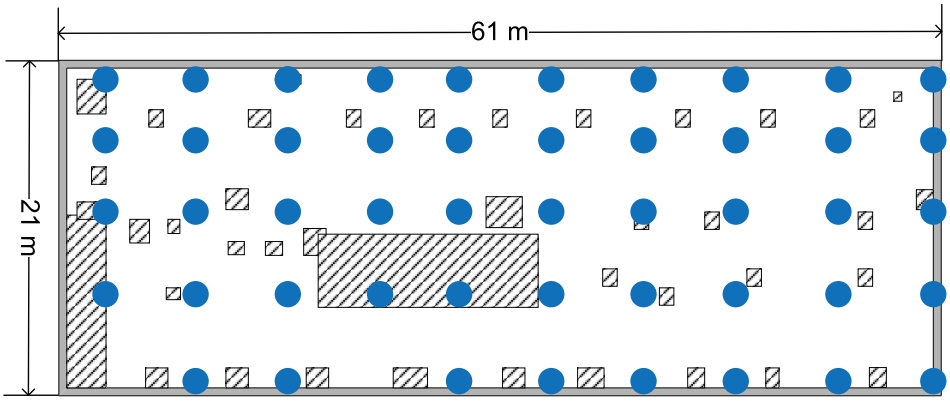

Figure 4.4: Floor plan of w.iLab.t testbed.

- *InFRA* [80]: ad-hoc version of InFRA.
- *ViMOR (Origianl)* [**?**]: the original version of ViMOR. For fair comparison, we set K to 10.
- *ViMOR (Multi-rate)*: multi-rate extension of ViMOR. We extend ViMOR to utilize multiple PHY rates. The source determines the PHY rates of relay nodes based on the shortest path in terms of estimated transmission time (ETT), and assigns N minimizing the average packet error ratio as in [**?**].

4.4.2 Micro-benchmark

Through the measurement under specific scenarios, we verify the featured operation of EV-CAST and impact of the factors addressed in Section 4.2.

Impact of battery status

In order to observe the impact of the battery status, we set up the topology as in Fig. 4.5a. We vary the battery level of node 1, while fixing the other nodes' battery levels to 50%.

The measurement results are presented in Fig. 4.6. Fig. 4.6a presents the fractional

transmit time of each node with respect to the battery level of node 1. We observe that EV-CAST changes the relay node from node 1 to node 2 when node 1's battery level is 40%, while ViMOR selects relay nodes independently of node 1's battery level. We also observe that EV-CAST consumes lower transmission time due to its intelligent selection of TPs. Fig. 4.6b presents the APLR of each node, and we observe that both EV-CAST and original ViMOR achieve the target APLR, while multi-rate ViMOR yields higher APLR in some cases due to the incorrect estimation of link quality. Fig. 4.6c presents the network lifetime. When node 1's battery level is higher than 50%, the bottleneck node to determine lifetime is node 2, and hence, the gain of lifetime is achieved by the reduction of airtime as shown in Fig. 4.6d. On the other hand, when node 1's battery level is lower than 50%, the lifetime is determined by node 1, and hence, the gain of lifetime is due to the battery-aware relay selection. We observe that EV-CAST achieves up to 17% and 12% higher lifetime than original ViMOR and multi-rate ViMOR, respectively.

Impact of spatial reuse

In order to observe the impact of the spatial reuse, we set up the topology as in Fig. 4.5b, where nodes 1 and 2 are hidden with each other, i.e., they are the SRP. Distance from node 0 to node 1 is shorter than that from node 0 to node 3. As in scenario 1, we vary the battery level of node 1, while fixing the other nodes' battery levels to 50%.

The measurement results are presented in Fig. 4.7. From Fig. 4.7a, we observe that EV-CAST selects node 1 as a relay as well as node 2 while ViMOR only selects node 2 as a relay. In order for the source node to serve node 3, which has the longest distance from the source, large airtime is required, thus incurring higher airtime for ViMOR schemes. On the other hand, EV-CAST achieves lower airtime thanks to the spatial reuse, while all the schemes achieve the target APLR as shown in Fig. 4.6b. Note that the fractional transmit time of node 1 decreases as the battery level of node 1

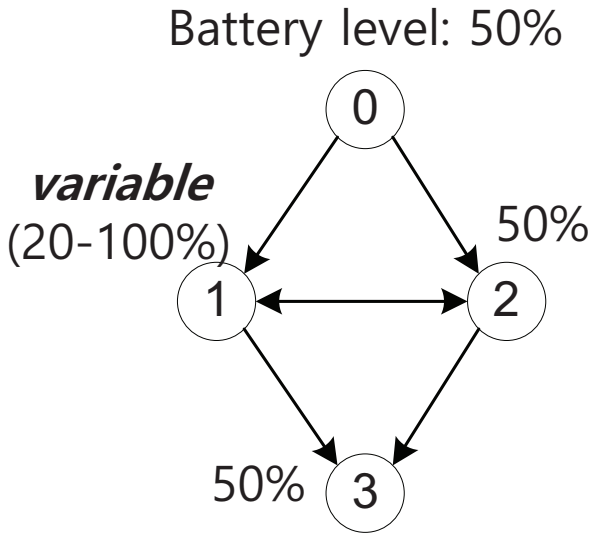

(a)

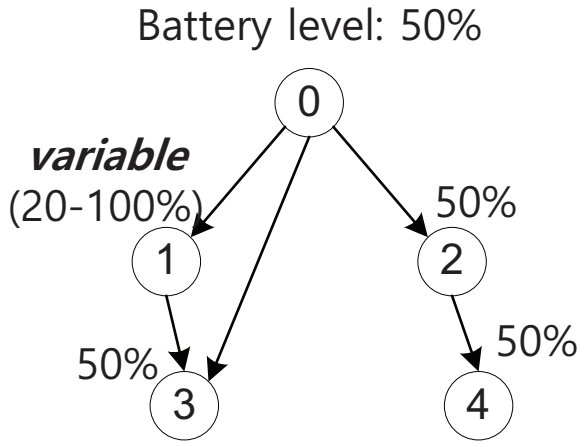

(b)

Figure 4.5: Scenarios for micro-benchmark: (a) scenario 1: impact of battery status and (b) scenario 2: impact of spatial reuse.

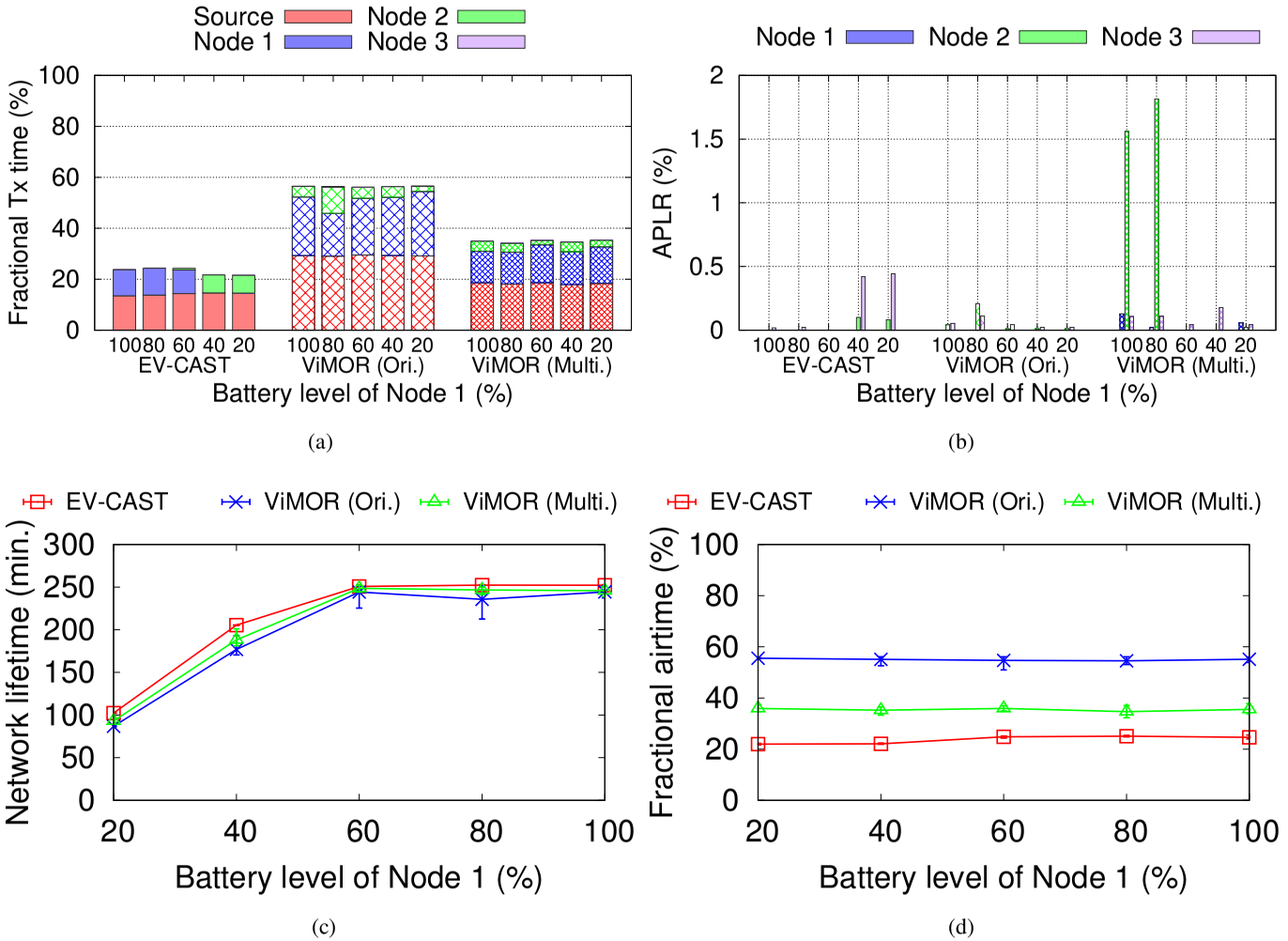

Figure 4.6: Measurement results for scenario 1: (a) distribution of fractional tx time, (b) network lifetime, (c) distribution of APLR, and (d) fractional airtime.

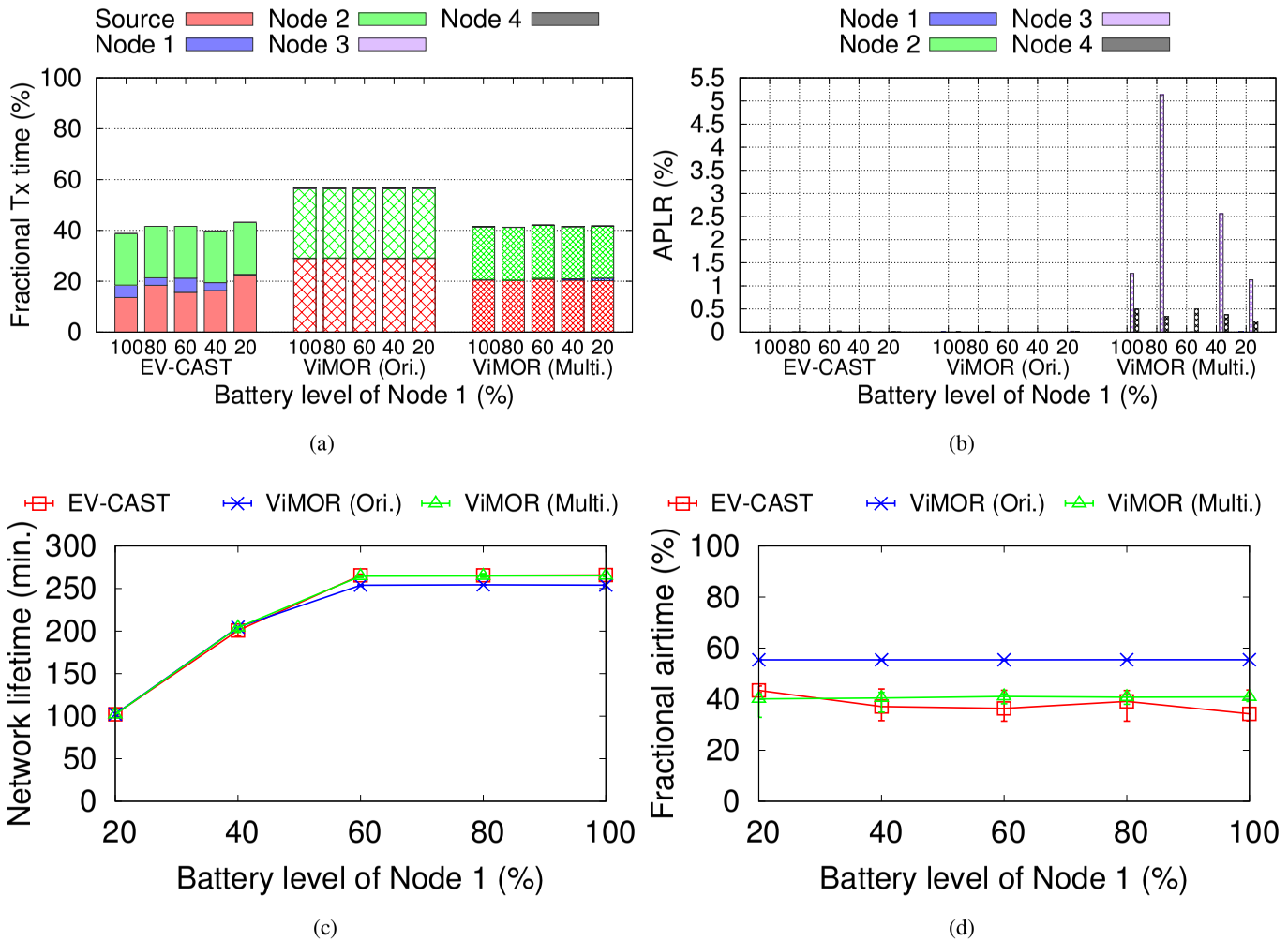

Figure 4.7: Measurement results for scenario 2: (a) distribution of fractional tx time, (b) network lifetime, (c) distribution of APLR, and (d) fractional airtime.

decreases due to the battery-aware relay selection. In Fig. 4.6c, we observe that EV-CAST achieves higher lifetime than ViMOR schemes especially when node 1's battery level is higher than 50%.

4.4.3 Macro-benchmark

We evaluate the performance with 30 destination nodes for various transmit power values. The network shrinks as the transmit power decreases, and hence, we evaluate the impact of the network size by varying the transmit power. The battery level of each node is 50% or 100% with the equal probability of 0.5 and the charging probability is 0.5. We set the bottom leftmost node as the source node.

Fig. 4.8a presents NSR results. We observe that NSR increases as the transmit power increases since more nodes can be served with higher transmit power. EV-CAST achieves the highest NSR for all the transmit power values thanks to the intelligent selection of relay nodes. Fig. 4.8b presents the fractional airtime results. Since larger airtime is required to serve nodes with lower transmit power, EV-CAST consumes more airtime as the transmit power decreases. Whereas, the original ViMOR decreases the airtime as the transmit power decreases, which is related to the philosophy of ViMOR. ViMOR consumes airtime as much as possible while ensuring all the relay nodes have the same N. However, if the source node cannot allocate N to all the relay nodes within the available airtime, it does not allow the relay nodes to relay. Due to such an all-or-none mechanism, the source node does not allocate N when the transmit power is low. As a consequence, EV-CAST achieves higher NSR at the cost of the airtime when the transmit power is low, while achieving lower airtime with the maximum NSR when the transmit power is high. Fig. 4.8c presents the network lifetime results. We observe that EV-CAST achieves higher lifetime especially when the transmit power is 17 dBm due to its low airtime. Moreover, when the transmit power is low and airtime is large, EV-CAST still achieves the moderate lifetime due to its energy-aware relay selection.

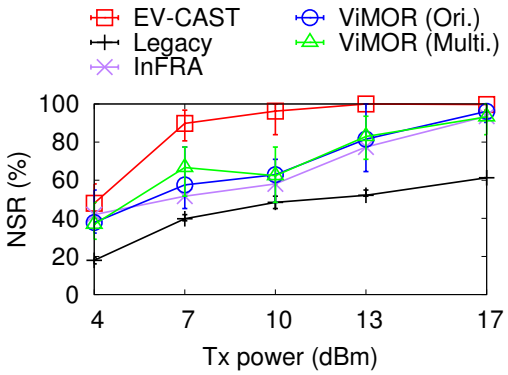

(a)

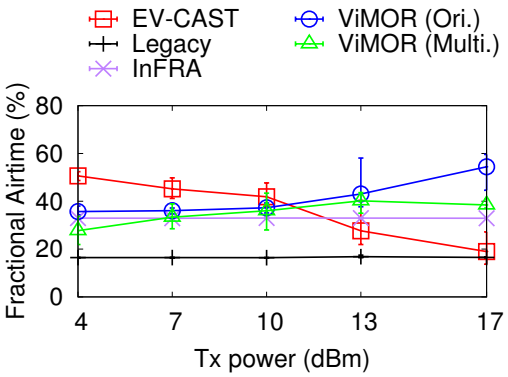

(b)

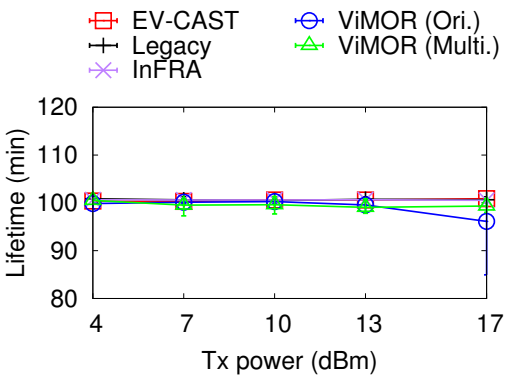

(c)

Figure 4.8: Measurement results with respect to the transmit power (a) NSR, (b) fractional airtime, and (c) network lifetime.

4.5 Related Work

This section discusses related work in two contexts: (1) multicast opportunistic routing and (2) video multicast over WLAN.

4.5.1 Multicast Opportunistic Routing

The concept of collaborative relaying has been utilized in the context of opportunistic routing (OR) for multicast [**?**, 16, 17, 82]. Instead of designating fixed next-hop nodes, all the neighboring nodes of a sender node have opportunities to relay packets.

MORE [82], the most well-known OR protocol, firstly employ intra-flow NC to enhance reliability and the routing gain.

Pacifier [16] is proposed to solve so called "crying baby" problem, which is a problematic phenomenon that overall throughput is bounded by the worst user. Pacifier solves the "crying baby" problem by proposing the tree-based OR and round-robin batch transmission.

Uflood [17] identifies major factors such as PDR, number of neighbor nodes, PHY rate, in selection of relay nodes and proposes a distributed relay selection protocol based on them. Uflood is the first multi-rate multicast OR scheme. EV-CAST also considers the factors addressed in Uflood.

While aforementioned OR schemes target on applications requiring 100 $\%$ reliability such as file transfer, ViMOR [**?**] proposes a multicast OR scheme suited for the video streaming. With the philosophy of total denial of acknowledgement, ViMOR delivers video frames before their deadline.

None of them considers interference, battery status, and spatial reuse for selection of relay nodes.

4.5.2 Multicast over WLAN

Relay-based video multicast

Lin *et al.* [12] proposes that AP allocates transmission time and selects bit-rate for each relay node, while it transmits packets with the lowest PHY rate. PeerCast [14] proposes that AP selects a higher rate to deliver a batch of packets to the majority of clients, and a suitable subset of these clients relays the packets based on power-controlled ACKs. Alay *et al.* [15] proposes a two-hop relay multicast system using FEC. The users are divided into two groups such that receivers in group 1 have better average channel quality than those in group 2. T he selected receivers in group 1 relay packets to group 2. All of them considers the infrastructure mode where all nodes can receive from AP.

Multi-AP video multicast

Multiple AP-based multicast also enhances the coverage. Dircast [45] proposes a user association problem between multiple APs. Choi *et al.* [93] propose a cooperative FEC coding approach to harness the link diversity gain. Employing an adaptive video streaming, JurCast [94] proposes an approximation algorithm determining user association, PHY rate, and video source rate to maximize the network utility.

In addition to the research area, there are industrial practices to cover a large space with multiple APs. For example, Cisco StadiumVision Mobile [95] deploys multiple APs to cover a large sports stadium.

However, they require additional cost to deploy APs, and they are less flexible than collaborative relaying schemes.

4.6 Summary

We proposed EV-CAST, an interference and energy-aware video multicast system that exploits collaborative relays. On top of the proposed interference-aware link character-

ization, our algorithm determining the sender node set and their TPs takes into account the various factors including battery status and spatial reusability. The polling-based transmission mechanism reduces the collisions between sender nodes, and our feedback mechanism reduces the protocol overheads. Our prototype-based measurement results verify that EV-CAST improves NSR when the network is large and improves the fractional airtime when the network is small. As future work, we are planning to evaluate EV-CAST under more various scenarios.

Chapter 5

Conclusion

5.1 Research Contributions

In this dissertation, we dealt with the problem identification and performance enhancement of video multicast over WLAN.

In Chapter 2, we identified the practical issues with multicast power saving. The malfunctions of commercial WLAN devices and the coexistence problem with VoIP are identified. For the coexistence problem, we provide the analysis of the VoIP packet losses and a candidate solution to resolve the problem, which is verified by the prototype-based measurement results.

In Chapter 3, we propose InFRA to enable the differentiated selection of PHY/FEC rates depending on the cause of packet losses. Our proposed loss differentiation scheme suited for FEC-applied multicast diagnoses the cause of packet losses without hardware modification. The performance gain of InFRA compared with the state-of-the-art PHY/FEC rate adaptation scheme is demonstrated via small and large-scale experiments.

In Chapter 4, we propose EV-CAST to realize the interference, battery status, and spatial reusability-aware multi-hop multicast. Thanks to our elaborate design, EV-CAST manages the network topology efficiently, selects the sender node set with

appropriate transmission parameters, and transmits video packets reliably. The performance gain of EV-CAST compared with the state-of-the-art multi-hop as well as single-hop multicast schemes is demonstrated via measurements in an NGO-owned wireless testbed, imec w-iLab.t testbed.

5.2 Future Research Directions

Based on the results of this dissertation, there are several new research directions which require further investigation. We highlight some of them as follows.

First, regarding the practical issues with multicast power saving, as future work, we plan to investigate the impact of video multicast on more diverse types of traffic including HTTP-based unicast video streaming and instant messages. In addition to the legacy PSM, we plan to investigate the issues with newly defined power saving protocols such as flexible multicast service (FMS).

Second, regarding the PHY/FEC rate adaptation, we plan to enhance the rate decrease mechanism for weak interference. In the current version, we consider the worst weak interference, thus incurring the AP to select the lowest PHY rate in most cases. By analyzing the interference patterns, we believe that the AP can select more efficient PHY rate even with the weak interference.

Finally, regarding the multi-hop multicast, we plan to introduce the concept of auxiliary relay set in preparation for failure of relay nodes. When a relay does not receive the packets, it fails to relay, then the AP might schedule the auxiliary relays. We envision further reliability enhancement via such a mechanism.

Bibliography

[1] *Wireless LAN Medium Access Control (MAC) and Physical Layer (PHY) Specifications*, IEEE Std. 802.11-2016 (Revision of IEEE Std. 802.11-2012), Mar. 2016.

[2] IEEE 802.11aa, *Part 11: Wireless LAN Medium Access Control (MAC) and Physical Layer (PHY) Specifications Amendment 2: MAC Enhancements for Robust Audio Video Streaming*, IEEE Std., May 2012.

[3] Y. He, R. Yuan, X. Ma, and J. Li, "The IEEE 802.11 Power Saving Mechanism: an Experimental Study," in *Proc. IEEE WCNC*, Mar. 2008.

[4] T. Hiraguri, M. Ogawa, M. Umeuchi, and T. Sakata, "Study of Power Saving Scheme Suitable for Wireless LAN in Multimedia Communication," in *Proc. IEEE WCNC*, Apr. 2009.

[5] G. Lee, Y. Shin, J. Koo, and S. Choi, "ACT-AP: ACTivator Access Point for Multicast over WLAN," in *Proc. IEEE INFOCOM*, May 2017.

[6] Ö. Alay, T. Korakis, Y. Wang, and S. Panwar, "Dynamic Rate and FEC Adaptation for Video Multicast in Multi-rate Wireless Networks," *Mobile Netw. Appl.*, vol. 15, no. 3, pp. 425–434, 2010.

[7] S. H. Wong, R. Raghavendra, Y. Song, and K.-W. Lee, "X-WING: A High-Speed Wireless Broadcasting Framework for IEEE 802.11 Networks," in *Proc. IEEE SECON*, Jun. 2013.

[8] B. Bulut, E. Mellios, D. Berkovskyy, F. A. Rahman, A. Doufexi, and A. Nix, "Cross-layer Design of Raptor Codes for Video Multicast over 802.11n MIMO Channels," in *Proc. IEEE PIMRC*, Aug. 2015.

[9] S. Jakubczak and D. Katabi, "A Cross-layer Design for Scalable Mobile Video," in *Proc. ACM MobiCom*, Sep. 2011.

[10] X. L. Liu, W. Hu, Q. Pu, F. Wu, and Y. Zhang, "Parcast: Soft Video Delivery in MIMO-OFDM WLANs," in *Proc. ACM MobiCom*, Aug. 2012.

[11] S. Aditya and S. Katti, "FlexCast: Graceful Wireless Video Streaming," in *Proc. ACM MobiCom*, Sep. 2011.

[12] K.-J. Lin and S.-T. Lee, "Relay-based Video Multicast with Network Coding in Multi-Rate Wireless Networks," in *Proc. IEEE GLOBECOM*, Dec. 2011.

[13] H. Schwarz, D. Marpe, and T. Wiegand, "Overview of the Scalable Video Coding Extension of the H. 264/AVC Standard," *IEEE Tran. Circuits Syst. Video Technol.*, vol. 17, no. 9, pp. 1103–1120, 2007.

[14] J. Xiong and R. R. Choudhury, "Peercast: Improving Link Layer Multicast Through Cooperative Relaying," in *Proc. IEEE INFOCOM*, Apr. 2011.

[15] O. Alay, T. Korakis, Y. Wang, E. Erkip, and S. S. Panwar, "Layered Wireless Video Multicast Using Relays," *IEEE Trans. Circuits Syst. Video Technol.*, vol. 20, no. 8, pp. 1095–1109, 2010.

[16] D. Koutsonikolas, Y. C. Hu, and C.-C. Wang, "Pacifier: High-Throughput, Reliable Multicast Without Crying Babies in Wireless Mesh Networks," *IEEE/ACM Trans. Networking (TON)*, vol. 20, no. 5, pp. 1375–1388, 2012.

[17] J. Subramanian, R. Morris, and H. Balakrishnan, "UFlood: High-Throughput Flooding over Wireless Mesh Networks," in *Proc. IEEE INFOCOM 2012*, Mar. 2012.

[18] K. Choumas, I. Syrigos, T. Korakis, and L. Tassiulas, "Video-aware Multicast Opportunistic Routing over 802.11 Two-Hop Mesh Networks," in *Proc. IEEE SECON*, Jul. 2014.

[19] B. G. Lee and S. Choi, *Broadband wireless access and local networks: mobile WiMAX and WiFi*. Artech House, 2008.

[20] Y. Shin, M. Choi, J. Koo, Y.-D. Kim, J.-T. Ihm, and S. Choi, "Empirical Analysis of Video Multicast over WiFi," in *Proc. ICUFN*, Jun. 2011.

[21] AirPort Extreme Base Station. [Online]. Available: http://www.apple.com/airportextreme/

[22] AIR-AP1232AG-A-K9. [Online]. Available: http://www.cisco.com/en/US/products/hw/wireless/

[23] MW-2060. [Online]. Available: http://www.mmctech.com/eng/product/index.htm/

[24] APD-2000. [Online]. Available: http://www.cybertan.com.tw/Products/Fixed.htm/

[25] Intel Pro/Wireless 3945 ABG Network Connection. [Online]. Available: http://www.intel.com/products/wireless/prowireless_mobile.htm/

[26] 802.11b/g Mini Card Wireless Adapter. [Online]. Available: http://www.realtek.com.tw/products/

[27] CB21AG. [Online]. Available: http://www.cisco.com/en/US/prod/collateral/wireless/

[28] WPU-7800. [Online]. Available: http://www.udcsystems.com/product/wpu7800.php/

[29] *Pulse Code Modulation (PCM) of Voice Frequencies*, ITU-T Recommendation G. 711, Dec. 1988.

[30] R. Krashinsky and H. Balakrishnan, "Minimizing Energy for Wireless Web Access with Bounded Slowdown," in *Proc. ACM MobiCom*, Sep. 2002.

[31] *The E-Model, a computational model for use in transmission planning*, ITU-T Recommendation G. 107, Dec. 1998.

[32] H. Lee, S. Byeon, B. Kim, K. B. Lee, and S. Choi, "Enhancing Voice over WLAN via Rate Adaptation and Retry Scheduling," *IEEE Trans. Mobile Comput.*, vol. 13, no. 12, pp. 2791–2805, 2014.

[33] V. Jacobson, R. Frederick, S. Casner, and H. Schulzrinne, "RTP: A Transport Protocol for Real-time Applications," *RFC 1889*, 2003.

[34] Y. He, R. Yuan, and W. Gong, "Modeling Power Saving Protocols for Multicast Services in 802.11 Wireless LANs," *IEEE Trans. Mobile Comput.*, vol. 9, no. 5, pp. 657–671, 2010.

[35] S. Mangold, S. Choi, G. R. Hiertz, O. Klein, and B. Walke, "Analysis of IEEE 802.11e for QoS Support in Wireless LANs," *IEEE Wireless Commun.*, vol. 10, no. 6, pp. 40–50, 2003.

[36] G. Peng, G. Zhou, D. T. Nguyen, and X. Qi, "All or None? The Dilemma of Handling WiFi Broadcast Traffic in Smartphone Suspend Mode," in *Proc. IEEE INFOCOM*, Apr. 2015.

[37] J. Koo, W. Lee, S. Choi, and Y. Park, "PIMM: Packet Interval-based Power Modeling of Multiple Network Interface-Activated Smartphones," in *Proc. ACM e-Energy*, Jul. 2015.

[38] Y. Shin, M. Choi, J. Koo, and S. Choi, "Video Multicast over WLANs: Power Saving and Reliability Perspectives," *IEEE Network*, vol. 27, no. 2, pp. 40–46, 2013.

[39] HostApd: IEEE 802.11 AP, IEEE 802.1X/WPA/WPA2/EAP/ RADIUS Authenticator. [Online]. Available: https://w1.fi/hostapd/

[40] Ixia IxChariot. https://www.ixiacom.com/products/ixchariot.

[41] Cisco Visual Networking Index, "Global Mobile Data Traffic Forecast Update, 2015–2020," *White paper*, 2015.

[42] V. Gupta, C. Gutterman, Y. Bejerano, and G. Zussman, "Experimental Evaluation of Large Scale WiFi Multicast Rate Control," in *Proc. IEEE INFOCOM*, Apr. 2016.

[43] J. Kim, S. Kim, S. Choi, and D. Qiao, "CARA: Collision-Aware Rate Adaptation for IEEE 802.11 WLANs," in *Proc. IEEE INFOCOM*, Apr. 2006.

[44] S. Sen, N. K. Madabhushi, and S. Banerjee, "Scalable WiFi Media Delivery through Adaptive Broadcasts," in *Proc. USENIX NSDI*, Apr. 2010.

[45] R. Chandra, S. Karanth, T. Moscibroda, V. Navda, J. Padhye, R. Ramjee, and L. Ravindranath, "DirCast: A Practical and Efficient Wi-Fi Multicast System," in *Proc. IEEE ICNP*, Oct. 2009.

[46] N. Choi, Y. Seok, T. Kwon, and Y. Choi, "Leader-based Multicast Service in IEEE 802.11v Networks," in *Proc. IEEE CCNC*, Jan. 2010.

[47] J. Villalón, P. Cuenca, L. Orozco-Barbosa, Y. Seok, and T. Turletti, "Cross-layer Architecture for Adaptive Video Multicast Streaming over Multirate Wireless LANs," *IEEE J. Sel. Areas Commun.*, vol. 25, no. 4, pp. 699–711, 2007.

[48] W.-S. Lim, D.-W. Kim, and Y.-J. Suh, "Design of Efficient Multicast Protocol for IEEE 802.11n WLANs and Cross-layer Optimization for Scalable Video Streaming," *IEEE Trans. Mobile Comput.*, vol. 11, no. 5, pp. 780–792, 2012.

[49] B.-S. Kim, S. W. Kim, and R. L. Ekl, "OFDMA-based Reliable Multicasting MAC Protocol for WLANs," *IEEE Trans. Vehicular Technol.*, vol. 57, no. 5, pp. 3136–3145, 2008.

[50] Y. Zhang, H. Hu, and M. Fujise, *Resource, Mobility, and Security Management in Wireless Networks and Mobile Communications*. CRC Press, 2006.

[51] A. Nafaa, T. Taleb, and L. Murphy, "Forward Error Correction Strategies for Media Streaming over Wireless Networks," *IEEE Commun. Mag.*, vol. 46, no. 1, pp. 72–79, 2008.

[52] R. Immich, E. Cerqueira, and M. Curado, "Adaptive Video-aware FEC-based Mechanism with Unequal Error Protection Scheme," in *Proc. ACM SAC*, Mar. 2013.

[53] H.-r. Lee, Y.-W. Jeong, J.-s. Kim, D. Wu, and K.-d. Seo, "Estimation of Accurate Effective Loss Rate for FEC Video Transmission," *Signal Processing: Image Communication*, vol. 29, no. 6, pp. 678–698, 2014.

[54] V. Sgardoni, M. Sarafianou, P. Ferré, A. Nix, and D. Bull, "Robust video broadcasting over 802.11 a/g in time-correlated fading channels," *IEEE Tran. Consum. Electron.*, vol. 55, no. 1, pp. 69–76, 2009.

[55] K. Kang, J. Ryu, S. Choi, K.-J. Park, and J. Hur, "Toward Energy-Efficient Error Control in 3G Broadcast Video," *IEEE Wireless Commun.*, vol. 19, no. 6, pp. 60–67, 2012.

[56] X. Wang, L. Wang, Y. Wang, Y. Zhang, and A. Yamada, "Supporting MAC layer Multicast in IEEE 802.11n: Issues and Solutions," in *Proc. IEEE WCNC*, Apr. 2009.

[57] A. Basalamah and T. Sato, "Adaptive FEC reliable multicast MAC protocol for WLAN," in *Proc. IEEE VTC-Fall*, Oct. 2007.

[58] Y. Bejerano, J. Ferragut, K. Guo, V. Gupta, C. Gutterman, T. Nandagopal, and G. Zussman, "Scalable WiFi Multicast Services for Very Large Groups," in *Proc. IEEE ICNP*, Oct. 2013.

[59] W.-H. Kuo, R. Kaliski, and H.-Y. Wei, "A QoE-based Link Adaptation Scheme for H. 264/SVC Video Multicast over IEEE 802.11," *IEEE Trans. on Circuits and Syst. Video Technol.*, vol. 25, no. 5, pp. 812–826, 2015.

[60] C. Zhou, X. Zhang, L. Lu, and Z. Guo, "Collision-Detection based Rate-Adaptation for Video Multicasting over IEEE 802.11 Wireless Networks," in *Proc. IEEE ICIP*, Sep. 2010.

[61] S. H. Wong, H. Yang, S. Lu, and V. Bharghavan, "Robust Rate Adaptation for 802.11 Wireless Networks," in *Proc. ACM MobiCom*, Sep. 2006.

[62] R. Anwar, K. Nishat, M. Ali, Z. Akhtar, H. Niaz, and I. A. Qazi, "Loss Differentiation: Moving onto High-speed Wireless LANs," in *Proc. IEEE INFOCOM*, Apr. 2014.

[63] I. Pefkianakis, Y. Hu, S. H. Wong, H. Yang, and S. Lu, "MIMO Rate Adaptation in 802.11n Wireless Networks," in *Proc. ACM MobiCom*, Sep. 2010.

[64] S. Rayanchu, A. Mishra, D. Agrawal, S. Saha, and S. Banerjee, "Diagnosing Wireless Packet Losses in 802.11: Separating Collision From Weak Signal," in *Proc. IEEE INFOCOM*, Apr. 2008.

[65] J.-H. Hauer, A. Willig, and A. Wolisz, "Mitigating the Effects of RF Interference Through RSSI-based Error Recovery," in *Proc. EWSN*, Feb. 2010.

[66] T. Ho, M. Médard, R. Koetter, D. R. Karger, M. Effros, J. Shi, and B. Leong, "A Random Linear Network Coding Approach to Multicast," *IEEE Trans. Inf. Theory*, vol. 52, no. 10, pp. 4413–4430, 2006.

[67] J. Lee, W. Kim, S.-J. Lee, D. Jo, J. Ryu, T. Kwon, and Y. Choi, "An Experimental Study on The Capture Effect In 802.11a Networks," in *Proc. ACM WiNTECH*, Sep. 2007.

[68] J. del Prado, K. Challapali, S. Shankar, and P. Li, "Application Characteristics for HT Usage Scenarios," IEEE 802.11-03/364r0, 2003.

[69] Wireshark 2.2.3. [Online]. Available: https://www.wireshark.org/

[70] M. Médard, F. H. Fitzek, M.-J. Montpetit, and C. Rosenberg, "Network Coding Mythbusting: Why It Is Not About Butterflies Anymore," *IEEE Commun. Mag.*, vol. 52, no. 7, pp. 177–183, 2014.

[71] A. Shokrollahi, "Raptor Codes," *IEEE Trans. Inf. Theory*, vol. 52, no. 6, pp. 2551–2567, 2006.

[72] M. Luby, "LT-codes," in *Proc. 43rd Annu. IEEE Symp. Foundations of Computer Science (FOCS)*, 2002.

[73] T. S. Rappaport *et al.*, *Wireless Communications: Principles and Practice*. Prentice Hall PTR New Jersey, 1996, vol. 2.

[74] J. Zhang, K. Tan, J. Zhao, H. Wu, and Y. Zhang, "A Practical SNR-guided Rate Adaptation," in *Proc. IEEE INFOCOM*, Apr. 2008.

[75] D. Son, B. Krishnamachari, and J. Heidemann, "Experimental Study of Concurrent Transmission in Wireless Sensor Networks," in *Proc. ACM SenSys*, Oct. 2006.

[76] G. Judd, X. Wang, and P. Steenkiste, "Efficient Channel-aware Rate Adaptation in Dynamic Environments," in *Proc. ACM MobiSys*, June 2008.

[77] J. Klaue, B. Rathke, and A. Wolisz, "Evalvid–A Framework for Video Transmission and Quality Evaluation," in *Proc. 13th Int. Conf. TOOLS*, Sep. 2003.

[78] YouTube. [Online]. Available: https://www.youtube.com/watch?v=ttz4Sr0tZFg/

[79] Cisco Digital Fandom. [Online]. Available: http://www.cisco.com/c/dam/en_us/solutions/industries/sports/Digital-Fan-2-0-Brochure-final.pdf

[80] Y. Shin, G. Lee, J. Choi, J. Koo, S.-J. Lee, and S. Choi, "InFRA:Interference-Aware PHY/FEC Rate Adaptation for Video Multicast over WLAN," in *Proc. IEEE SECON*, Jun. 2017.

[81] imec w-iLab.t wireless testbed. [Online]. Available: https://http://wilab2.ilabt.iminds.be/

[82] S. Chachulski, M. Jennings, S. Katti, and D. Katabi, "Trading Structure for Randomness in Wireless Opportunistic Routing," in *Proc. ACM SigComm*, Aug. 2007.

[83] S.-J. Lee, M. Gerla, and C.-C. Chiang, "On-demand Multicast Routing Protocol," in *Proc. IEEE WCNC*, Sep. 1999.

[84] J. Fan, J. Chen, Y. Du, W. Gao, J. Wu, and Y. Sun, "Geocommunity-based Broadcasting for Data Dissemination in Mobile Social Networks," *IEEE Trans. Parallel Distrib. Syst.*, vol. 24, no. 4, pp. 734–743, 2013.

[85] Stoker's MANET Manager. [Online]. Available: https://www.play.google.com/store/apps/details?id=org.span&hl=en

[86] Y. Zhang, L. Song, C. Jiang, N. H. Tran, Z. Dawy, and Z. Han, "A Social-Aware Framework for Efficient Information Dissemination in Wireless Ad Hoc Networks," *IEEE Commun. Mag.*, vol. 55, no. 1, pp. 174–179, 2017.

[87] E. Soares, P. Brandão, R. Prior, and A. Aguiar, "Experimentation with MANETs of smartphones," in *Proc. IEEE Wireless Days*, Mar. 2017.

[88] *Generic coding of moving pictures and associated audio information: Systems*, ISO/IEC 13818-1 4rd edition, 2013.

[89] J.-P. Sheu, C.-C. Kao, S.-R. Yang, and L.-F. Chang, "A Resource Allocation Scheme for Scalable Video Multicast in WiMAX Relay Networks," *IEEE Trans. Mobile Comput.*, vol. 12, no. 1, pp. 90–104, 2013.

[90] Linux kernel backports website. http://drvbp1.linux-foundation.org/∼mcgrof/rel-html/backports/.

[91] W.-S. Lim and K. G. Shin, "EMS: Efficient Multicast Streaming Scheme for Multicasting within Wi-Fi Hotspot," in *Proc. IEEE ICNP*, Nov. 2015.

[92] Data sheet for BCM4356. [Online]. Available: http://www.cypress.com/file/298796/download

[93] M. Choi, W. Sun, J. Koo, S. Choi, and K. G. Shin, "Reliable Video Multicast over Wi-Fi Networks with Coordinated Multiple APs," in *Proc. IEEE INFOCOM*, Apr. 2014.

[94] H. Wang, W. T. Ooi, and M. C. Chan, "JurCast: Joint User and Rate Allocation for Video Multicast over Multiple APs," in *Proc. IEEE INFOCOM*, Apr. 2016.

[95] Cisco StadiumVision Mobile. [Online]. Available: http://www.cisco.com/web/strategy/sports/stadiumvision_mobile.html

초 록

무선랜에서 실시간 비디오를 멀티캐스트로 전송하는 무선랜 비디오 멀티캐스트는 동일한 장소에 있는 사용자들에게 실시간 비디오를 전송하는데 있어 유망한 기술이다. 무선 채널의 브로드캐스트 특성으로 인해 비디오 멀티캐스트는 기본적으로 scale-free한 비디오 전송, 즉 수신자의 수와 관계없이 고정된 무선 자원을 사용한 비디오 전송을 가능하게 한다. 하지만, 비디오 멀티캐스트는 실생활에서 널리 사용되지 못하였는데, 그 원인으로는 세 가지 문제점, 즉 1) 전력 관리와 관련된 문제점, 2) 낮은 신뢰성과 효율성, 3) 제한된 전송 범위가 대표적으로 거론된다. 본 학위 논문에서는 1) 멀티캐스트 전력 관리와 관련된 실제적 문제들의 확인, 2) 단일-홉에서 물리 계층 전송 속도(PHY 레이트)와 Forward Erasure Correction(FEC) 레이트 적응 기법, 3) 다중-홉 멀티캐스트 기법을 다루어 상기한 세가지 문제점을 해결하고자 한다.

첫째, 대부분의 무선랜 기기들은 배터리로 동작한다는 점에서 비디오 멀티캐스트는 전력 관리 모드에 있는 단말에 신뢰성있게 전송되어야 한다. 따라서, 멀티캐스트 전력 관리의 영향을 분석하고, 이와 관련된 두 가지 현실적인 문제점들을 고찰한다. 다양한 상용 무선랜 기기들을 이용한 실험을 통해 많은 기기들이 표준을 따르지 않고 있고, 이로 인해 비디오 멀티캐스트 성능이 심각하게 저하됨을 밝힌다. 본 저자는 이러한 멀티캐스트의 전력 관리와 관련된 오동작들을 분류하고, 그로 인한 성능 저하를 보고한다. 또한, 비디오 멀티캐스트와 Voice over IP (VoIP)가 공존할 때 멀티캐스트 전력 관리로 인한 공존 문제를 밝힌다. 표준에 따른 동작을 하더라도 멀티캐스트 동작이 VoIP의 성능을 저하시킬 수 있음을 실측과 수학적 분석을 통해

밝히고, 이를 해결할 수 있는 방안을 제시한다. 또한, 제안하는 기법을 오픈 소스 무선랜 디바이스 드라이버에 구현하였고, 이를 바탕으로 실측을 통해 제안하는 기법이 비디오 멀티캐스트의 성능을 저하시키지 않으면서 VoIP 성능을 증가시킴을 입증한다.

둘째, FEC를 적용한 다중 PHY 레이트 무선 멀티캐스트는 적절한 PHY 레이트와 FEC 레이트가 선택될 때 효율적이고 신뢰적인 비디오 멀티캐스트를 가능하게 한다. 이 때, 최적의 PHY/FEC 레이트는 패킷 손실의 원인에 따라 달라지는데, 기존의 연구들에서는 PHY/FEC 레이트를 간섭에 의한 손실이 발생하는 경우에도 단순히 채널에 의한 손실만을 고려하여 선택해왔다. 따라서, 본 저자는 InFRA라고 하는 간섭 인지적 PHY/FEC 레이트 적응 프레임워크를 제시한다. InFRA는 간섭의 원인을 수신 신호 강도(received signal strength indicator, RSSI)와 순환 중복 검사(cyclic redundancy check, CRC) 오류 발생 알림을 이용해 패킷 손실의 원인을 유추하고, 이를 바탕으로 최적의 PHY/FEC 레이트를 선택한다. 상용 무선랜 칩셋을 이용해 프로토타입을 만들고 이를 이용한 측정 실험을 통해 InFRA가 다양한 네트워크 시나리오에서 멀티캐스트 성능을 향상시킴을 보인다. InFRA는 최신의 기존 기법보다 경쟁 간섭원(contention interferer)이 있을 때는 2.3배의 많은 노드에게 목표로하는 비디오 성능을 제공할 수 있고, 은닉 간섭원(hidden interferer)이 있을 때는 1.8배의 많은 노드에게 목표로하는 비디오 성능을 제공할 수 있다. 아는 바에 의하면 InFRA는 최초로 간섭을 고려한 PHY/FEC 레이트 적응 기법이다.

셋째, 일부 수신 노드들이 소스 노드로부터 받은 패킷을 릴레이하는 협업 릴레이(collaborative relay)방식은 비디오 멀티캐스트의 전송 범위를 확장시킬 뿐만 아니라 신뢰성과 효율성을 향상시킨다. 이 때, 소스 노드와 릴레이 노드를 포함한 전송자 노드와 그들의 전송 파라미터 (PHY 레이트와 전송할 패킷의 수) 결정에 따라 멀티캐스트 성능이 크게 달라진다. 따라서, 본 저자는 EV-CAST라고 하는 협업 릴레이를 사용한 에너지 인지적 비디오 멀티캐스트 기법을 제한한다. EV-CAST는 송신자 노드들과 그들의 전송 파라미터를 동시에 결정하는 알고리즘, 간섭 인지적 링크 특징화 기반의 실시간 네트워크 관리 기법, Polling 기반의 릴레이 전송 프로토콜로 구성된다. 최적의 전송자 노드 집합을 찾기 위해 기존에 알고 있던 요소들과

더불어 배터리 상태, 공간 재사용의 새로운 요소들을 고려한다. 프로토타입 기반의 측정 결과를 통해 EV-CAST가 최신의 기존 기법들보다 더 나은 성능을 보임을 입증한다.

요약하자면, 2장에서 4장까지 앞서 설명한 세가지 세부 연구 주제들, 즉 전력 관리와 관련된 실제적인 문제의 확인, 간섭에 강인한 단일-홉 멀티캐스트를 위한 InFRA, 효율적인 다중-홉 멀티캐스트를 위한 EV-CAST를 각각 제시한다. 결론적으로 이상의 연구를 통해 무선랜 비디오 멀티캐스트가 실생활에서 광범위하게 사용되는 데 기여하고자 한다.

주요어: 비디오 멀티캐스트, 무선랜, 멀티캐스트 전력 관리, 적응적 PHY/FEC 레이트 조절, 다중-홉 멀티캐스트.

학번: 2010-20828